




5-2013

Adsorption of Antimony by Birnessite and the Impact of Antimony on the Electrostatic Surface Properties of Variable-Charge Soil Minerals

Kalyn Alaine Vergeer
kvergeer@utk.edu

Follow this and additional works at: https://trace.tennessee.edu/utk_gradthes

 Part of the [Environmental Chemistry Commons](#), [Environmental Monitoring Commons](#), [Geochemistry Commons](#), and the [Soil Science Commons](#)

Recommended Citation

Vergeer, Kalyn Alaine, "Adsorption of Antimony by Birnessite and the Impact of Antimony on the Electrostatic Surface Properties of Variable-Charge Soil Minerals. " Master's Thesis, University of Tennessee, 2013.

https://trace.tennessee.edu/utk_gradthes/1693

This Thesis is brought to you for free and open access by the Graduate School at TRACE: Tennessee Research and Creative Exchange. It has been accepted for inclusion in Masters Theses by an authorized administrator of TRACE: Tennessee Research and Creative Exchange. For more information, please contact trace@utk.edu.

To the Graduate Council:

I am submitting herewith a thesis written by Kalyn Alaine Vergeer entitled "Adsorption of Antimony by Birnessite and the Impact of Antimony on the Electrostatic Surface Properties of Variable-Charge Soil Minerals." I have examined the final electronic copy of this thesis for form and content and recommend that it be accepted in partial fulfillment of the requirements for the degree of Master of Science, with a major in Environmental and Soil Sciences.

Michael E. Essington, Major Professor

We have read this thesis and recommend its acceptance:

Jaehoon Lee, Phillip Jardine

Accepted for the Council:

Carolyn R. Hodges

Vice Provost and Dean of the Graduate School

(Original signatures are on file with official student records.)

Adsorption of Antimony by Birnessite and the Impact of Antimony on
the Electrostatic Surface Properties of Variable-Charge Soil Minerals

A Thesis Presented for the
Master of Science
Degree
The University of Tennessee, Knoxville

Kalyn Alaine Vergeer
May 2013

Acknowledgements

This thesis would not have been possible without the immense knowledge, and patience of my Major Professor, Dr. Michael Essington. I am grateful for your assistance and support throughout this entire process. I would also like to thank my committee members Dr. Jaehoon Lee and Dr. Phillip Jardine for their willingness to lend their expertise and insight to this project.

I also owe special thanks to Jeffrey Conner who kept me grounded and managed put up with all my shit.

To my parents, Bob and Janice, who motivated me more than I could have ever imagined, thank you for showing me what hard work looks like.

And finally, to my older siblings, who have continually challenged me to prove myself, I am now more educated than all of you.

Dedication

I dedicate this Masters Thesis to my grandparents, Donald and Elinor Rasmussen.

Abstract

Antimony (Sb) is a toxin that can be found in high concentrations in the soil due to anthropogenic sources. Antimony exists in soil as Sb(V) in the monovalent antimonate hydroxyanion. The adsorption mechanisms of Sb(V) are not well-characterized. The objective of this study was to further elucidate Sb(V) adsorption mechanisms by examining the impact of adsorption on surface charging characteristics of gibbsite, goethite, birnessite, and kaolinite. Also examined was Sb(V), SO₄ [sulfate], and PO₄ [phosphate] adsorption by birnessite.

Electrophoretic mobility and potentiometric titrations were employed to examine the ζ -potential and net proton surface charge density as a function of pH and ionic strength, and in the presence or absence of adsorbed Sb(V), phosphate, or sulfate. Competitive batch adsorption studies were performed to examine Sb(V), SO₄, and PO₄ adsorption as a function of pH, ionic strength, and competitive environment. Results suggest that Sb(V) participates in inner-sphere adsorption by gibbsite, goethite, and kaolinite in acidic conditions, PO₄ participates in inner-sphere adsorption by gibbsite, goethite and kaolinite in the pH range studied, and that SO₄ participates in inner- and outer-sphere adsorption by gibbsite, goethite, and kaolinite with the former mechanisms becoming more important in acidic conditions. Adsorption of Sb(V) and PO₄ by birnessite had little impact on the surface charge characteristics indicating outer-sphere adsorption. Batch adsorption edge studies showed Sb(V) and PO₄ retention to be dependent on pH and ionic strength, supporting electrostatic adsorption mechanisms. Batch adsorption studies showed SO₄ was not adsorbed by birnessite in the pH 3 to 11 range. The adsorption data was modeled using FITEQL 4.0 and the diffuse layer model (DLM). The DLM adequately described Sb(V) and PO₄ adsorption by birnessite using electrostatic surface complexes.

Table of Contents

Chapter	Page
I. Introduction	1
II. Electrostatic Properties of Variable Charge Minerals as Influenced by the Adsorption of Inorganic Ligands	6
Materials and Methods	14
Results and Discussion	18
Summary	26
III. Competitive Adsorption of Inorganic Ligands onto Birnessite: Effects of pH and Ionic Strength	28
Materials and Methods	34
Results and Discussion	39
Summary	43
IV. Conclusions	45
Appendix	48
References	102
VITA	114

List of Tables

Table	Page
1. Mineral specific surface area, the point of zero charge (pH_{PZC}), and isoelectric point (IEP) of minerals used in this study.	49
2. Diffuse layer model parameters used to develop chemical models of $\text{Sb}(\text{OH})_6$ and PO_4 adsorption by birnessite.	50
3. Conditional formation constants for aqueous species and surface complexation reactions used to model $\text{Sb}(\text{OH})_6$, and PO_4 adsorption by birnessite in 10 mM KNO_3 and 100 mM KNO_3 .	51
4. Birnessite surface complexation reactions and associated FITEQL-optimized intrinsic equilibrium constants in 10 mM KNO_3 and 100 mM KNO_3 .	52
5. Goodness-of-fit parameters (WSOS/DF) for ligand adsorption to birnessite.	53

List of Figures

Figure	Page
1. X-ray diffraction profile (powder mount) of alumina-hydrate SF-4 (gibbsite).	54
2. X-ray diffraction profile (powder mount) of Fe-OOH solid precipitated using the procedure of Schwertmann et al. (2000).	55
3. X-ray diffraction profile (powder mount) of MnO ₂ prepared using the procedure of Cole et al. (1947) and McKenzie (1971).	56
4. X-ray diffraction profile (powder mount) of kaolinite (KGa-1B).	57
5. The influence of nitrate (NO ₃) and sulfate (SO ₄) on the ζ-potential (mV) of gibbsite as a function of pH, and counterion type and concentration (ionic strength).	58
6. The influence of nitrate (NO ₃) and sulfate (SO ₄) on proton adsorption (Q _h , mmol _c kg ⁻¹) by gibbsite as a function of pH, and counterion type and concentration (ionic strength).	59
7. The influence of nitrate (NO ₃) and phosphate (PO ₄) on the ζ-potential (mV) of gibbsite as a function of pH, and counterion type and concentration (ionic strength).	60
8. The influence of nitrate (NO ₃) and phosphate (PO ₄) on proton adsorption (Q _h , mmol _c kg ⁻¹) by gibbsite as a function of pH, and counterion type and concentration (ionic strength).	61
9. The influence of nitrate (NO ₃) and antimonate (Sb(OH) ₆) on the ζ-potential (mV) of gibbsite as a function of pH, and counterion type and concentration (ionic strength).	62
10. The influence of nitrate (NO ₃) and antimonate (Sb(OH) ₆) on proton adsorption (Q _h , mmol _c kg ⁻¹) by gibbsite as a function of pH, and counterion type and concentration (ionic strength).	63

- 11.** The influence of nitrate (NO_3) and sulfate (SO_4) on the ζ -potential (mV) of goethite as a function of pH, and counterion type and concentration (ionic strength). 64
- 12.** The influence of nitrate (NO_3) and sulfate (SO_4) on proton adsorption (Q_h , $\text{mmol}_c \text{kg}^{-1}$) by goethite as a function of pH, and counterion type and concentration (ionic strength). 65
- 13.** The influence of nitrate (NO_3) and phosphate (PO_4) on the ζ -potential (mV) of goethite as a function of pH, and counterion type and concentration (ionic strength). 66
- 14.** The influence of nitrate (NO_3) and phosphate (PO_4) on proton adsorption (Q_h , $\text{mmol}_c \text{kg}^{-1}$) by goethite as a function of pH, and counterion type and concentration (ionic strength). 67
- 15.** The influence of nitrate (NO_3) and antimonate ($\text{Sb}(\text{OH})_6$) on the ζ -potential (mV) of goethite as a function of pH, and counterion type and concentration (ionic strength). 68
- 16.** The influence of nitrate (NO_3) and antimonate ($\text{Sb}(\text{OH})_6$) on proton adsorption (Q_h , $\text{mmol}_c \text{kg}^{-1}$) by goethite as a function of pH, and counterion type and concentration (ionic strength). 69
- 17.** The influence of nitrate (NO_3) on the ζ -potential (mV) of birnessite as a function of pH and counterion concentration (ionic strength). 70
- 18.** The influence of nitrate (NO_3) and sulfate (SO_4) on proton adsorption (Q_h , $\text{mmol}_c \text{kg}^{-1}$) by birnessite as a function of pH, and counterion type and concentration (ionic strength). 71
- 19.** The influence of nitrate (NO_3) and sulfate (SO_4) on the ζ -potential (mV) of birnessite as a function of pH, and counterion type and concentration (ionic strength). 72
- 20.** The influence of nitrate (NO_3) and phosphate (PO_4) on the ζ -potential (mV) of birnessite as a function of pH, and counterion type and concentration (ionic strength). 73

- 21.** The influence of nitrate (NO_3) and phosphate (PO_4) on proton adsorption (Q_h , $\text{mmol}_c \text{ kg}^{-1}$) by birnessite as a function of pH, and counterion type and concentration (ionic strength). 74
- 22.** The influence of nitrate (NO_3) and antimonate ($\text{Sb}(\text{OH})_6$) on the ζ -potential (mV) of birnessite as a function of pH, and counterion type and concentration (ionic strength). 75
- 23.** The influence of nitrate (NO_3) and antimonate ($\text{Sb}(\text{OH})_6$) on proton adsorption (Q_h , $\text{mmol}_c \text{ kg}^{-1}$) by birnessite as a function of pH, and counterion type and concentration (ionic strength). 76
- 24.** The influence of nitrate (NO_3) on the ζ -potential (mV) of kaolinite as a function of pH, and concentration (ionic strength). 77
- 25.** The influence of nitrate (NO_3) and sulfate (SO_4) on proton adsorption (Q_h , $\text{mmol}_c \text{ kg}^{-1}$) by kaolinite as a function of pH, and counterion type and concentration (ionic strength). 78
- 26.** The influence of nitrate (NO_3) and sulfate (SO_4) on the ζ -potential (mV) of kaolinite as a function of pH, and counterion type and concentration (ionic strength). 79
- 27.** The influence of nitrate (NO_3) and phosphate (PO_4) on the ζ -potential (mV) of kaolinite as a function of pH, and counterion type and concentration (ionic strength). 80
- 28.** The influence of nitrate (NO_3) and phosphate (PO_4) on proton adsorption (Q_h , $\text{mmol}_c \text{ kg}^{-1}$) by kaolinite as a function of pH, and counterion type and concentration (ionic strength). 81
- 29.** The influence of nitrate (NO_3) and antimonate ($\text{Sb}(\text{OH})_6$) on the ζ -potential (mV) of kaolinite as a function of pH, and counterion type and concentration (ionic strength). 82
- 30.** The influence of nitrate (NO_3) and antimonate ($\text{Sb}(\text{OH})_6$) on proton adsorption (Q_h , $\text{mmol}_c \text{ kg}^{-1}$) by kaolinite as a function of pH, and counterion type and concentration (ionic strength). 83

- 31.** The adsorption of antimonate (Sb(V)), sulfate (SO₄), and phosphate (PO₄) by birnessite in 10 mM KNO₃ as a function of pH. The solid lines represent the diffuse layer model description of the adsorption data. 84
- 32.** The adsorption of antimonate (Sb(V)), sulfate (SO₄), and phosphate (PO₄) by birnessite in 100 mM KNO₃ as a function of pH. The solid lines represent the diffuse layer model description of the adsorption data. 85
- 33.** The influence of sulfate (SO₄) on the adsorption of antimonate (Sb(V)) by birnessite in 10 mM KNO₃ as a function of pH and order of ligand addition. 86
- 34.** The influence of sulfate (SO₄) on the adsorption of antimonate (Sb(V)) by birnessite in 100 mM KNO₃ as a function of pH and order of ligand addition. 87
- 35.** The predicted and experimentally-determined adsorption of antimonate (Sb(V)) and sulfate (SO₄) by birnessite under direct competition in 10 mM KNO₃ as a function of pH. The solid lines represent the diffuse layer model description of the adsorption data. 88
- 36.** The predicted and experimentally-determined adsorption of antimonate (Sb(V)) and sulfate (SO₄) by birnessite under direct competition in 100 mM KNO₃ as a function of pH. The solid lines represent the diffuse layer model description of the adsorption data. 89
- 37.** The predicted and experimentally-determined adsorption of antimonate (Sb(V)) and sulfate (SO₄) by birnessite under indirect competition in 10 mM KNO₃ as a function of pH. The solid lines represent the diffuse layer model description of the adsorption data. 90
- 38.** The predicted and experimentally-determined adsorption of antimonate (Sb(V)) and sulfate (SO₄) by birnessite under indirect competition in 100 mM KNO₃ as a function of pH. The solid lines represent the diffuse layer model description of the adsorption data. 91
- 39.** The predicted and experimentally-determined adsorption of antimonate (Sb(V)) and sulfate (SO₄) by birnessite under indirect competition in 10 mM KNO₃ as a function of pH. The solid lines represent the diffuse layer model description of the adsorption data. 92
- 40.** The predicted and experimentally-determined adsorption of antimonate (Sb(V)) and sulfate (SO₄) by birnessite under indirect competition in 100 mM KNO₃ as a function of pH. The solid lines represent the diffuse layer model description of the adsorption data. 93
- 41.** The influence of phosphate (PO₄) on the adsorption of antimonate (Sb(V)) in 10 mM KNO₃ as a function of pH and order of ligand addition. 94
- 42.** The influence of phosphate (PO₄) on the adsorption of antimonate (Sb(V)) in 100 mM KNO₃ as a function of pH and order of ligand addition. 95

- 43.** The predicted and experimentally-determined adsorption of antimonate (Sb(V)) and phosphate (PO₄) by birnessite under direct competition in 10 mM KNO₃ as a function of pH. The solid lines represent the diffuse layer model description of the adsorption data. 96
- 44.** The predicted and experimentally-determined adsorption of antimonate (Sb(V)) and phosphate (PO₄) by birnessite under direct competition in 100 mM KNO₃ as a function of pH. The solid lines represent the diffuse layer model description of the adsorption data. 97
- 45.** The predicted and experimentally-determined adsorption of antimonate (Sb(V)) and phosphate (PO₄) by birnessite under indirect competition in 10 mM KNO₃ as a function of pH. The solid lines represent the diffuse layer model description of the adsorption data. 98
- 46.** The predicted and experimentally-determined adsorption of antimonate (Sb(V)) and phosphate (PO₄) by birnessite under indirect competition in 100 mM KNO₃ as a function of pH. The solid lines represent the diffuse layer model description of the adsorption data. 99
- 47.** The predicted and experimentally-determined adsorption of antimonate (Sb(V)) and phosphate (PO₄) by birnessite under indirect competition in 10 mM KNO₃ as a function of pH. The solid lines represent the diffuse layer model description of the adsorption data. 100
- 48.** The predicted and experimentally-determined adsorption of antimonate (Sb(V)) and phosphate (PO₄) by birnessite under indirect competition in 100 mM KNO₃ as a function of pH. The solid lines represent the diffuse layer model description of the adsorption data. 101

CHAPTER I

INTRODUCTION

Antimony (Sb) is a potentially toxic metal with no known biological function (Filella et al., 2002; Shtangeeva et al., 2011). The concentration of Sb in uncontaminated soil is generally less than 10 mg kg⁻¹ (Johnson, et al., 2005; Kabata-Pendias et al., 1984; Filella et al., 2002) with a median concentration of 1 mg kg⁻¹ (Arai, 2010). Elevated soil concentrations of Sb, up to and in excess of 5000 mg kg⁻¹ (Arai, 2010), are a result of anthropogenic activities such as mining and smelting. Antimony is also elevated in road side soils due to its use in brake pads, and in shooting range soils where it is a component in lead bullets (Tschan et al., 2010; Filella et al., 2002). Antimony is of concern to regulatory agencies, and it has been identified as a priority pollutant by the US EPA and the European Union (USEPA, 2006; Council of European Union, 1998).

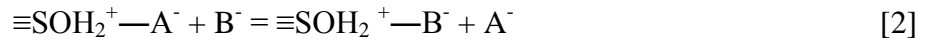
Antimony may exist in several oxidation states (-III, 0, III V). In soil, Sb principally exists as Sb(V) in oxic conditions, and in soil solutions the hydroxide anion Sb(OH)₆⁻ dominates (Okkenhaug, et al., 2011; Bencze, 1994). The aqueous speciation of Sb(V) is controlled by the hydrolysis reaction:



(pK_a = 2.84 at 25°C) (Accornero et al., 2008; Zakaznova-Herzog et al., 2006). Additional aqueous speciation reactions, such as ion pairing with metal cations, or complexation by dissolved soil organic matter, has not been well-characterized. The fate and behavior of metal contaminants in natural systems is regulated by precipitation and adsorption mechanisms.

Proposed mechanisms of retention for $\text{Sb}(\text{OH})_6^-$ include mineral precipitation, ligand exchange, and anion exchange.

Anion and ligand exchange reactions are those that occur on mineral surfaces that develop positive surface charge through isomorphic substitution or the protonation of surface hydroxyl groups. Non-specific (outer-sphere) surface complexation results from electrostatic interactions and occurs when an anion is unable to displace surface H_2O or OH^- , and at least one molecule of water remains between a positive charge surface site and the adsorbed anionic species. Conversely, specific (inner-sphere) surface complexation results in bonds with covalent character and occur when a ligand is able to displace surface H_2O or OH^- , and no water molecules remain between the ligand and the surface coordinating metal ion (Essington, 2003; Karamalidis, 2010). Non-specific, anion exchange reactions at surface hydroxyl functional groups can be described by:



where, A^- and B^- are exchangeable anions and $\equiv\text{S}$ is a surface-exposed metal. Specific, ligand exchange reactions can be described by:



where, L is a ligand with l - charge.

Generally, ligands that participate in outer-sphere complexation are strong acid anions, whose pK_a values are negative (e.g. HSO_4^- , NO_3^- , and Cl^-), while ligands that participate in inner-sphere complexation are weak acid anions, whose pK_a values lie between 0 and 14 (e.g. AsO_4 and PO_4) (Essington, 2003).

The fate and behavior of contaminants in the environment is strongly influenced by surface reactive mineral phases in soil. Metal oxide (Al, Fe, Mn) surfaces consist of variable charge (amphoteric) hydroxyl groups; these exhibit increasing negative charge with increasing pH and increasing positive charge with decreasing pH (Kampf et al, 2012). The metal oxide minerals have important environmental implications because they are able to adsorb metal and ligand ions from soil solution (Dixon et al., 2002; Kampf et al, 2012). Toxic metals that are specifically adsorbed are not likely to become phytoavailable, bioaccessible, or mobile.

Numerous surface-reactive minerals exist in soil. Gibbsite is present in all soil, and is particularly ubiquitous in highly weathered soils, weathered volcanic ash, and moderately acidic soils (e.g., Oxisols, Andisols, and Ultisols). Goethite is also widespread in nature, occurring in almost every soil type and climatic region (Schwertmann et al., 2000). Birnessite is a hydrous manganese oxide and a common form of mineralized manganese in redoximorphic soil (McKenzie, 1971). Kaolinite is possibly the most ubiquitous non-swelling aluminosilicate mineral in soil (Dixon, 1989). All these minerals are responsible for ligand retention in soil; thus they are important regulators of contaminant transport.

The adsorption of Sb(V) by metal oxide and aluminosilicate minerals has received limited attention. However, studies suggest that adsorption proceeds through an inner-sphere mechanism (Eq. [3]), particularly in acidic environments. Adsorption studies on Al and Fe (oxy)hydroxides show that the greatest retention of Sb(V) occurs when solution pH is less than 5, with retention decreasing with increasing pH (Rakshit et al., 2011; Leuz et al., 2006; Tighe et al., 2005). Similarly, McComb et al (2007) showed increasing inner-sphere retention of Sb(V) by goethite with decreasing pH using Attenuated Total Reflectance-Infrared (ATR-IR) spectroscopy. Ambe et al. (1986) showed strong adsorption of Sb(V) on hematite below pH 7,

with the percentage of adsorbed Sb(V) decreasing rapidly with increasing pH above pH 7.

Scheinost et al. (2006) showed inner-sphere retention of Sb(V) using Extended X-ray Adsorption Fine Structure (EXAFS) spectroscopy on shooting range soils. Ilgen et al. (2012) showed Sb(V) participating in inner-sphere mechanism on gibbsite and kaolinite using EXAFS spectroscopy. Xi et al. (2009) showed Sb(V) retention by kaolinite was greatest at pH 3.6, and decreased with increasing pH. Wang et al. (2012) showed Sb(V) adsorption by magnetite was unaffected by ionic strength, and decreased with increasing pH suggesting inner-sphere adsorption mechanisms.

The adsorption of phosphate and sulfate by metal oxide and aluminosilicate minerals has been well characterized. In a comprehensive study by Goldberg (1984) phosphate was shown to participate in specific adsorption by various Al and Fe oxide minerals as a function of pH. Balistrieri et al. (1990) showed phosphate adsorption by iron oxide and manganese oxide to increase with decreasing pH. Su and Harsh (1993) examined phosphate and sulfate adsorption mechanisms by amorphous aluminosilicates using electrophoretic mobility studies and suggested phosphate was participating in specific adsorption while sulfate was participating in nonspecific adsorption. He et al. (1997) examined phosphate and sulfate adsorption as a function of pH and ionic strength and concluded that phosphate participates in inner-sphere adsorption while sulfate participates in outer-sphere adsorption mechanisms on kaolinite and γ -Al₂O₃. Juang et al. (2002) examined sulfate adsorption by goethite using electrophoretic mobility and concluded that sulfate participated in an outer-sphere adsorption mechanism. Tripathy et al. (2001) found sulfate to participate in outer-sphere adsorption on hydrous manganese oxide in the pH 2.5 to 9 range.

Phosphate and sulfate adsorption mechanisms on metal oxides and aluminosilicates are well established, the former participates in specific adsorption mechanisms while the latter

predominantly participates in nonspecific adsorption. Antimony(V) adsorption studies by metal oxides and aluminosilicates are limited. Even though literature is beginning to illuminate how Sb(V) is retained, further evidence is needed to establish a comprehensive understanding of antimony's interactions with common soil constituents. Further, elucidating the retention mechanisms for Sb(V) by metal oxides will allow for informed predictions about transport and bioavailability, and aid in the promulgation of regulations, *in-situ* remediation strategies, and environmental management programs (Erdemoglu, 2006; Tserenpil et al., 2011; Arai, 2010).

In this study, the influence of Sb(OH)_6^- , $\text{H}_2\text{PO}_4^-/\text{HPO}_4^{2-}$, and SO_4^{2-} adsorption on the surface charge properties of gibbsite, goethite, birnessite, and kaolinite as a function of pH and ionic environment were examined using electrophoretic mobility and potentiometric titration studies. These studies provide the evidence to identify ligand adsorption mechanisms. The adsorption of Sb(OH)_6^- , $\text{H}_2\text{PO}_4^-/\text{HPO}_4^{2-}$, and SO_4^{2-} , by birnessite was also examined using batch adsorption studies as a function of pH, ionic strength, and competitive ligand environment. The competitive effects of phosphate and sulfate on antimony adsorption lend further evidence for prediction of antimony behavior in the presence of competing ligands (Essington, 2011).

CHAPTER II

ELECTROSTATIC PROPERTIES OF VARIABLE CHARGE MINERALS AS INFLUENCED BY ADSORPTION OF INORGANIC LIGANDS

Antimony (Sb) is a potentially toxic metal with no known biological function (Filella et al., 2002; Shtangeeva et al., 2011). The concentration of Sb in uncontaminated soil is generally less than 10 mg kg⁻¹ (Johnson, et al., 2005; Kabata-Pendias et al., 1984; Filella et al., 2002) with a median concentration of 1 mg kg⁻¹ (Arai, 2010). Elevated soil concentrations of Sb, up to and in excess of 5000 mg kg⁻¹ (Arai, 2010), are a result of anthropogenic activities such as mining and smelting. Antimony is also elevated in road side soils due to its use in brake pads, and in shooting ranges where it is a component in lead bullets (Tschan et al., 2010; Filella et al., 2002). Antimony is of concern to regulatory agencies, and it has been identified as a priority pollutant by the US EPA and the European Union (USEPA, 2006; Council of European Union, 1998).

Antimony may exist in several oxidation states (-III, 0, III V). In soil, Sb principally exists as Sb(V) in oxic conditions, and in soil solutions the hydroxycyanion Sb(OH)₆⁻ dominates (Okkenhaug, et al., 2011; Bencze, 1994). The aqueous speciation of Sb(V) is controlled by the hydrolysis reaction:

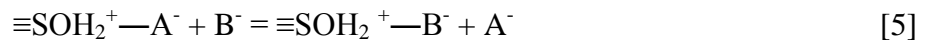


(pK_a = 2.84 at 25°C) (Accornero et al., 2008; Zakaznova-Herzog et al., 2006). Additional aqueous speciation reactions, such as ion pairing with metal cations, or complexation by dissolved soil organic matter, has not been well-characterized.

The fate and behavior of metal contaminants in natural systems is regulated by precipitation and adsorption mechanisms. Proposed mechanisms of retention for Sb(OH)₆⁻

include mineral precipitation, ligand exchange, and anion exchange. Precipitation of Sb(V) minerals such as $\text{Pb}[\text{Sb}(\text{OH})_6]_2$ or $\text{Ca}[\text{Sb}(\text{OH})_6]_2$ have been proposed. However, these precipitates are unstable compared to adsorbed forms of Sb(V) and there is no evidence of precipitation in soils, even in high contaminated environments (Johnson et al., 2005).

Anion and ligand exchange reactions are those that occur on mineral surfaces that develop positive surface charge through isomorphous substitution or the protonation of surface hydroxyl groups. Non-specific (outer-sphere) surface complexation results from electrostatic interactions and occurs when an anion is unable to displace surface H_2O or OH^- , and at least one molecule of water remains between a positive charge surface site and the adsorbed anionic species. Conversely, specific (inner-sphere) surface complexation results in bonds with covalent character and occur when a ligand is able to displace surface H_2O or OH^- , and no water molecules remain between the ligand and the surface coordinating metal ion (Essington, 2003; Journey, 2008; Karamalidis, 2010). Non-specific, anion exchange reactions at surface hydroxyl functional groups can be described by:



where, A^- and B^- are exchangeable anions and $\equiv\text{S}$ is a surface-exposed metal. Specific, ligand exchange reactions can be described by:



where, L is a ligand with l - charge.

Generally, ligands that participate in outer-sphere complexation are strong acid anions, whose pK_a values are negative (e.g. HSO_4^- , NO_3^- , and Cl^-) while ligands that participate in inner-sphere complexation are weak acid anions, whose pK_a values lie between 0 and 14 (e.g. AsO_4 ,

and PO_4) (Essington, 2003; Anderson, 2006). Adsorption mechanisms of phosphate and sulfate have been well established. Phosphate participates in specific adsorption on hydrous metal oxides and aluminosilicates; conversely, sulfate has been shown to participate in predominantly nonspecific adsorption on hydrous oxides and aluminosilicates (Ali et al., 1996; Goldberg, 1984; He et al., 1997; Anderson, 2006; Violante et al., 2002; Balistrieri, 1999; Su, 1993; Tripathy et al., 2001; Juang et al., 2002). Recent literature suggests that Sb(V) may participate in specific adsorption with gibbsite, goethite, manganite, and kaolinite (Rakshit, et al., 2011; Martinez-Llado et al., 2008; Wang et al. 2012; Ilgen et al., 2012).

Metal oxides and layer silicates are two major soil constituents that bear reactive surface functional groups. Oxides of aluminum, iron, and manganese have variable charge surfaces. Kaolinite also bears variable charge functional groups. Gibbsite, Al(OH)_3 , is an aluminum hydroxide that is ubiquitous in soil, particularly in highly weathered soils, weathered volcanic ash, and moderately acidic soils (e.g., Oxisols, Andisols, and Ultisols). Gibbsite consists of stacked dioctahedral sheets of Al(OH)_3 that are held together by hydrogen bonds. Surface hydroxyls on the planar surface and half of the hydroxyls on the edge surface are doubly-coordinated by two Al^{3+} atoms and bear neutral charge. Conversely, half of the hydroxyls on the sheet edges are singly-coordinated with one Al^{3+} atom and are not charge-satisfied. These edge hydroxyls will be predominantly undercoordinated ($\equiv\text{Al-OH}^{-0.5}$) when the solution $\text{pH} > \text{pH}_{\text{PZC}}$. As solution pH decreases, the extent of undercoordinated surface hydroxyls will decrease in relation to the extent of protonated hydroxyls ($\equiv\text{Al-OH}_2^{+0.5}$). The pH_{PZC} is the pH at which the surface bears neutral net charge, meaning the proportion of undercoordinated surface hydroxyls and protonated surface hydroxyls is equal.

Goethite is a hydrous iron oxide that is widespread in nature, occurring in almost every soil type and climatic region (Schwertmann et al., 2000). Goethite consists of chains of edge-sharing Fe^{III} octahedral that are bound to adjacent chains by hydrogen bonding and sharing polyhedron corners. The surface charge of goethite is primarily independent of structural charge, unless significant isomorphous substitution is occurring for Fe^{III} for a lower valency cation. Doubly-coordinated hydroxyls are charge satisfied ($\equiv\text{Fe}_2\text{—OH}^0$). Singly- coordinated and triply-coordinated hydroxyls are primarily negatively charged when $\text{pH} > \text{pH}_{\text{PZC}}$ ($\equiv\text{Fe—OH}^{-0.5}$, $\equiv\text{Fe}_3\text{—O}^{-0.5}$), and primarily positive charged when $\text{pH} < \text{pH}_{\text{PZC}}$ ($\equiv\text{Fe—OH}_2^{+0.5}$, $\equiv\text{Fe}_3\text{—OH}^{+0.5}$).

Birnessite, MnO_2 , is a hydrous manganese oxide and common form of mineralized manganese in redoximorphic soil (McKenzie, 1971). Birnessite, a phyllo-manganate, consists of layer structures of edge linked Mn octahedral that are connected to adjacent layers by water and exchangeable cations. Birnessite has permanent structural charge from vacancies in the layer structure or from the substitution of Mn^{III} for Mn^{IV} . This structural charge is satisfied by exchangeable cations. Considered inert is the doubly coordinated hydroxyl $\equiv\text{Mn}^{\text{III}}_2\text{—OH}^0$, which is charge satisfied. Negative variable surface charge arises from the singly-coordinated and doubly-coordinated hydroxyls ($\equiv\text{Mn}^{\text{IV}}\text{—OH}^{-1.33}$, $\equiv\text{Mn}^{\text{IV}}\text{—OH}^{-0.33}$, $\equiv\text{Mn}_2^{\text{III}}\text{—O}^{-0.5}$, and $\equiv\text{Mn}^{\text{IV}}_2\text{—O}^{-0.33}$). In strongly acidic environments $\equiv\text{Mn}^{\text{IV}}_2\text{—OH}_2^{+0.67}$ and $\equiv\text{Mn}^{\text{IV}}\text{—OH}_2^{+0.67}$ may exist. The undercoordinated surface hydroxyls lend to predominantly negative surface charge when $\text{pH} > \text{pH}_{\text{PZC}}$.

Kaolinite, $\text{Al}_2\text{Si}_2\text{O}_5(\text{OH})_4$, is possibly the most ubiquitous non-swelling aluminosilicate mineral in soil (Dixon, 1989). Kaolinite consists of 1:1 layered ratio of tetrahedral and octahedral sheets that are held together with hydrogen bonding. The hydrogen bonded interlayer lends much stability to the mineral. The protonation and deprotonation of $\equiv\text{Si—OH}$ and $\equiv\text{Al—OH}$

groups, along with minor amounts of Al^{3+} for Si^{4+} isomorphic substitution, creates surface charge. Singly-coordinated edge hydroxyls will have predominantly negative charge when $\text{pH} > \text{pH}_{\text{PZC}}$ ($\equiv\text{Al}-\text{OH}^{-0.5}$ and $\equiv\text{Si}-\text{O}^-$) and predominately positive charge when $\text{pH} < \text{pH}_{\text{PZC}}$ ($\equiv\text{Al}-\text{OH}^{+0.5}$) (Jiang et al., 2009). Doubly coordinated $\equiv\text{Al}_2-\text{OH}^0$ and $\equiv\text{Si}_2-\text{O}^0$ are considered to be inert, along with the $\begin{matrix} \equiv\text{Si} \\ \equiv\text{Al}_2 \end{matrix} > \text{O}^0$ surface group.

Charge on a mineral has influence beyond its surface into the bulk solution. This region between the mineral surface and the bulk solution is called the solid-solution interface, and consists of various layers of charge density (Essington, 2003). The total net surface charge on a particle (σ_p) is:

$$\sigma_p = \sigma_s + \sigma_H + \sigma_{is} + \sigma_{os} = -\sigma_d \quad [7]$$

where σ_s is the permanent structural charge, σ_H is the proton surface charge resulting from the specific adsorption of proton and hydroxyl ions, σ_{is} is the inner-sphere charge resulting from specific ion adsorption, σ_{os} is the outer-sphere charge resulting from non-specific ion adsorption, and σ_d is the counterion diffuse swarm charge that exactly balances σ_p (Goldberg et al., 2010). Ligands that participate in adsorption in the σ_{is} plane will affect surface charging characteristics that are measureable by electrokinetic and potentiometric analysis. Conversely, ions that participate in adsorption in the σ_{os} plane will affect these methods of analysis.

Ligand adsorption mechanisms, outer- vs. inner-sphere complexation, may be directly determined through electrokinetic experiments, and indirectly by potentiometric titrations. Electrokinetic experiments measure the electric double layer potential at the shear plane between the solid and the bulk solution. This electric potential is known as the zeta potential (ζ). The ζ -potential is assumed to be approximate to the diffuse double layer potential (Goldberg et al.,

2012). To measure the ζ -potential, the movement of a suspended charged particle is tracked under an applied electric field. The mobility of the particle is measured as electrophoretic mobility, which is related to ζ by the Smoluchowski equation (Hunter, 1989):

$$\mu_E = \frac{\epsilon\zeta}{\eta} \quad [8]$$

where μ_E is the electrophoretic mobility (microns sec^{-1} per volt cm^{-1}), ϵ is the dielectric constant of solution, ζ is the zeta potential (mV), and η is the viscosity of the suspending liquid (poises). The electrophoretic mobility of a particle within an indifferent electrolyte will reflect the surface charge created by proton adsorption and desorption on mineral surface functional groups. When a ligand other than the indifferent electrolyte is present, electrophoretic mobility will reflect the adsorption mechanism. Adsorption of a ligand in the σ_{is} plane will decrease μ_E , while adsorption of a ligand in the σ_{os} plane will not affect μ_E , relative to the indifferent electrolyte. The electrophoretic mobility may be used to predict adsorption mechanisms because the influence a ligand adsorbed in the σ_{is} plane affects the intrinsic surface charge of a mineral. Conversely, a ligand adsorbed in the σ_{os} plane is relatively mobile. The electrophoretic mobility of a particle is also influenced by ionic strength. Increased concentrations of electrolyte in the σ_d plane tend to shield the particle charge, decreasing the extent of charge influence in the solid-solution interface and decrease the response within an electric field (Yu, 1997).

Potentiometric titrations may be employed to indirectly characterize ligand adsorption mechanisms. Potentiometric titrations measure variation in σ_H , as a function of pH, by quantifying protonation and deprotonation reactions on surface functional groups. Variations in σ_H are determined by measuring proton concentration without the solid (blank) and measuring proton concentration when the solid is present, the difference is considered adsorbed proton per

mass of solid, in $\text{mmol}_c \text{ kg}^{-1}$. To accurately relate blank $[\text{H}^+]$ to suspension $[\text{H}^+]$, a standard curve must be developed to relate the total proton hydrogen concentration (TOTP) to pH:

$$\text{TOTP} = [\text{H}^+] - [\text{OH}^-] = f(10^{-\text{pH}} - 10^{-(14-\text{pH})}) \quad [9]$$

where $[\text{H}^+]$ is the free proton and $[\text{OH}^-]$ is the free hydroxide concentrations. The concentration of adsorbed proton is computed by subtracting the blank from the titration data:

$$Q_h = \left[c_A - c_B - ([\text{H}^+] - [\text{OH}^-]) \right] \times \frac{V}{m_s} \quad [10]$$

where Q_h is adsorbed proton in $\text{mmol}_c \text{ kg}^{-1}$, c_A is the concentration of strong acid added to the suspension, c_B is the concentration of strong base added, V is the suspension volume in L, and m_s is the mass of solid in kg. When a ligand is present (in addition to the background electrolyte), proton adsorption will reflect the ligand adsorption mechanism. Adsorption of a ligand in the σ_{is} plane will increase Q_h in response to the addition of intrinsic negative surface charge, while adsorption of a ligand in the σ_{os} plane will not have an effect on Q_h . Potentiometric titrations are used to indirectly measure adsorption because the initial protonation status of surface functional groups is unknown (Sposito, 2004), only changes in Q_h are quantified. Nonspecific adsorption of a ligand, occurring in the σ_{os} plane will not influence the σ_H plane, and will not cause a shift in Q_h . Conversely, specific adsorption of a ligand in the σ_{is} plane will displace water and hydroxyl ions on surface functional groups influencing the σ_H plane. Further, the influence a negatively charged ligand extends into the solid-solution interface, from its point of adsorption, requiring additional protons to satisfy the charge, thus increasing Q_h (Sposito, 1989).

Electrophoretic mobility and potentiometric titrations provide the evidence necessary to identify ligand adsorption mechanisms. In addition to variations in μ_E and Q_h , points of zero

charge (pH_{PZC}) and common intersection points (CIP) of potentiometric titration curves obtained under differing ionic strength conditions also indicate surface charging characteristics. When the electrophoretic mobility of a particle is zero, this is the point of zero charge: the pH at which the concentrations of negative and positive functional groups on a mineral surface are equal (Goldberg, 2012). When determined by electrophoretic mobility, the point of zero charge is known as the isoelectric point (Appel et al., 2003; Sposito, 1989). Ligand adsorption occurring in the σ_{is} plane will decrease the number of positive surface sites, shifting the pH_{PZC} to lower values (Goldberg and Kabenji, 2010). In a potentiometric titration, a common intersection point will occur when proton adsorption curves of varying ionic strength cross at a common pH. When the electrolytes are indifferent, the CIP is point of zero salt effect (pH_{PZSE}) and is equal to the pH_{PZC} (Avena et al., 1998; Appel et al., 2003). However, when the specific adsorption of a ligand occurs, the point of zero salt effect is not equal to the pH_{PZC} (Sposito, 2004).

Adsorption of phosphate by goethite and aluminum oxides has been shown to decrease electrophoretic mobility supporting inner-sphere complexation mechanisms (Antelo et al., 2005; Del Nero et al., 2010; Arai et al., 2001; Celi et al., 2000). Goldberg (2010) showed phosphate and sulfate adsorption by gibbsite to shift pH_{PZC} to lower values, and decrease electrophoretic mobility throughout the pH range examined. Juang (2002) found sulfate adsorption by goethite to decrease electrophoretic mobility, but not shift the pH_{PZC} . Su and Harsh (1993) examined phosphate and sulfate adsorption mechanisms by amorphous aluminosilicates using electrophoretic mobility studies and suggested that phosphate was participating in specific adsorption while sulfate was participating in nonspecific adsorption.

The influence of $\text{Sb}(\text{OH})_6^-$ adsorption on the gibbsite, goethite, birnessite, and kaolinite surface charge properties as a function of pH and ionic environment were examined using

electrophoretic mobility studies and potentiometric titrations. Similarly, the impact of PO₄ and SO₄ adsorption of the surface charge of these solids was examined. The adsorption characteristics of PO₄ and SO₄ are well-established, and their impact on electrophoretic mobility and proton adsorption is also well-known (Anderson, 2006; Essington, 2003; He et al, 1997; Juang et al., 2002).

MATERIALS AND METHODS

Preparation of Solids

All chemicals used in the preparation and pretreatment of the solids were reagent-grade or better. Gibbsite (Al(OH)₃), alumina hydrate SF-4, was obtained from Alcan Chemicals (Beachwood, OH). The gibbsite was pretreated according to Sarkar et al. (1999). Briefly, 30-g of gibbsite was placed in a 250-ml centrifuge bottle, with 150-ml of 10 mM NaOH. The bottle was vortexed and then placed on the platform shaker for 30 min to remove poorly crystalline Al(OH)₃. The gibbsite is then repeatedly washed with Type-1 (18-MΩ) water, and centrifuged until a supernatant of pH 7 was obtained. The solid was stored in 1 mM KNO₃ suspension at ambient temperature (20-22°C).

Goethite (FeOOH) was synthesized using the method of Schwertmann et al. (2000). A 1.0 M Fe(NO₃)₃ solution was created by dissolving anhydrous (Fe(NO₃)₃) in Type-1 water. A 100-mL volume of 1.0 M Fe(NO₃)₃ solution was placed in a 2-L polyethylene flask. A 180-mL volume of 5 M KOH was rapidly added with vigorous stirring, yielding a red-brown precipitate. The solution was then quickly diluted to a 2-L volume using Type-1 water to quench the reaction. The flask was sealed and placed in a 70°C oven for 60 h. The precipitate was then washed and centrifuged with 1 mM HCl until pH 5, then with 1 mM KNO₃ until all traces of

chloride ion were removed (determined by a silver nitrate test). The solid was stored in 1 mM KNO₃ suspension at ambient temperature (20-22°C).

Birnessite (MnO₂) was synthesized using the method of Cole et al. (1947) as modified by McKenzie (1971). A 1.0 M KMnO₄ solution was created with solid KMnO₄. The solution was brought to a boil. To this was slowly added 165-mL of 12.1 M HCl. The suspension was boiled for an additional 10 min following the HCl addition. The resulting precipitate was washed and centrifuged with 1 mM HCl until pH 5 was obtained. The resulting solid was then washed and centrifuged with 1 mM KNO₃ until all traces of chloride ion were removed as determined by a silver nitrate test. The solid was then stored in 1 mM KNO₃ suspension at ambient temperature (20-22°C).

Kaolinite (Al₂Si₂O₅(OH)₄), KGa-1B, was obtained from the Clay Minerals Society (West Lafayette, IN). The kaolinite was treated according to the procedure of Mattigod et al. (1985). The kaolinite was suspended in Type-1 water and dispersed in a blender for 20 min. The pH of the suspension was adjusted to 9.5 using 100 mM NaOH, and the <20 μm fraction was collected by Stokes' Law. The <20 μm kaolinite suspension was placed in 250-ml centrifuge bottles. The solid was then centrifuge-washed ten times with Type-1 water to remove excess salts. The solid was stored in 1 mM KNO₃ suspension at ambient temperature (20-22°C).

The solids were characterized using x-ray diffraction. Gibbsite and kaolinite were found to be without detectable impurities (Figs. 1 and 2). Goethite and birnessite (Fig. 3 and 4) were found to be poorly-crystalline. Surface area measurements were performed using the BET N₂ adsorption isotherm method and a SA 3100 Surface Area Analyzer (Beckman Coulter, Brea, CA). The specific surface area of the mineral precipitates is presented in Table 1.

Preparation of Solutions

All swamping electrolytes were prepared using CO₂-free Type 1 water. Both 10 mM and 100 mM KNO₃ solutions were prepared using solid potassium nitrate; 10 mM KSb(OH)₆ was prepared using solid hexahydroxoantimonate; 10 mM K₂SO₄ was prepared using solid potassium sulfate; 1 mM and 10 mM KH₂PO₄ were prepared using solid potassium phosphate. Adjustments of pH were made using either 10 mM, 100 mM, 500 mM, or 1 M KOH or HNO₃. All reagents were analytical grade or better.

Electrokinetic Mobility

Surface charging characteristics of gibbsite, goethite, birnessite, and kaolinite in various swamping electrolytes was determined by microelectrophoresis using Zeta-Meter System 4.0 (Zeta Meter, Staunton, VA). The suspensions for testing were prepared in 50-ml polypropylene tubes. After a volume of mineral suspension (gibbsite, goethite, birnessite or kaolinite) was placed in the tubes, they were placed in a N₂-filled glove box to ensure a CO₂-free environment. A volume of a swamping electrolyte was added to each tube to yield a solid-to-solution ratio of 0.2 g L⁻¹ for gibbsite and kaolinite, and 0.15 g L⁻¹ for goethite and birnessite. The suspension pH was adjusted in each tube individually with HNO₃ or KOH in order to achieve a pH range between 3.5 and 10. The tubes were removed from the glove box and shaken for 24 h to reach equilibrium at ambient temperature (20°C to 22°C). The tubes were placed back into the CO₂-free, N₂ environment for pH determinations using a calibrated (pH 4, 7, and 10 buffers) combination pH electrode. Suspensions were then manually loaded into a GT-2 electrophoresis cell according to the Zeta-Meter 4.0 operating instructions. A minimum of 10 particles were tracked across a single scale of division for each suspension. An average ζ-potential (mV)

reading was recorded for each suspension. The Zeta-Meter 4.0 unit automatically calculated the zeta potential in millivolts for aqueous systems using the Smoluchowski equation Eq. [8]. Zeta potential was then plotted as a function of pH. The impact of antimonate, sulfate, and phosphate on ζ -potential was determined by varying the swamping background electrolyte compositions to include KSb(OH)_6 , K_2SO_4 , and KH_2PO_4 . The swamping electrolytes used are as follows: 10 mM KNO_3 ; 100 mM KNO_3 ; 10 mM KSb(OH)_6 ; 10 mM K_2SO_4 ; 10 mM KH_2PO_4 ; 10 mM KNO_3 with 10 mM KSb(OH)_6 ; 10 mM KNO_3 with 10 mM K_2SO_4 ; 10 mM KNO_3 with 10 mM KH_2PO_4 ; 100 mM KNO_3 with 10 mM KSb(OH)_6 ; 100 mM KNO_3 with 10 mM K_2SO_4 ; and 100 mM KNO_3 with 10 mM KH_2PO_4 .

Potentiometric Titrations

The surface charging characteristics of gibbsite, goethite, birnessite, and kaolinite were determined via potentiometric titrations. The titrations were conducted using a batch method in 50-ml polypropylene tubes. After a volume of mineral suspension (gibbsite, goethite, birnessite or kaolinite) was placed in the tubes, they were moved into a N_2 -filled glove box to ensure a CO_2 -free environment. A volume of a swamping electrolyte was added to each tube to yield a solid-to-solution ratio of 10 g L^{-1} for gibbsite and kaolinite, and 5 g L^{-1} for goethite and birnessite. The suspension pH was adjusted in each tube individually with HNO_3 or KOH in order to achieve a pH range between 3.5 and 10. Blank tubes were prepared without solid under otherwise identical conditions. All tubes were capped, removed from the glove box, and placed on a platform shaker for a 2 h equilibration at ambient temperature (20°C to 22°C). The solid and solution phases were then separated by centrifugation and the tubes were placed back into the CO_2 -free, N_2 environment for pH determinations. Mineral and blank pH was determined using a calibrated (pH 4, 7, and 10 buffers) combination pH electrode.

The impact of antimonate, sulfate, and phosphate on proton adsorption was determined by varying the swamping background electrolyte compositions to include KSb(OH)_6 , K_2SO_4 , and KH_2PO_4 . The swamping electrolytes used were identical to the electrophoretic mobility studies with the addition of: 10 mM KNO_3 with 1 mM KH_2PO_4 ; and 100 mM KNO_3 with 1 mM KH_2PO_4 . All potentiometric titrations were performed as described above.

Analysis of Potentiometric Titration Results

CoStat 6.0 software (Monterey, CA) was used for analysis of titration data. A standard curve was developed to relate the pH of the blanks to the total hydrogen concentrations Eq. [9]. The concentration of adsorbed proton (Q_h) was computed by subtracting the fitted blank from the titration data Eq. [10]. Adsorbed proton was plotted as a function of pH. Titration curves of gibbsite and goethite were shifted to match zero proton adsorption to pH_{PZC} found in electrophoretic mobility studies. Birnessite titrations were not adjusted, as birnessite gave no pH_{PZC} , and kaolinite titrations did not require shifting, the IEP was equivalent to the pH_{PZC} given by potentiometric titrations.

RESULTS AND DISCUSSION

Gibbsite

Electrophoretic mobility studies reveal a pH_{PZC} of 10.5 for gibbsite in indifferent electrolyte (KNO_3) (Fig. 5). This finding is slightly higher than reported values in Karamalidis and Dzombak (2011) (Table 1). Below the pH_{PZC} , gibbsite mobility is decreased with 100 mM KNO_3 compared to 10 mM KNO_3 due to the screening effect of counterions (Adekola et al., 2011). Conversely, potentiometric titrations of gibbsite in 10 mM KNO_3 and 100 mM KNO_3 show only a negligible influence of ionic strength on Q_h (Fig. 6). Jodin et al. (2005) and

Rosenqvist et al. (2002) found large variations in Q_h for gibbsite as a function of ionic strength. However, Adekola et al. (2011) and Yang et al. (2007) found only small differences in Q_h as a function of ionic strength.

In the presence of both NO_3 and SO_4 , the IEP of gibbsite is similar to that determined in the presence of NO_3 alone. However, the ζ -potential of gibbsite shifts to lower values as pH decreases below approximately 10, relative to the NO_3 systems. In the presence of SO_4 only, the pH_{PZC} shifts to the 7.6 to 9.6 range (Fig. 5). This may be due to colloid instability when the ζ -potential is less than ± 10 mV (Zeta-Meter 4.0). Little variation exists in the ζ -potentials between the 10 mM KNO_3 + 10 mM K_2SO_4 and 100 mM KNO_3 + 10 mM K_2SO_4 systems throughout the pH range studied. The influence of sulfate on Q_h supports the μ_e findings (Fig. 6). At pH values greater than 7, Q_h is not affected by the background electrolyte. However, at pH values less than 7, the Q_h of the SO_4 systems is greater than that of the NO_3 systems. This indicates that sulfate is participating in predominantly outer-sphere adsorption in $\text{pH} > 7$ systems and that increasing inner-sphere adsorption occurs with decreasing pH below 7 (resulting in greater proton adsorption). This is consistent with literature, which indicates the inner-sphere complexation of SO_4 by gibbsite in acidic systems (Goldberg, 2010; Essington, 2011).

The ζ -potential of gibbsite under the influence of phosphate (PO_4) is decreased throughout the entire pH range studied relative to the NO_3 systems. Further, PO_4 adsorption shifted the pH_{PZC} from 10.5 to 4.8 (Fig. 7). Above pH 4.8, ζ -potential of phosphate with 100 mM KNO_3 is less negative than phosphate and phosphate with 10 mM KNO_3 due to counterion shielding (Yu, 1997). The influence of phosphate on Q_h supports the μ_e findings (Fig. 8). The increased proton adsorption throughout the entire pH range studied, relative to the NO_3 systems,

indicates that phosphate is mainly participating in inner-sphere adsorption mechanisms, a finding that is consistent with the literature (Goldberg, 2010; Essington, 2011).

The ζ -potential of gibbsite under the influence of antimonate ($\text{Sb}(\text{OH})_6$) is decreased throughout the entire pH range studied relative to the NO_3 systems (Fig 9). Similar to PO_4 , the ζ -potential of $\text{Sb}(\text{OH})_6$ with 100 mM KNO_3 is less negative compared to the lower ionic strength systems. However, unlike the ζ -potentials of gibbsite with PO_4 , the presence of $\text{Sb}(\text{OH})_6$ does not increase the ζ -potentials to positive values with decreasing pH (no pH_{PZC}). Indeed, the ζ -potentials tend to become even more negative in strongly acidic systems. The potentiometric titration results support those of the electrophoretic mobility studies, showing an increase in Q_h throughout the entire pH range (Fig. 10). These results suggest $\text{Sb}(\text{OH})_6$ is participating in specific adsorption on the gibbsite surface, similar to PO_4 .

Goethite

Electrophoretic mobility studies reveal a pH_{PZC} of 9.8 for goethite in indifferent electrolyte (KNO_3) (Fig. 11). This finding is within the reported values of Kosmulski (2009) (Table 1). Below the pH_{PZC} , goethite mobility is decreased in 100 mM KNO_3 compared to that in 10 mM KNO_3 due to counterion shielding. The potentiometric titration results show that Q_h is influenced by ionic strength (10 mM KNO_3 and 100 mM KNO_3) (Fig. 12). The Q_h results are consistent with those of other studies (Shuai et al., 2009; Boily et al., 2001).

The ζ -potential of goethite in the presence of sulfate (SO_4) alone is generally negative for all pH values studied. This is also the case for the 10 mM KNO_3 + 10 mM K_2SO_4 systems (Fig. 11). However, the ζ -potential of goethite with 100 mM KNO_3 and 10 mM K_2SO_4 shifts from negative to positive values as pH decreases below 9.3 (Fig.11). The pH_{PZC} is similar to that

observed in the NO_3 systems. The influence of sulfate on Q_h is similar to that observed for the NO_3 systems (Fig.12). However, when NO_3 and SO_4 are present in combination, there is an upward shift in Q_h at pH values less than 7. The results from electrophoretic mobility and potentiometric titration studies suggest that sulfate adsorption by goethite is primarily outer-sphere in alkaline systems, with increasing inner-sphere character in neutral to acidic systems. Juang et al.(2002) suggested that sulfate adsorption to goethite was electrostatic, but the bonding was strong enough to decrease particle mobility. However, numerous other studies have clearly established this inner-sphere complexation of sulfate by goethite in acidic systems. Using Fourier Transformed Infrared (FTIR) spectroscopy, Hug (1997) confirmed the monodentate complexation of SO_4 by goethite in pH 3 and 5 suspensions. Similarly, Peak et al. (1999) showed that SO_4 was retained by outer-sphere mechanisms by goethite in $\text{pH} > 6$ systems, and by inner- and outer-sphere adsorption mechanisms in $\text{pH} < 6$ suspensions. Rietra et al. (1999) successfully modeled the adsorption edge of SO_4 by goethite by considering only inner-sphere complexation.

The ζ -potential of goethite under the influence of phosphate (PO_4) is negative throughout the entire pH range studied, becoming less negative with decreasing pH (Fig. 13). Due to the large variability in the data, the ζ -potentials are not influenced by ionic strength, although the 100 mM KNO_3 + 10 mM PO_4 system tends to generate more positive ζ -potential values than the 10 mM PO_4 and 10 mM KNO_3 + 10 mM PO_4 systems consistent with the shielding effect. The influence of phosphate on Q_h (Fig. 14) is highly variable, relative to the NO_3 systems. Proton adsorption on goethite under the influence of phosphate is not strongly influenced by ionic strength. The electrophoretic mobility studies suggest the specific adsorption of phosphate; however, proton adsorption results are inconclusive. Li et al. (2000) suggested that the surface precipitation of phosphate on goethite may contribute more acidic functional groups to the

goethite surface via proton adsorption. They also reported that the ζ -potentials of goethite were similar in the presence of absence of PO_4 when up to 3 mmol g^{-1} phosphate was present in solution. With higher PO_4 loadings, the ζ -potentials were similar to that found for strengite. The maximum phosphate in solution for the potentiometric titrations was 2 mmol g^{-1} , and 66 mmol g^{-1} for electrophoretic mobility. Analysis of stability indices of iron phosphate in the presence of goethite using Visual MINTEQ 3.0 shows that both the ζ -potential and Q_h solutions are supersaturated with respect to $\text{FePO}_4 \cdot 2\text{H}_2\text{O}(\text{s})$ when $\text{pH} < 5.5$. The phosphate precipitation may impact the Q_h and ζ -potential results.

The ζ -potential of goethite with adsorbed $\text{Sb}(\text{OH})_6$ is negative throughout the entire pH range studied (Fig. 15). The influence of $\text{Sb}(\text{OH})_6$ adsorption on Q_h (Fig. 16) is inconsistent with the ζ -potential findings. Above pH 8, Q_h is greater than that in the NO_3 systems. However, below pH 9, Q_h is erratic. The proton adsorption curve of $\text{Sb}(\text{OH})_6$ with 10 mM and 100 mM KNO_3 are similar to that of the indifferent electrolyte when $\text{pH} < 7$. When $\text{Sb}(\text{OH})_6$ alone is the swamping electrolyte, Q_h is positive when $\text{pH} > 4.5$, then decreases precipitously when $\text{pH} < 4.5$. The Q_h curves of $\text{Sb}(\text{OH})_6$ adsorption by goethite do not provide a clear picture of adsorption mechanisms. Further, they do not support the ζ -potential results. Electrophoretic mobility studies suggest $\text{Sb}(\text{OH})_6$ is participating in specific adsorption at the goethite surface. This is supported by Essington (2011) who reported $\text{Sb}(\text{OH})_6$ adsorption by goethite occurs through ligand exchange at all pH values, and McComb et al. (2007) who found the specific adsorption of $\text{Sb}(\text{OH})_6$ on iron oxides to increase with decreasing pH using ATR-IR spectroscopy

Birnessite

Electrophoretic mobility studies reveal no pH_{PZC} by birnessite in indifferent electrolyte (KNO_3) within the pH range studied (Fig. 17). This finding is consistent with reported pH_{PZC} values from Kosmulski (2009), which range between 1.8 and 2.8 (Table 1). The ζ -potentials for the 100 mM KNO_3 system are less negative than those of the 10 mM KNO_3 system due to counterion shielding effect. The ζ -potential values for the NO_3 suspensions are relatively constant as a function of pH, averaging -28 mV in 10 mM KNO_3 and -21 mV in 100 mM KNO_3 . Further, potentiometric titrations of birnessite show less negative Q_h values in 10 mM KNO_3 compared to 100 mM KNO_3 (Fig. 18). Extrapolation of Q_h data indicates a pH_{PZC} of approximately 3 for birnessite.

The ζ -potential of birnessite in all SO_4 systems is negative at all pH values (Fig. 19). The ζ -potentials of the 10 mM SO_4 and 10 mM KNO_3 + 10 mM SO_4 are similar and do not vary consistently with pH. The average ζ -potential of 10 mM SO_4 is -30 mV, while that of 10 mM KNO_3 + 10 mM SO_4 is -29 mV. These average values are similar to that of the 10 mM KNO_3 suspensions (-28 mV). The ζ -potentials of birnessite in 100 mM KNO_3 + 10 mM SO_4 averages -17 mV, which is less negative than the 100 mM KNO_3 suspension (-21 mV). Similar to the ζ -potential findings, SO_4 did not influence Q_h relative to the NO_3 systems (Fig. 18). These results suggest SO_4 is participating in outer-sphere adsorption at the birnessite surface.

The ζ -potential of birnessite, under the influence of phosphate (PO_4), is negative throughout the pH range studies (Fig. 20). The ζ -potentials in the 10 mM PO_4 and the 10 mM KNO_3 + 10 mM PO_4 are similar, with the former averaging -32mV and the later -29 mV. The ζ -potentials of birnessite with 100 mM KNO_3 + 10 mM PO_4 are more positive than the 10 mM PO_4

and the 10 mM KNO₃ + 10 mM PO₄ suspensions, averaging -20 mV (Fig. 20). The ζ -potentials for the PO₄ suspensions are similar to those of the SO₄ suspensions. The Q_h results indicate PO₄ is not impacting the intrinsic surface charge of birnessite, as the Q_h data for these systems are similar to those with NO₃ alone (Fig. 21). Electrophoretic mobility and potentiometric titration results suggest phosphate is participating in outer-sphere adsorption at the birnessite surface.

The ζ -potential of birnessite under the influence of Sb(OH)₆ is negative throughout the pH range studied (Fig. 22). The ζ -potential of birnessite when Sb(OH)₆ is the swamping electrolyte is generally invariant with pH, averaging -34 mV. The ζ -potentials of birnessite suspensions with 10 mM Sb(OH)₆ + 100 mM KNO₃ are more positive (averaging -21 mV) compared to 10 mM Sb(OH)₆ + 10 mM KNO₃ (averaging -30 mV). The influence of Sb(OH)₆ on Q_h as a function of pH (Fig. 23) are also similar to the 10 mM and 100 mM KNO₃ suspensions. The electrophoretic mobility and potentiometric titration results suggest that Sb(OH)₆ may participate in outer-sphere adsorption mechanisms at the birnessite surface.

Kaolinite

Electrophoretic mobility studies reveal a pH_{PZC} 4.5 for kaolinite in 10 mM KNO₃ and 6.5 in 100 mM KNO₃ (Fig. 24). The pH_{PZC} of kaolinite in 10 mM KNO₃ is consistent with reported values in Kosmulski (2009) (Table 1). Variations in pH_{PZC} as a function of ionic strength have been reported in the literature (Chassange et al., 2009; Kosmulski and Dahlsten, 2006) who concluded that ζ -potentials of kaolinite are ionic strength and salt specific. Kosmulski (2012) states that the inert character of 1 to 1 indifferent electrolytes with respect to metal oxides is well documented, and the effect of the nature and concentration of electrolyte on the pH_{PZC} is insignificant, however due to literature discrepancies of reported pH_{PZC} values of variable charge

minerals (other than metal oxides), the assumption of indifference by 1-1 electrolytes by these minerals may not be correct. Therefore, specific interactions of K^+ with kaolinite may explain the increase in pH_{PZC} with increasing K^+ concentration. Potentiometric titrations of kaolinite in 10 mM KNO_3 and 100 mM KNO_3 are similar throughout pH range studied (Fig. 25) a result of the low surface reactivity of kaolinite, similar to that of gibbsite.

The ζ -potential of kaolinite under the influence of SO_4 is negative throughout the pH range studied (Fig. 26). Further, the ζ -potential values for the SO_4 suspensions deviate (become more negative) from the values in the NO_3 suspensions as pH decreases below approximately 7. The influence of SO_4 on Q_h is consistent with the ζ -potential findings (Fig. 25). The Q_h values increase in the presence of SO_4 , relative to NO_3 , as solution pH decreases below approximately 5. These results suggest that SO_4 is participating in predominantly outer-sphere adsorption in pH > 7 suspensions due to lack of influence on Q_h and ζ -potential measurements relative to the NO_3 suspensions. The retention of SO_4 in pH < 7 suspensions appears to have greater inner-sphere character, as indicated by an upward shift in Q_h and a downward shift in the ζ -potentials, relative to the NO_3 systems. This is consistent with Essington (2011) who found sulfate adsorption by kaolinite to be hysteretic at low pH, but inconsistent with He et al. (1997) who proposed sulfate adsorption by kaolinite to be primarily outer-sphere.

The ζ -potential of kaolinite, under the influence of PO_4 is negative throughout the pH range studied (Fig. 27). The ζ -potentials of 10 mM PO_4 suspensions (with and without 10 mM KNO_3) are similar, and that of the 100 mM KNO_3 + 10 mM PO_4 is more positive. The ζ -potentials of all PO_4 systems are more negative than the NO_3 systems. These results suggest PO_4 is participating in inner-sphere adsorption surface complexation, which is consistent with Essington (2011), as well as He et al. (1997). The influence of PO_4 on Q_h does not appear to

suggest inner-sphere complexation (Fig. 28). Proton adsorption results for kaolinite under the influence of PO_4 generally do not differ from the NO_3 suspensions. These finding may be a result of the low surface reactivity of kaolinite.

The ζ -potential of kaolinite suspensions with $\text{Sb}(\text{OH})_6$ show a clear deviation from that with NO_3 (Fig. 29). The strongly alkaline conditions, the ζ -potential of $\text{Sb}(\text{OH})_6$ suspensions is similar to that of the NO_3 suspensions; however with decreasing pH the ζ -potentials of the Sb systems do not increase. Similar to SO_4 and PO_4 , the ζ -potential of $\text{Sb}(\text{OH})_6$ suspensions with 100 mM KNO_3 is less negative compared to $\text{Sb}(\text{OH})_6$ alone and $\text{Sb}(\text{OH})_6$ with 10 mM KNO_3 as a result of counterion shielding. The potentiometric titration results indicate that $\text{Sb}(\text{OH})_6$ adsorption is generating negative surface charge, particularly as pH decreases below approximately 7 (Fig. 30). These results suggest $\text{Sb}(\text{OH})_6$ adsorption by kaolinite displays inner-sphere complexation character, particularly in acidic pH environments.

SUMMARY

The impact of NO_3 , $\text{Sb}(\text{OH})_6$, SO_4 , and PO_4 on surface charging characteristics of variable-charge minerals were examined using electrophoretic mobility and proton adsorption analyses. Antimony (V) was found to participate in inner-sphere surface complexation reactions on gibbsite, goethite, and kaolinite. Adsorption $\text{Sb}(\text{OH})_6$ by birnessite, however, did not impact the surface charging relative to an indifferent electrolyte. The ζ -potential and Q_h data suggest that SO_4 participated in both inner- and outer-sphere complexation on gibbsite, goethite, and kaolinite with the former mechanism becoming important in acidic suspensions. Adsorption of SO_4 by birnessite was outer-sphere at all pH values. The adsorption of PO_4 by gibbsite, goethite, and kaolinite displayed strong inner-sphere character throughout the pH range studied. Phosphate

adsorption by birnessite, however, had little impact on surface charging characteristics compared to the indifferent electrolyte, indicating that PO_4 retention by birnessite proceeds through an outer-sphere mechanism. Elucidating the retention mechanisms of Sb(V) , a toxic substance, by common soil components lends important information concerning mobility and bioaccessibility. Given its ability to adsorb specifically to gibbsite, goethite, and kaolinite, Sb(V) could potentially be immobilized in the soil with the use of soil amendments and other remediation strategies involving these minerals, particularly in acidic environments.

CHAPTER III

COMPETITIVE ADSORPTION OF INORGANIC LIGANDS ONTO BIRNESSITE: EFFECTS OF PH AND IONIC STRENGTH

Antimony (Sb) is a metalloid that is toxic to most living organisms and has no known biological function (Filella et al., 2002; Shtangeeva et al., 2011). The concentration of Sb in uncontaminated soil is generally less than 10 mg kg^{-1} with a median concentration of 1 mg kg^{-1} (Bowen, 1979; Johnson, et al., 2005; Kabata-Pendias et al., 1984; Filella et al., 2002a).

Antimony is used in a number of industrial applications. It is a component in flame retardants, semiconductors, brake pads, and it is used as a metal hardening agent. Elevated soil concentrations of Sb are generally a result of anthropogenic activities such as mining and smelter, along road side soils due to its prevalence in brake pads, and in shooting range soils where it is a component of lead ammunition (Tschan et al., 2010; Filella et al., 2002). The concentration of Sb in contaminated soil has been reported as high as 5000 mg kg^{-1} . It is estimated that Sb release into the environment has increased at least 10-fold in recent decades (Shtangeeva et al., 2011). Antimony contamination is of concern to regulatory agencies and has been identified as a priority pollutant by the US EPA and the European Union, which have set drinking water guidelines at 6 and $10 \text{ } \mu\text{g L}^{-1}$ (USEPA, 2006; Council of European Union, 1998).

Antimony is a group 15 element on the Periodic Table of Elements. It may exist in several oxidation states (-III, 0, III, V). In nature, Sb principally exists as Sb(V) in oxic (O_2 present) and Sb(III) in anoxic (O_2 absent) environments. In the 3-11 pH range, Sb(III) exists as Sb(OH)_3^0 , while Sb(V) exists as Sb(OH)_6^- (Guo et al., 2009; Filella et al., 2002). In soil solutions, the Sb(OH)_6^- species is more common than the Sb(OH)_3^0 species, although the latter is shown to be more toxic to living organisms and is known to prompt chronic health problems (Okkenhaug,

et al., 2011; Bencze, 1994). The aqueous speciation of Sb(V) is controlled by the hydrolysis reaction:



($\text{pK}_a=2.84$ at 25°C) (Accornero et al., 2008; Zakaznova-Herzog et al., 2006). Therefore, at pH values above 2.84 the hydroxyanion Sb(OH)_6^- predominates in soil solution. Additional aqueous speciation reactions such as ion pairing with metal cations, or complexation by dissolved soil organic matter, has not been well-characterized.

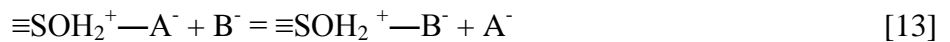
There is growing concern in the environmental fate, behavior and bioaccessibility of Sb due to the increased anthropogenic input into the soil environment (Filella et al., 2002; Filella et al., 2003; Leuz et al, 2006; Lintschinger et al., 1998). Due to the anionic behavior of the predominant Sb(V) redox state (Sb(OH)_6^-), Sb may not be strongly retained by soil. Proposed mechanisms of retention for Sb(OH)_6^- include mineral precipitation, ligand exchange and anion exchange. Precipitation of minerals such as $\text{Pb}[\text{Sb(OH)}_6]_2$ or $\text{Ca}[\text{Sb(OH)}_6]_2$ are possible for Sb(V). However, these precipitates are unstable in soil compared to adsorbed forms of Sb(V) (Johnson et al., 2004). Further, there is no evidence of precipitation in soil affected by elevated Sb levels (Johnson et al., 2004).

Anion and ligand exchange are adsorption reactions that occur on mineral surfaces that have developed positive surface charge through isomorphic substitution or the protonation of surface hydroxyl groups (Essington, 2003; Yu, 1997). Anions and ligands in solution are able to adsorb to surface sites through a combination of both specific and non-specific mechanisms. Non-specific (outer-sphere) exchange reactions occur when an anion is unable to displace surface H_2O and at least one molecule of water remains between surface site and the anionic

species. These anions are exchangeable and are held at the surface by electrostatic interactions. Specific (inner-sphere) complexes are formed when a ligand is able to displace surface H₂O and no water molecules remain between the ligand and the surface metal ion (Essington, 2003; Karamalidis, 2010). These surface complexes display considerable stability due to the covalent bonding character of the ligand-metal surface bond. Specific, inner-sphere exchange reactions can be described through the following ligand exchange:



Non-specific, outer-sphere exchange reactions can be described as anion exchange:



where $\equiv\text{S}$ is a surface-exposed metal, L is a ligand with l - charge, and A^{-} and B^{-} are exchangeable anions. Anion exchange is sensitive to the ionic strength of the soil solution. Thus, anion exchange is influenced by the presence of exchangeable anions, like NO_3^{-} and Cl^{-} . Conversely, the adsorption of ligands retained by inner-sphere mechanism is generally not influenced by ionic strength (Zhang, et al. 1996; Zhang, et al. 2009).

Metal oxides (Al, Fe, Mn) are variable charge soil minerals that exhibit increasing negative charge with increasing pH and increasing positive charge with decreasing pH (Kampf et al., 2012). They have important environmental implications because they have high capacity to adsorb both metals and ligands from soil solution (Dixon et al., 2002; Kampf et al., 2012).

Hydrous manganese (Mn) oxides are surface-reactive and an important sink for metals and ligands. Manganese oxides are most commonly found in soils formed from mafic and ultramafic metamorphic and igneous rocks. Although found in soils of different ages and from different parent materials, hydrous Mn oxides tend to occur in seasonally wet and imperfectly

drained soils (Essington, 2003; Dixon et al. 2002; Post, 1999). Hydrrous manganese oxides, ranging from black to brown in color, exist ubiquitously as fine-grained coatings on surfaces of soils and sediments in low concentrations. Hydrrous Mn oxides have both permanent negative structural charge and pH dependent surface charge (Essington, 2003). Because they have net negative surface charge when the pH is greater than 2, they are important adsorbents of metal ions, even when present in low concentrations (Dixon et al. 2002; McKenzie, 1989; Negra et al. 2005; Tan et al. 2008). Weakly hydrolyzable cations (i.e. Pb, Cu, Mn, Co, Zn, Zr, Ni) and ligands derived from weak acids (i.e. molybdate, phosphate, selenite) have been found to strongly adsorb to Mn oxides, generally in excess of surface charge (Dixon et al., 2002; McKenzie, 1989). Birnessite (MnO_2) is a common Mn oxide (Essington, 2003; Wei et al., 2010). It is a phyllosilicate existing as layered sheets of edge-linked Mn^{4+}O_6 octahedra with substantial isomorphic substitution by Mn^{3+} and numerous cation vacancies; both of which lend a permanent negative structural charge that is satisfied by an interlayer of hydrated exchangeable cations (Dixon et al., 2002; Essington, 2003; Sposito, 2008, Wei et al., 2010).

Adsorption of Sb(V) by metal oxides has recently received considerable attention. Adsorption studies on Al and Fe (oxy)hydroxides show that the greatest retention of Sb(V) occurs when the pH of the system is less than 5, with retention decreasing with increasing pH (Rakshit et al., 2011; Leuz et al., 2006; Tighe et al., 2005). Similarly, McComb et al. (2007), showed increasing inner-sphere retention of Sb(V) with decreasing pH via ATR-IR spectroscopy on goethite. Ambe et al. (1986) showed strong adsorption of Sb(V) on hematite below pH 7, with the percentage adsorbed decreasing rapidly above pH 7. Scheinost et al. (2006) showed inner-sphere retention of Sb(V) via EXAFS spectroscopy on shooting range soils. Rakshit et al. (2011) showed Sb(V) adsorbed strongly to gibbsite, possibly via inner-sphere

adsorption mechanism with the highest adsorption occurring at pH values less than 4. Ilgen (2012) showed that Sb(V) participated in inner-sphere surface complexation on gibbsite and kaolinite using EXAFS spectroscopy. Xi et al. (2009) suggested that Sb(V) may form inner-sphere complexes at low pH on kaolinite surface, and mainly outer-sphere complexes at high pH. Wang et al. (2012) showed inner-sphere adsorption of Sb(V) on synthetic manganite. Despite the growing knowledge of Sb(V) behavior relative to soil minerals, there is a general dearth of knowledge relative to Sb(V) adsorption by manganese oxides. Conversely, SO_4 is known to participate in both inner- and outer-sphere adsorption by metal oxides and PO_4 is known to participate in primarily inner-sphere adsorption by metal oxides, including manganese oxides (Ali et al., 1996; Goldberg, 1984; He et al., 1997; Violante et al., 2002; Su, 1993; Juang et al., 2002; Saeki, 1995; Tripathy et al., 2001; Balistrieri et al., 1990).

To aid in the description of chemical and electrostatic ion retention, surface complexation models (SCM) are commonly employed. SCMs are used to describe adsorption phenomena using an equilibrium approach (Goldberg, 1992). They are based on a balance of surface charge expression. They contain columbic correction factors to account for the effect of surface charge on surface complexation, and explicitly define equilibrium constant expressions for surface complexes. The diffuse layer model (DLM), proposed by Stumm et al. (1970), is a simple surface complexation model frequently used to describe the oxide mineral-aqueous solution interface. Adsorption is based on electrostatic mechanisms, which is consistent with the zeta-potential and proton adsorption findings for Sb(V) retention in Chapter II.

The model does not consider surface complexes with ions in the background electrolyte, and the relationship between surface charge and surface potential is given by the following equation:

$$\sigma_d = \frac{Sa}{F} \text{sgn } \psi_d \left\{ 2\varepsilon_0 DRT \sum_i C_i \left[\exp\left(\frac{-z_i F \psi_d}{RT}\right) - 1 \right] \right\}^{1/2} \quad [14]$$

where σ_d is expressed in C m^{-2} (Coulombs per square meter), S is specific surface area ($\text{m}^2 \text{g}^{-1}$), a is the concentration of solid in aqueous suspension, F is the Faraday constant (C mol^{-1}), ψ_d is the diffuse layer potential in volts, ε_0 is the permittivity of vacuum, D is the dielectric constant of bulk water, R is the gas constant ($\text{J K}^{-1} \text{mol}^{-1}$) T is temperature (K), sgn is the signum function: $\text{sgn } \psi_d = 1$ if $\psi_d > 0$ and $\text{sgn } \psi_d = -1$ if $\psi_d < 0$, and c_i and z_i are the concentration and charge of solutions species i . The application of the DLM requires knowledge of surface parameters of the adsorbent and formation constants for all aqueous species and surface protonation reactions. To apply the DLM to adsorption data, general surface complexation reactions and reactions describing intrinsic equilibrium constants must be defined.

The object of this study was to examine noncompetitive adsorption of Sb(V) , SO_4 , and PO_4 by birnessite as a function of pH and ionic strength. Direct competitive adsorption of Sb(V) , SO_4 , and PO_4 studies were performed, as well as indirect competitive adsorption of Sb(V) and SO_4 , and Sb(V) and PO_4 . The competitive effects of phosphate and sulfate on antimony adsorption will lend further evidence for prediction of Sb(V) behavior in the presence of common soil ligands.

MATERIALS AND METHODS

Preparation of Solutions

All solutions were prepared using CO₂-free Type I water. The 10 mM and 100 mM KNO₃ background electrolytes were prepared using solid potassium nitrate, 10 mM K₂Sb(OH)₆⁻ was prepared using solid hexahydroxoantimonate, 10 mM K₂SO₄ was prepared using solid potassium sulfate, and 10 mM KH₂PO₄ was prepared using solid potassium phosphate.

Adjustments to solution pH were made with HCl or HNO₃. All solids, acids, and bases used were analytical grade or better.

Preparation of Solid

Birnessite (MnO₂) was synthesized using the method of Cole et al. (1947) as modified by McKenzie (1971). A 1.0 M KMnO₄ solution was created with 395.075-g of solid KMnO₄ and 2.5-L Type-I water. The solution was brought to a boil. To this was added, slowly over the course of 15 minutes, 165-mL of 12.1 M HCl. The suspension was boiled for an additional 10 min following the HCl addition. The resulting precipitate was washed by centrifuge washing with 0.001M HCl until pH 5, and then with 1mM KNO₃ until all traces of chloride ion were removed (determined by a silver nitrate test). The solid was suspended in 1mM KNO₃, and stored at ambient temperature. The solid was characterized using x-ray diffraction and found to be birnessite (Fig. 4). Surface area measurements were performed using the BET N₂ adsorption isotherm method and a SA 3100 Surface Area Analyzer (Beckman Coulter, Brea, CA). The specific surface area of birnessite is 46.30 m² g⁻¹.

Antimony (V) Adsorption on Birnessite

Batch adsorption studies were performed to quantify the adsorption of Sb(V) on birnessite as a function of pH and ionic strength. All studies were performed in duplicate, with a blank (no solid) for each pH increment. Birnessite suspensions of 5 g L^{-1} were created in 50-mL polypropylene tubes with 0.125-g solid and 25-mL of either 10 mM or 100 mM KNO_3 . Birnessite suspensions were prepared in an N_2 -filled glove box to insure a CO_2 -free environment. To achieve a pH range between 3.5 and 10, each tube was individually adjusted with HNO_3 or KOH . The tubes were then hand shaken, and allowed to stabilize for 30 min before volumes of ligand were added. Adsorption edge studies were performed in three competitive environments as described below.

Noncompetitive Adsorption

Noncompetitive adsorption studies were performed first by equilibrating solutions of either $\text{Sb}(\text{OH})_6$, SO_4 or PO_4 with the birnessite suspensions. Here, volumes of 10mM $\text{KSb}(\text{OH})_6$, 10mM K_2SO_4 or 10mM KH_2PO_4 were added to each tube of suspended birnessite, to yield an initial concentration of $80 \text{ } \mu\text{mol L}^{-1}$ of ligand. The tubes were then shaken on a platform shaker for 24 h at ambient temperature (20°C to 22°C). Following equilibration, the tubes were placed back into the CO_2 -free, N_2 environment for pH determinations using a calibrated (pH 4, 7, and 10 buffers) combination pH electrode. The supernatant was removed from the tubes and filtered through a $0.20\text{-}\mu\text{m}$ nylon syringe filter (Restek, China) and analyzed by ICP-AES (Spectro, Mahwah, NJ) for total Sb, S, or P.

Direct Competition

Direct competition adsorption studies were performed by introducing birnessite suspensions to solutions containing Sb(V) and SO₄ or Sb(V) and PO₄. In these systems, an initial concentration of 80 μmol L⁻¹ of each ligand was added to each tube of suspended birnessite, simultaneously, followed by a 24 h equilibration at ambient temperature (20°C to 22°C). Following equilibration, the tubes were placed back into the CO₂-free, N₂ environment for pH determinations using a calibrated (pH 4, 7, and 10 buffers) combination pH electrode. The supernatant was removed from the tubes and filtered through a 0.20-μm nylon syringe filter and analyzed by ICP-AES for total Sb, S, or P.

Indirect Competition

Indirect competition adsorption studies were performed by first equilibrating 80 μmol L⁻¹ of Sb(V) solution with suspended birnessite for a 24 h period. Next, 80 μmol L⁻¹ of either SO₄ or PO₄ was added to each tube, and the systems were equilibrated for an additional 24 h period at ambient temperature (20°C to 22°C). Following equilibration, the tubes were placed back into the CO₂-free, N₂ environment for pH determinations using a calibrated (pH 4, 7, and 10 buffers) combination pH electrode. The supernatant was removed from the tubes and filtered through a 0.20-μm nylon syringe filter and analyzed by ICP-AES for total Sb, S, or P.

Indirect competition adsorption studies with preadsorbed SO₄ or PO₄ were similarly performed. In these systems, 80 μmol L⁻¹ of either SO₄ or PO₄ solutions were equilibrated with suspended birnessite for a 24 h period. Next, 80 μmol L⁻¹ of Sb(V) was added to each tube, and the systems were equilibrated for an additional 24 h period at ambient temperature (20°C to 22°C). Following equilibration, the tubes were placed back into the CO₂-free, N₂ environment

for pH determinations using a calibrated (pH 4, 7, and 10 buffers) combination pH electrode. The supernatant was removed from the tubes and filtered through a 0.20- μm nylon syringe filter and analyzed by ICP-AES for total Sb, S, or P.

Adsorption Data Analysis

Initial concentrations of adsorbed ligand (C_{in} , $\mu\text{mol L}^{-1}$) were determined through analysis of the blank systems. Equilibrium concentrations of adsorbed ligand (C_{eq} , mol L^{-1}) were determined through analysis of adsorption suspensions at equilibrium. The concentration of adsorbed ligand (q , $\mu\text{mol kg}^{-1}$) was determined by difference:

$$q = \frac{V(C_{in} - C_{eq})}{m_s} \quad [15]$$

where V is the volume of solution (0.025 L) and m_s is the mass of solid (1.25×10^{-4} kg).

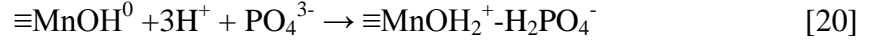
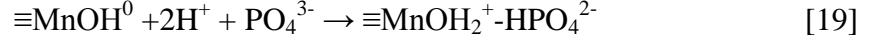
Adsorption edge (q vs pH) plots were constructed for all systems.

Surface Complexation Modeling

FITEQL 4.0 software (Herbelin and Westall, 1999) was used to optimize the adsorption constants for ligand retention using the DLM. FITEQL employs a nonlinear least squares method to determine intrinsic equilibrium constants from experimental data. The model requires values for surface parameters of the adsorbent (Table 2), and formation constants for aqueous species and surface protonation reactions (Table 3).

The application of the DLM to antimonate and phosphate adsorption requires the definitions of the following surface complexation reactions





The intrinsic equilibrium constants for these reactions are defined by the following equations:

$$K_+(int) = \frac{[\equiv\text{MnOH}_2^+]}{[\equiv\text{MnOH}^0](\text{H}^+)} \exp\left(\frac{F\psi_d}{RT}\right) \quad [21]$$

$$K_-(int) = \frac{[\equiv\text{MnO}^-](\text{H}^+)}{[\equiv\text{MnOH}^0]} \exp\left(\frac{-F\psi_d}{RT}\right) \quad [22]$$

$$K_1(int) = \frac{[\equiv\text{MnOH}_2^+ - \text{Sb}(\text{OH})_6^-]}{[\equiv\text{MnOH}^0](\text{Sb}(\text{OH})_6^-)(\text{H}^+)} \exp\left(\frac{F\psi_d}{RT}\right) \quad [23]$$

$$K_2(int) = \frac{[\equiv\text{MnOH}_2^+ - \text{HPO}_4^{2-}]}{[\equiv\text{MnOH}^0](\text{PO}_4^{3-})(\text{H}^+)^2} \exp\left(\frac{F\psi_d}{RT}\right) \quad [24]$$

$$K_3(int) = \frac{[\equiv\text{MnOH}_2^+ - \text{H}_2\text{PO}_4^-]}{[\equiv\text{MnOH}^0](\text{PO}_4^{3-})(\text{H}^+)^3} \exp\left(\frac{F\psi_d}{RT}\right) \quad [25]$$

where R is the molar gas constant, T is the absolute temperature, and square brackets indicate concentrations (mol kg⁻¹), and parentheses indicates activities.

The general mass balance expression for the reactive surface functional group is:

$$S_T = [\equiv\text{MnOH}^0] + [\equiv\text{MnOH}_2^+] + [\equiv\text{MnO}^-] + [\equiv\text{MnOH}_2^+ - \text{Sb}(\text{OH})_6^-] + [\equiv\text{MnOH}_2^+ - \text{HPO}_4^{2-}] + [\equiv\text{MnOH}_2^+ - \text{H}_2\text{PO}_4^-] \quad [26]$$

The charge balance expression for the surface is:

$$\sigma_d = [\equiv\text{MnOH}_2^+] - [\equiv\text{MnO}^-] - [\equiv\text{MnOH}_2^+ \cdot \text{HPO}_4^{2-}] \quad [27]$$

These reactions, the adsorption edge data, and the data from Table 2 and Table 3 allowed FITEQL to optimize intrinsic equilibrium constants for specific adsorption of $\text{Sb}(\text{OH})_6$ and PO_4 by birnessite. A goodness-of-fit parameter is calculated by FITEQL, and indicates the overall variance associated with the model prediction. The parameter is the weighed sums of squares of residuals divided by the degrees of freedom (WSOS/DF). In general, values less than 20 indicate the model adequately describes the experimentally-determined data.

RESULTS AND DISCUSSION

Noncompetitive Adsorption

Antimonate adsorption by birnessite in 10 mM KNO_3 (Fig. 31) and 100 mM KNO_3 (Fig. 32) increases with decreasing pH. Adsorption is at a maximum at pH values below 4 in 10 mM KNO_3 and below pH 6 in 100 mM KNO_3 . FITEQL optimized equilibrium constants are found in Table 4. This adsorption data are well-described by surface speciation results from the DLM (Table 5), which assumes all adsorption is electrostatic. Increased $\text{Sb}(\text{OH})_6$ retention with decreasing pH, suggest adsorption is dependent upon surface charge. This mechanistic interpretation is also in agreement with the ζ -potential and proton adsorption studies presented in Chapter II (Fig. 22 and 23).

The adsorption of SO_4 by birnessite in 10 mM KNO_3 (Fig. 31) and 100 mM KNO_3 (Fig. 32) is less than 5 percent of the amount added throughout the entire pH range studied, regardless

of ionic strength. This is in agreement with surface charge studies of Chapter II which show adsorption of SO_4 to have no influence on ζ -potential and proton adsorption studies.

The adsorption of PO_4 by birnessite is electrostatic, as indicated by the ζ -potential and proton adsorption findings in Chapter II (Fig. 20 and 21), and could be predicted using the DLM (Table 4). Phosphate adsorption is similar to that of $\text{Sb}(\text{OH})_6$, showing increasing adsorption with decreasing pH in both ionic strengths (Fig. 31 and 32). Adsorption maximum occurred at pH 3 (88% of what was added) in 10 mM KNO_3 and pH 4 (99% of what was added) in 100 mM KNO_3 . This data is well-described by surface speciation results from the DLM (Table 5). Phosphate adsorption by birnessite is less than antimonate in acidic media and in 10 mM KNO_3 . Overall, PO_4 retention is greater in 100 mM KNO_3 than 10 mM KNO_3 .

Competitive Adsorption

Competitive adsorption between SO_4 and $\text{Sb}(\text{OH})_6$ in 10 mM KNO_3 shows $\text{Sb}(\text{OH})_6$ retention is not influenced by SO_4 , in any competitive environment, throughout the pH range studied (Fig. 33). Similarly, competition between SO_4 and $\text{Sb}(\text{OH})_6$ in 100 mM KNO_3 shows $\text{Sb}(\text{OH})_6$ is not influenced by SO_4 throughout the entire pH range and regardless of competitive environment (Fig.34). Adsorption of SO_4 in both 10 mM KNO_3 and 100 mM KNO_3 is minimal (Fig. 33 and 34), and this is the reason there was no impact on $\text{Sb}(\text{V})$ retention.

Direct competition between SO_4 and $\text{Sb}(\text{OH})_6$ in 10 mM KNO_3 (Fig. 35) was well-described by the DLM (Table 4 and 5). However, in the 100 mM KNO_3 system (Fig. 36), the DLM poorly described the experimentally-determined adsorption above pH 8, leading to a high WSOS/DF value (Table 5). Maximum $\text{Sb}(\text{OH})_6$ retention occurred at pH 4 (99%) in 10 mM

KNO_3 and pH 4.6 (99%) in 100 mM KNO_3 . Sulfate adsorption was not considered in the model, as adsorption was minimal (Fig. 35 and 36).

Indirect competition (preadsorbed $\text{Sb}(\text{OH})_6$ followed by the addition of SO_4) between SO_4 and $\text{Sb}(\text{OH})_6$ in 10 mM KNO_3 (Fig. 37) was well-described by the DLM (Table 4 and 5). However, in the 100 mM KNO_3 system (Fig. 38), the DLM poorly described the experimentally-determined adsorption above pH 8, leading to a high WSOS/DF value (Table 5). Maximum $\text{Sb}(\text{OH})_6$ retention occurred at pH 3.3 (98%) in 10 mM KNO_3 and pH 4.6 (99%) in 100 mM KNO_3 . Sulfate adsorption was not considered in the model, as adsorption was minimal (Fig. 37 and 38). Similar results were found in the 10 mM KNO_3 and 100 mM KNO_3 systems when SO_4 was preadsorbed to birnessite, and $\text{Sb}(\text{OH})_6$ was added after equilibration (Fig. 39 and 40). The DLM model well-described both ionic strength systems (Table 5), and maximum retention of $\text{Sb}(\text{OH})_6$ occurred at pH 3.6 (98%) in 10 mM KNO_3 and pH 5 (99%) in 100 mM KNO_3 . Sulfate adsorption was not considered in the model, as adsorption was minimal.

Competitive adsorption between PO_4 and $\text{Sb}(\text{OH})_6$ in 10 mM KNO_3 shows phosphate has little impact on antimonate adsorption throughout the entire pH range (Fig. 41). Similar results were found in 100 mM KNO_3 (Fig. 42); antimonate adsorption is not influenced by phosphate in any competitive environment. Antimonate adsorption is influenced by the ionic strength. Direct competition between PO_4 and $\text{Sb}(\text{OH})_6$ in 10 mM KNO_3 shows $\text{Sb}(\text{OH})_6$ retention to be greater than PO_4 throughout the pH range studied (Fig. 43), this was well described by the DLM (Table 5). Noncompetitive $\text{Sb}(\text{OH})_6$ adsorption in 10 mM KNO_3 reached a maximum of 96% at pH 3 (Fig. 31). When in competition with PO_4 , maximum $\text{Sb}(\text{OH})_6$ adsorption decreased slightly to 94% at pH 3 (Fig. 43). Noncompetitive phosphate adsorption in 10 mM KNO_3 reached a maximum of 88% at pH 3 (Fig. 31). When in competition with $\text{Sb}(\text{OH})_6$ maximum PO_4

adsorption decreased to 58% at pH 3 (Fig. 43). In 100 mM KNO₃, Sb(OH)₆ adsorption is greater than PO₄ in acidic conditions (Fig. 44), and was not well-described by the DLM (Table 5).

Noncompetitive Sb(OH)₆ adsorption in 100 mM KNO₃ reached a maximum of 100% below pH 5 (Fig. 32). When in competition with PO₄ maximum adsorption was not affected (Fig. 44).

Noncompetitive phosphate adsorption in 100 mM KNO₃ reached a maximum of 94% at pH 4 (Fig.32). When in competition with Sb(OH)₆ maximum adsorption decreased to 85% at pH 3 (Fig. 43).

Indirect competition (preadsorbed Sb(OH)₆ followed by the addition of PO₄) between PO₄ and Sb(OH)₆ in 10 mM KNO₃ (Fig. 45) was well-described by the DLM (Table 5).

Antimonate reaches maximum adsorption (97%) at pH 3, and PO₄ reaches maximum adsorption (68%) at pH 3. In 100 mM KNO₃ (Fig. 46), indirect competition between Sb(OH)₆ and PO₄ was similar to the direct competition results and was well-described by the DLM (Table 5).

Antimonate adsorption was not influenced by the presence of PO₄, while PO₄ adsorption was decreased in the presence of Sb(OH)₆. For the indirect competition between PO₄ and Sb(OH)₆ in 10 mM KNO₃ with preadsorbed PO₄, the maximum Sb(OH)₆ retention was 95% and that of PO₄ was 71% at pH 3 (Fig. 47). The DLM did not adequately describe the experimentally-determined data (Table 5). The DLM poorly described the data in the 100 mM KNO₃ system (Table 5), where maximum Sb(OH)₆ adsorption reached 98% and maximum PO₄ adsorption was 90% at pH 4 (Fig. 48).

The impact of these ligands on birnessite surface charge (Chapter II) coupled with the ability of the DLM to describe the adsorption data suggest that the Sb(OH)₆ and PO₄ retention mechanisms are electrostatic. When the adsorption mechanism is electrostatic, increased background electrolyte concentration tends to decrease overall adsorption, due to competition

between the background electrolyte and the ligand, known as classical ionic strength effect (Lutzenkirchen, 1997). Ligand (Sb(OH)_6 and PO_4) adsorption by birnessite is affected by changes in ionic strength; however, the affect is not that of the classical ionic strength effect, but a promotive effect. In all studies, the adsorption of ligand (Sb(OH)_6 or PO_4) by birnessite was greater in 100 mM KNO_3 than 10 mM KNO_3 which may accounted for by the promotive effect from increased background electrolyte concentration. Tao (2004) suggested that increasing the ionic strength increases the shielding of the charged surface, thus reducing the repulsion or attraction between ions and charged surfaces. Although Tao (2004) experimentally illustrated this promotive effect using cations, the same theory may be used to explain the increase in Sb(OH)_6 and PO_4 adsorption with increasing ionic strength. Further, Saeki (1995) found an increase in selenite (SeO_3^{2-}) adsorption by manganese oxide with increasing sodium concentration.

SUMMARY

The adsorption of inorganic ligands (Sb(V) , SO_4 , PO_4) by birnessite (MnO_2) was examined as a function of pH, ionic strength, and competitive environment using batch adsorption edge studies. Results show Sb(V) adsorption to be dependent on solution pH, and ionic strength, and relatively independent of competitive environment. Retention of Sb(V) increased with decreasing pH, and was greatest in 100 mM KNO_3 systems. Phosphate adsorption by birnessite was shown to increase with decreasing pH, increase with increasing background electrolyte concentration, and decrease when in competition with Sb(OH)_6 . These results are indicative of electrostatic adsorption, and were successfully modeling using the diffuse layer model. The adsorption of SO_4 by birnessite was minimal, with adsorption never exceeding 10% of the amount added in the pH 3.5 to 10 range. In all competitive environments, PO_4 adsorption

was greatest in 100 mM KNO₃ and was most affected by the presence of Sb(OH)₆ in 10 mM KNO₃. Antimonate was most affected by the presence of PO₄ in direct competition and when PO₄ was preadsorbed by birnessite, although maximum Sb(OH)₆ retention was never below 95% of what was added to the systems. Overall, Sb(OH)₆ retention by birnessite was greater than PO₄. This study provides information for the prediction of Sb(V) transport in soil systems. These findings are supported by Saeki (1995) and Balistieri et al. (1990), who found PO₄ retention on Mn oxides to increase with decreasing pH. Zhang et al. (2009) found SO₄ adsorption by Fe-Mn oxide to have no impact on As(III) adsorption, and Tripathy et al. (2001) found SO₄ to have little impact on surface charging of amorphous Mn oxides relative to the indifferent background electrolyte, and concluded adsorption above the point of zero charge was highly unlikely. Yao et al. (1996) successfully modeled PO₄ adsorption by δ-MnO₂ using outer-sphere surface complexes (e.g., Eq. [19] and [20]) with the triple layer model and found similar log K values, they also concluded the adsorption of SO₄ is not important in pH range 2-8.5.

CHAPTER IV

CONCLUSIONS

Antimony (Sb) is a toxin that can be found in high concentrations in the soil due to anthropogenic input from sources such as mining, and smelting. Elevated soil concentrations, up to and in excess of 5000 mg kg^{-1} , are also the results of Sb deposition from weathering of lead bullets, and wearing of automobile brake pads. Antimony contamination is of concern to both American and European regulatory agencies, yet knowledge of Sb behavior in soil is limited. In oxic and suboxic soil systems, pentavalent antimony (Sb(V)) is predicted to dominate. In a soil system above pH 2.85 antimonate (Sb(OH)_6^-) is the predominant species. Antimonate can participate in ligand exchange, anion exchange, and precipitation. However, it has been suggested that antimonate precipitates are unstable relative to adsorbed forms of Sb(V). Exchange mechanisms (ligand, anion) are those that occur on mineral surfaces bearing positive charge. In soil, metal oxides and layer silicates are two major components that bear reactive surface functional groups, and thus participate in ligand and anion exchange reactions. Ions that participate in anion exchange are electrostatically and weakly bonded to surface functional groups. Species that participate in ligand exchange are strongly bound to surface functional groups, with bonding mechanisms that have covalent character. A species that participates in the latter is less mobile in soils, while the former is more mobile. Establishing ligand retention for a potentially toxic contaminant, such as Sb(V), allows for accurate prediction of mobility and bioaccessibility. Antimony has recently received considerable attention; however, there is still a dearth of knowledge regarding its adsorption behavior in soils.

The objective of this study was to further elucidate Sb(V) adsorption mechanisms by examining the influence of adsorption on the surface charging characteristics of gibbsite,

goethite, birnessite, and kaolinite. To characterize surface charging characteristics in the presence or absence of Sb(V), SO₄, and PO₄ (two common soil ligands) electrophoretic mobility and potentiometric titrations were performed as a function of pH, and background electrolyte concentration (ionic strength). This study also aimed to characterize adsorption of Sb(V), SO₄, and PO₄ by birnessite as a function of pH, background electrolyte concentration, and competitive environment. Examining Sb(V) adsorption in the presence of potentially competing soil ligands (SO₄ or PO₄) assists in understanding antimony behavior in complex soil systems.

To directly characterize the influence of ligand adsorption on surface charge, electrophoretic mobility studies were used. Electrophoretic mobility directly characterizes variations in the net particle charge on a mineral surface, and is expressed as the ζ -potential (mV). To indirectly characterize the influence of ligand adsorption on surface charge, potentiometric titrations studies were performed. Potentiometric titrations, as proton adsorption curves, were used to characterize the adsorption or desorption of surface protons, expressed by Q_h (mmol_c kg⁻¹). Ligand exchange (specific retention) decreases the electrophoretic mobility, and causes an upward shift in proton adsorption. Anion exchange (non-specific adsorption) has less influence on the net particle charge, thus variations in ζ -potentials and Q_h are less apparent.

To quantitatively examine Sb(V), SO₄, and PO₄ adsorption by birnessite, a common Mn oxide, batch competitive adsorption studies were performed, and the subsequent data was modeled using the diffuse layer model (DLM) with FITEQL 4.0. The adsorption edge studies were performed in varying competitive environments and ionic strengths throughout the pH 3.5 to 10 range.

The electrokinetic and proton adsorption results suggest that Sb(V) participates in inner-sphere adsorption by gibbsite, goethite, and kaolinite under acidic conditions. Also, PO₄

participates in inner-sphere adsorption by gibbsite, goethite and kaolinite at all pH values studied, and SO_4 participates predominantly in outer-sphere adsorption by gibbsite, goethite, and kaolinite, with inner-sphere retention becoming important in acidic conditions. Adsorption of Sb(V) , PO_4 , and SO_4 by birnessite had little impact on the surface charge characteristics, indicating that the retention of ligand occurred through outer-sphere adsorption.

The adsorption of Sb(V) and PO_4 by birnessite was pH and ionic strength dependent and was modeled using FITEQL 4.0 and the diffuse layer model (DLM). The DLM adequately described Sb(V) and PO_4 surface complexation using electrostatic surface complexes. The adsorption of Sb(V) and PO_4 by birnessite increased with decreasing pH and increased with increasing background electrolyte concentration. Generally, Sb(V) and PO_4 reached maximum adsorption at pH values less than 4. Sulfate was not adsorbed by birnessite in all systems studied. Antimonate adsorption was not influenced by PO_4 ; however, PO_4 retention was reduced in the presence of Sb(OH)_6 .

This study aimed to elucidate adsorption and adsorption mechanisms of Sb(V) , PO_4 , and SO_4 by four variable charge minerals. The knowledge that Sb(V) is adsorbed by inner-sphere surface complexation mechanisms to gibbsite, goethite, and kaolinite in acidic environments lends valuable information for evaluating Sb(V) bioavailability in soil systems, and may give rise to effective remediation protocol of the toxic contaminant.

APPENDIX

Table 1. Mineral specific surface area obtained from BET N₂ adsorption (Beckman Coulter, Brea, CA), and the observed ranges of point of zero charge (pH_{PZC}) and isoelectric point (IEP) of minerals used in this study (Kosmulski, 2009).

Mineral, Formula	Surface Area m ² g ⁻¹	pH _{PZC} / IEP
Gibbsite, Al(OH) ₃	5.82	7.8-10.4 ^a
Goethite, FeOOH	34.25	6.7-10.2
Birnessite, δ-MnO ₂	46.3	1.8-2.8
Kaolinite, Al ₂ Si ₂ O ₅ (OH) ₄	13.08	2.9-5.0

^a Values obtained from Karamalidis and Dzombak (2010)

Table 2. Diffuse layer model parameters used to develop chemical models of Sb(OH)₆ and PO₄ adsorption by birnessite.

Property	Birnessite
Surface area, m ² g ⁻¹	46.3
Site density, nm ⁻² ^a	6.2
Total surface sites (x 10 ⁻⁴ mol L ⁻¹)	4.77
Suspension density, g L ⁻¹	5

^aGoldberg et al. (2012)

Table 3. Formation constants for aqueous species and surface complexation (protonation) reactions used to model Sb(OH)₆, and PO₄ adsorption by birnessite in 10 mM KNO₃ and 100 mM KNO₃.

Reactions	log K
$\text{H}_2\text{O} \rightarrow \text{H}^+ + \text{OH}^-$	-14.00
$\text{Sb}(\text{OH})_5 + \text{H}_2\text{O} \rightarrow \text{Sb}(\text{OH})_6^- + \text{H}^+$	2.85 ^a
$\text{PO}_4^{3-} + \text{H}^+ \rightarrow \text{HPO}_4^{2-}$	12.35
$\text{PO}_4^{3-} + 2\text{H}^+ \rightarrow \text{H}_2\text{PO}_4^-$	19.55
$\equiv\text{MnOH}^0 \rightarrow \equiv\text{MnO}^- + \text{H}^+$	-7.36 ^b
$\equiv\text{MnOH}^0 + \text{H}^+ \rightarrow \equiv\text{MnOH}^{2+}$	0.16 ^b

Values obtained from Martell et al. (2004) unless noted otherwise, and modified for ionic strength using Davies equation.

^a Accornero et al. (2008)

^b Sahai and Sverjensky (1997)

Table 4. Birnessite surface complexation reactions and associated FITEQL-optimized intrinsic equilibrium constants (log K values) in 10 mM KNO₃ and 100 mM KNO₃.

Reaction	log K	
	10 mM KNO ₃	100 mM KNO ₃
No Competition		
$\equiv\text{MnOH}^{1/3-} + \text{H}^+ + \text{Sb}(\text{OH})_6^- \rightarrow \equiv\text{MnOH}_2^{2/3+} - \text{Sb}(\text{OH})_6^-$	6.19	9.73
$\equiv\text{MnOH}^{1/3-} + 2\text{H}^+ + \text{PO}_4^{3-} \rightarrow \equiv\text{MnOH}_2^{+2/3} - \text{HPO}_4^{2-}$	20.75	22.24
$\equiv\text{MnOH}^{1/3-} + 3\text{H}^+ + \text{PO}_4^{3-} \rightarrow \equiv\text{MnOH}_2^{2/3+} - \text{H}_2\text{PO}_4^-$	25.00	28.26
Direct Competition SO₄		
$\equiv\text{MnOH}^{1/3-} + \text{H}^+ + \text{Sb}(\text{OH})_6^- \rightarrow \equiv\text{MnOH}_2^{2/3+} - \text{Sb}(\text{OH})_6^-$	7.99	9.11
Preadsorbed Sb(OH)₆, SO₄ added		
$\equiv\text{MnOH}^{1/3-} + \text{H}^+ + \text{Sb}(\text{OH})_6^- \rightarrow \equiv\text{MnOH}_2^{2/3+} - \text{Sb}(\text{OH})_6^-$	9.46	9.53
Preadsorbed SO₄, Sb(OH)₆ added		
$\equiv\text{MnOH}^{1/3-} + \text{H}^+ + \text{Sb}(\text{OH})_6^- \rightarrow \equiv\text{MnOH}_2^{2/3+} - \text{Sb}(\text{OH})_6^-$	8.60	9.49
Direct Competition PO₄		
$\equiv\text{MnOH}^{1/3-} + \text{H}^+ + \text{Sb}(\text{OH})_6^- \rightarrow \equiv\text{MnOH}_2^{2/3+} - \text{Sb}(\text{OH})_6^-$	8.04	9.42
$\equiv\text{MnOH}^{1/3-} + 2\text{H}^+ + \text{PO}_4^{3-} \rightarrow \equiv\text{MnOH}_2^{+2/3} - \text{HPO}_4^{2-}$	19.90	21.37
$\equiv\text{MnOH}^{1/3-} + 3\text{H}^+ + \text{PO}_4^{3-} \rightarrow \equiv\text{MnOH}_2^{2/3+} - \text{H}_2\text{PO}_4^-$	26.01	27.20
Preadsorbed Sb(OH)₆, PO₄ added		
$\equiv\text{MnOH}^{1/3-} + \text{H}^+ + \text{Sb}(\text{OH})_6^- \rightarrow \equiv\text{MnOH}_2^{2/3+} - \text{Sb}(\text{OH})_6^-$	8.59	9.60
$\equiv\text{MnOH}^{1/3-} + 2\text{H}^+ + \text{PO}_4^{3-} \rightarrow \equiv\text{MnOH}_2^{+2/3} - \text{HPO}_4^{2-}$	20.47	21.33
$\equiv\text{MnOH}^{1/3-} + 3\text{H}^+ + \text{PO}_4^{3-} \rightarrow \equiv\text{MnOH}_2^{2/3+} - \text{H}_2\text{PO}_4^-$	25.72	27.41
Preadsorbed PO₄, Sb(OH)₆ added		
$\equiv\text{MnOH}^{1/3-} + \text{H}^+ + \text{Sb}(\text{OH})_6^- \rightarrow \equiv\text{MnOH}_2^{2/3+} - \text{Sb}(\text{OH})_6^-$	8.44	9.59
$\equiv\text{MnOH}^{1/3-} + 2\text{H}^+ + \text{PO}_4^{3-} \rightarrow \equiv\text{MnOH}_2^{+2/3} - \text{HPO}_4^{2-}$	20.26	21.41
$\equiv\text{MnOH}^{1/3-} + 3\text{H}^+ + \text{PO}_4^{3-} \rightarrow \equiv\text{MnOH}_2^{2/3+} - \text{H}_2\text{PO}_4^-$	26.53	27.77

Table 5. Goodness-of-fit parameters (WSOS/DF) for ligand adsorption to birnessite.

Competitive Environment	WSOS/DF	
	10 mM KNO ₃	100 mM KNO ₃
No Competition	10.83	18.79
Sb(OH) ₆ and SO ₄ Direct Competition	12.79	45.51
Preadsorbed Sb(OH) ₆ , SO ₄ added	6.93	39.18
Preadsorbed SO ₄ , Sb(OH) ₆ added	7.11	13.84
Sb(OH) ₆ and PO ₄ Direct Competition	10.72	20.11
Preadsorbed Sb(OH) ₆ , PO ₄ added	14.2	14.67
Preadsorbed PO ₄ , Sb(OH) ₆ added	25.55	16.86

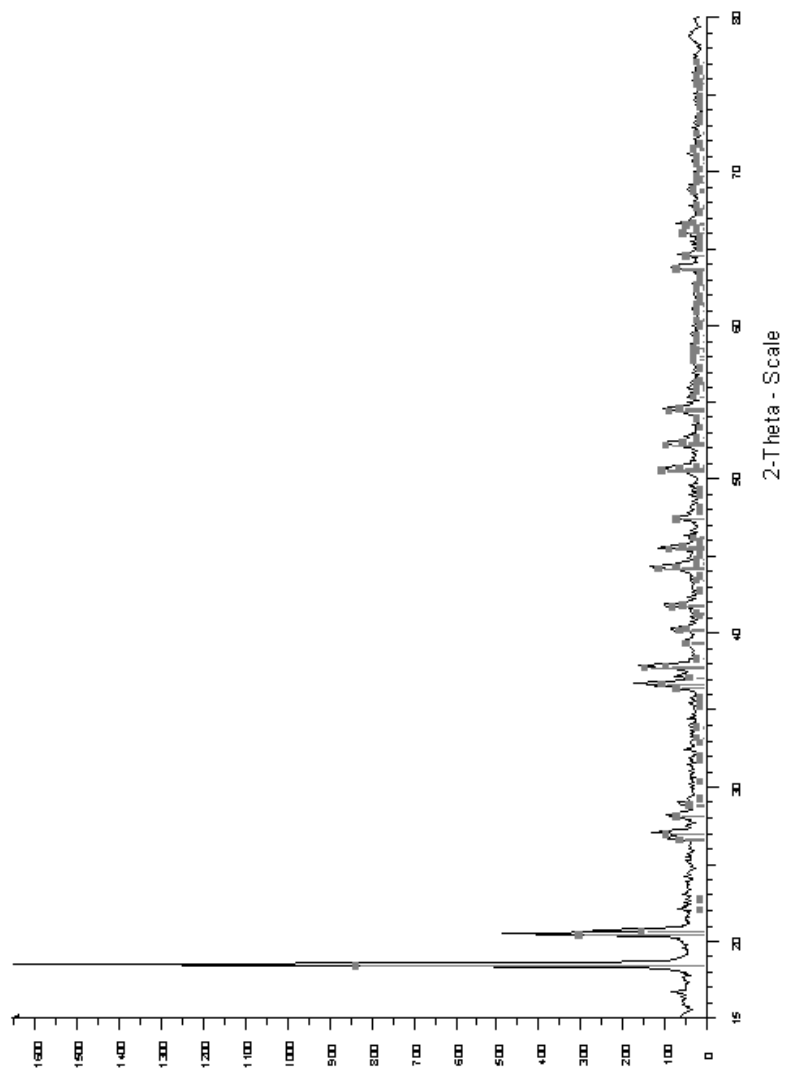


Figure 1. X-ray diffraction profile (powder mount) of alumina-hydrate SF-4 (gibbsite). The vertical lines are the gibbsite diffraction pattern Joint Committee Powder Diffraction Standards (JCPDS) file # 29-41.

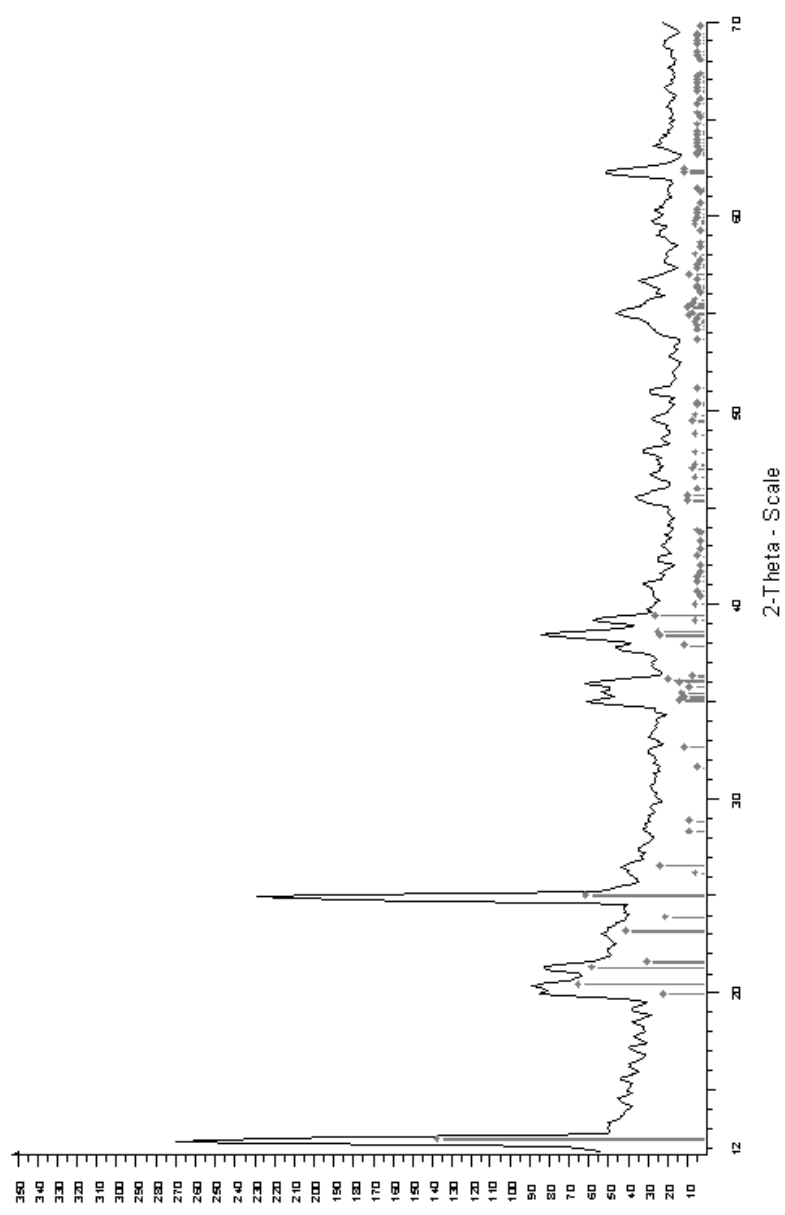


Figure 2. X-ray diffraction profile (powder mount) of kaolinite (KGa-1B). The vertical lines are the kaolinite diffraction pattern Joint Committee Powder Diffraction Standards (JCPDS) file #29-1488).

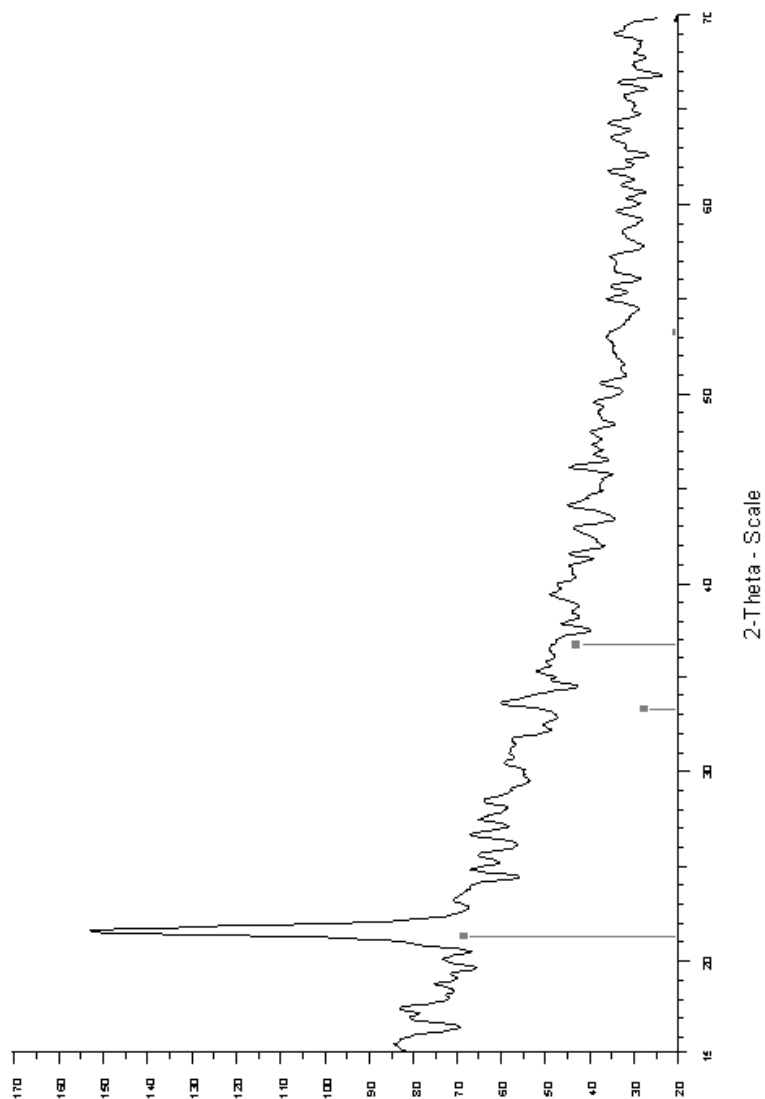


Figure 3. X-ray diffraction profile (powder mount) of the solid precipitated using the procedure of Schwertmann et al. (2000). The vertical lines are the goethite diffraction pattern Joint Committee Powder Diffraction Standards (JCPDS) file # 29-713.

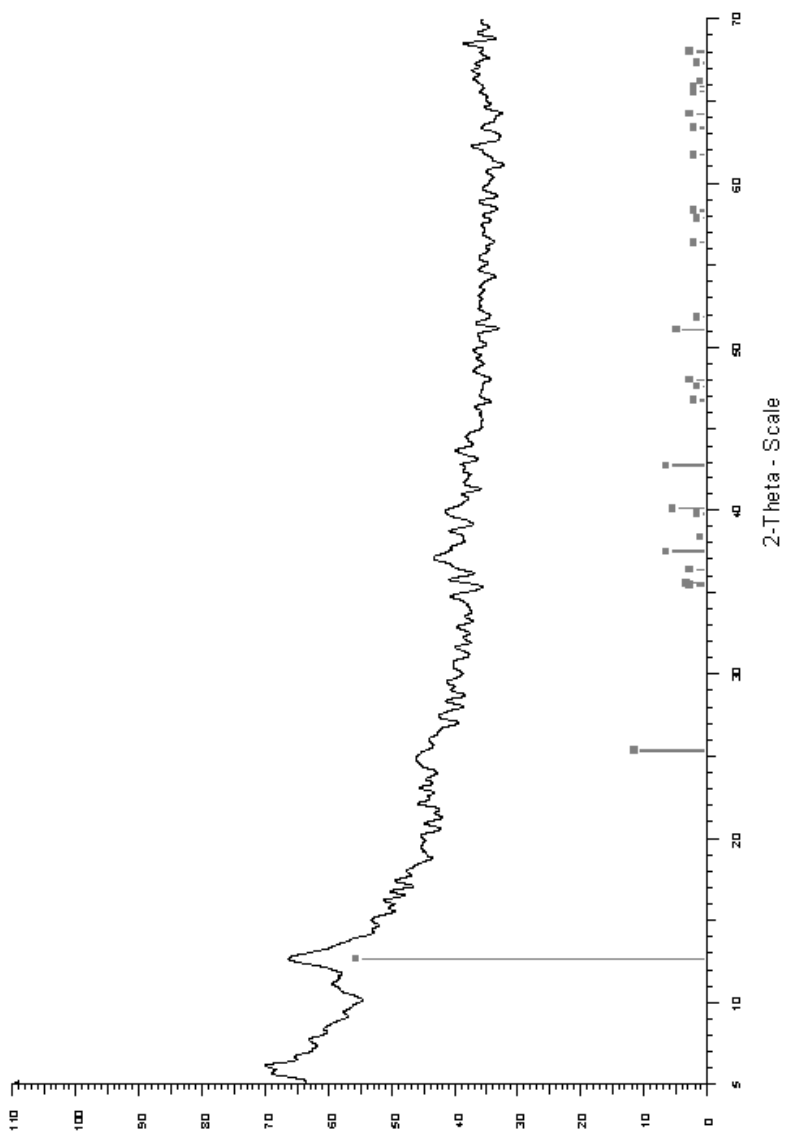


Figure 4. X-ray diffraction profile (powder mount) of the MnO₂ prepared using the procedure of Cole et al. (1947) and McKenzie (1971). The vertical lines are the birnessite diffraction pattern Joint Committee Powder Diffraction Standards (JCPDS) file # 23-1046.

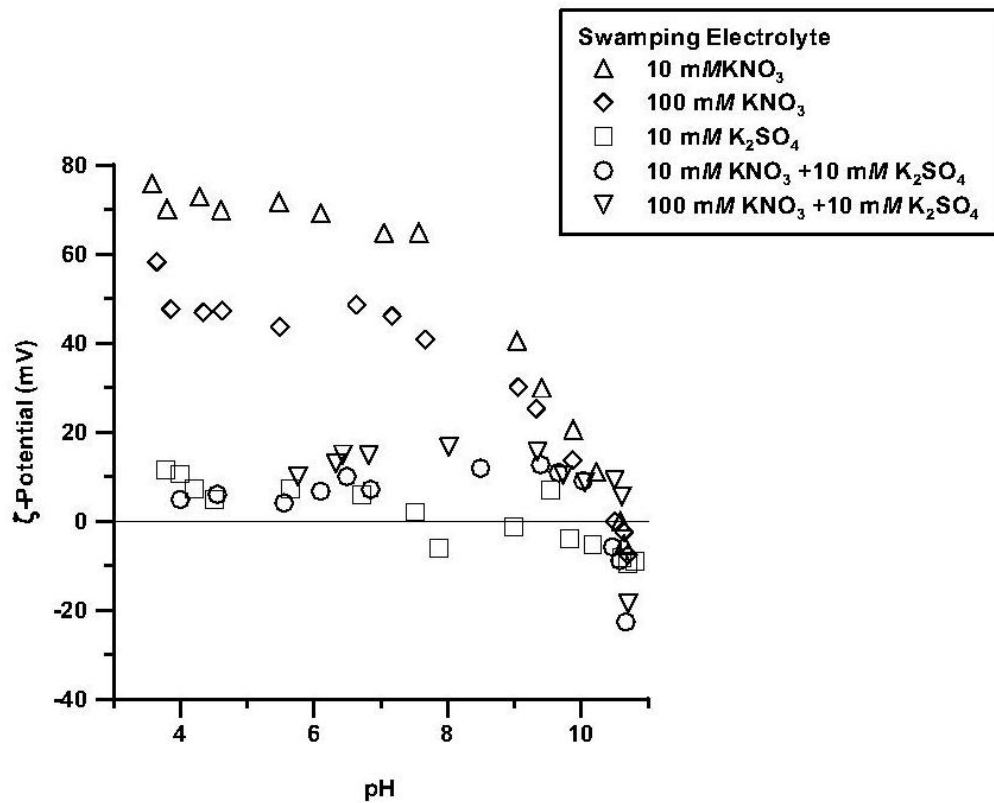


Figure 5. The influence of nitrate (NO₃) and sulfate (SO₄) on the ζ-potential (mV) of gibbsite as a function of pH, and counterion type and concentration (ionic strength).

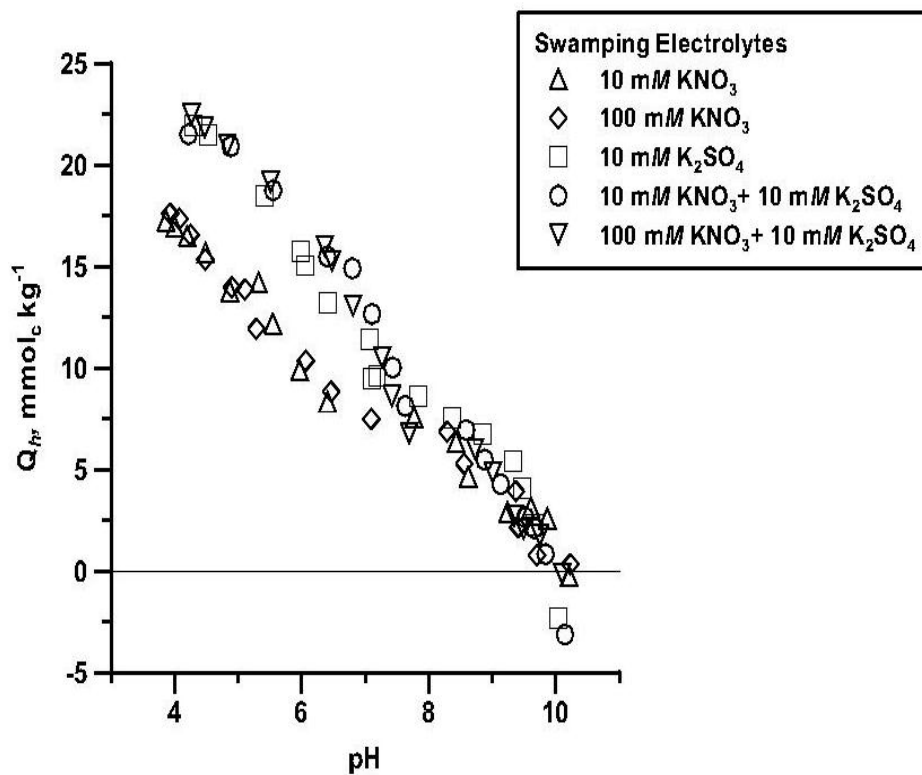


Figure 6. The influence of nitrate (NO₃) and sulfate (SO₄) on proton adsorption (Q_h , mmol_c kg⁻¹) by gibbsite as a function of pH, and counterion type and concentration (ionic strength).

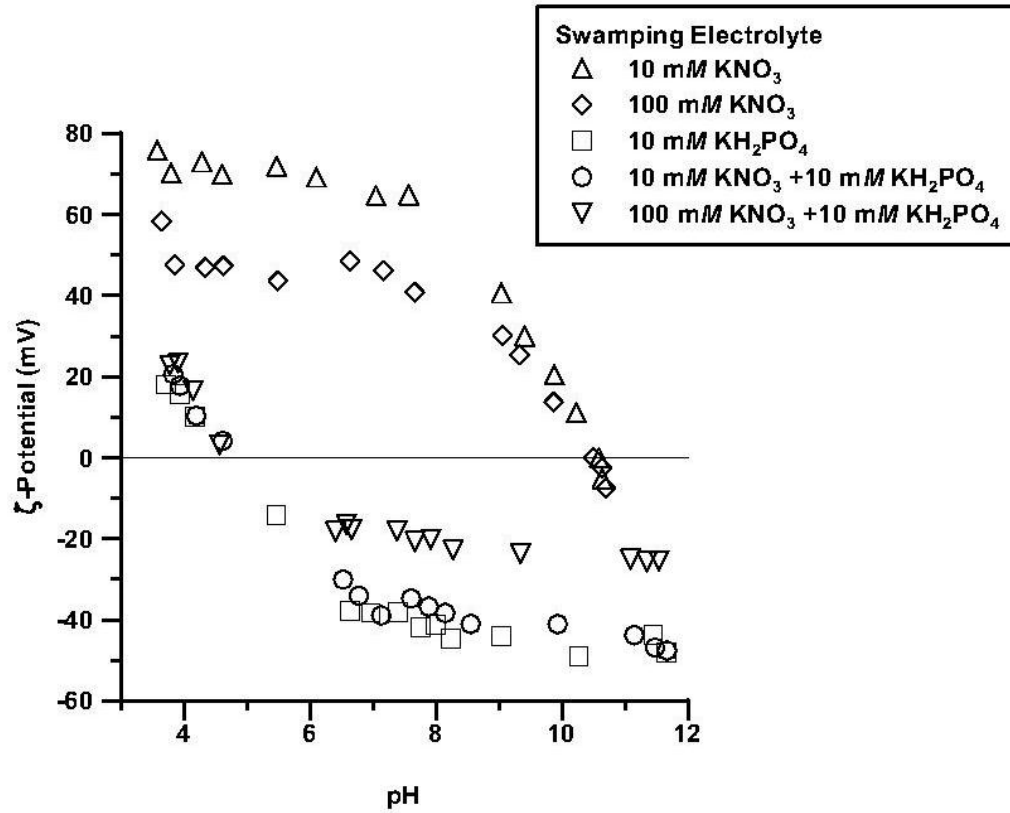


Figure 7. The influence of nitrate (NO_3) and phosphate (PO_4) on the ζ -potential (mV) of gibbsite as a function of pH, and counterion type and concentration (ionic strength).

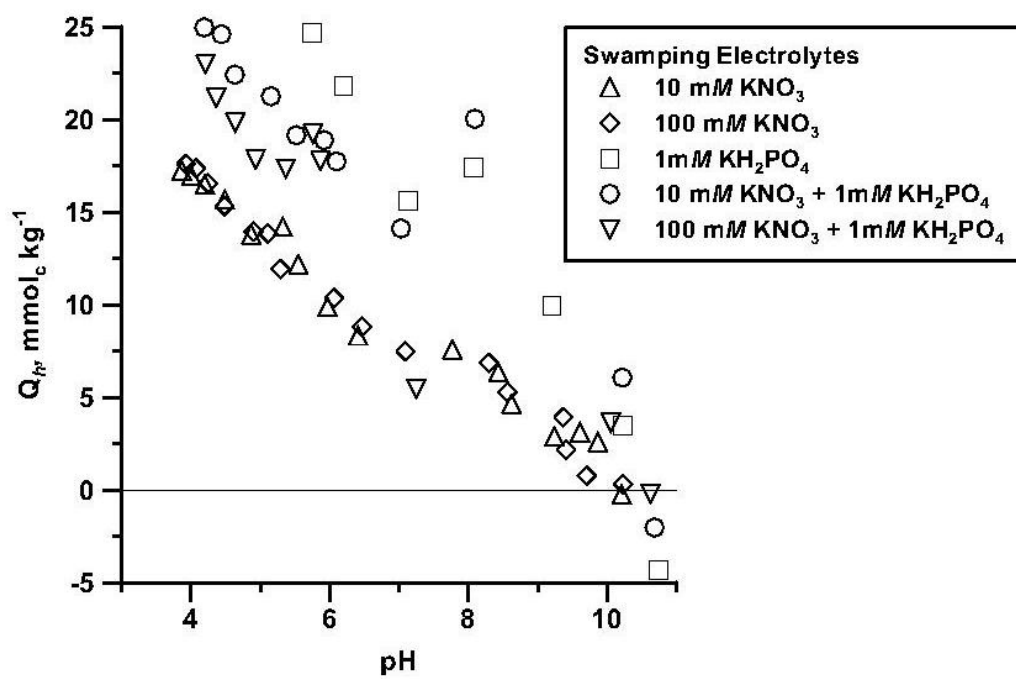


Figure 8. The influence of nitrate (NO₃) and phosphate (PO₄) on proton adsorption (Q_h , mmol_c kg⁻¹) by gibbsite as a function of pH, and counterion type and concentration (ionic strength).

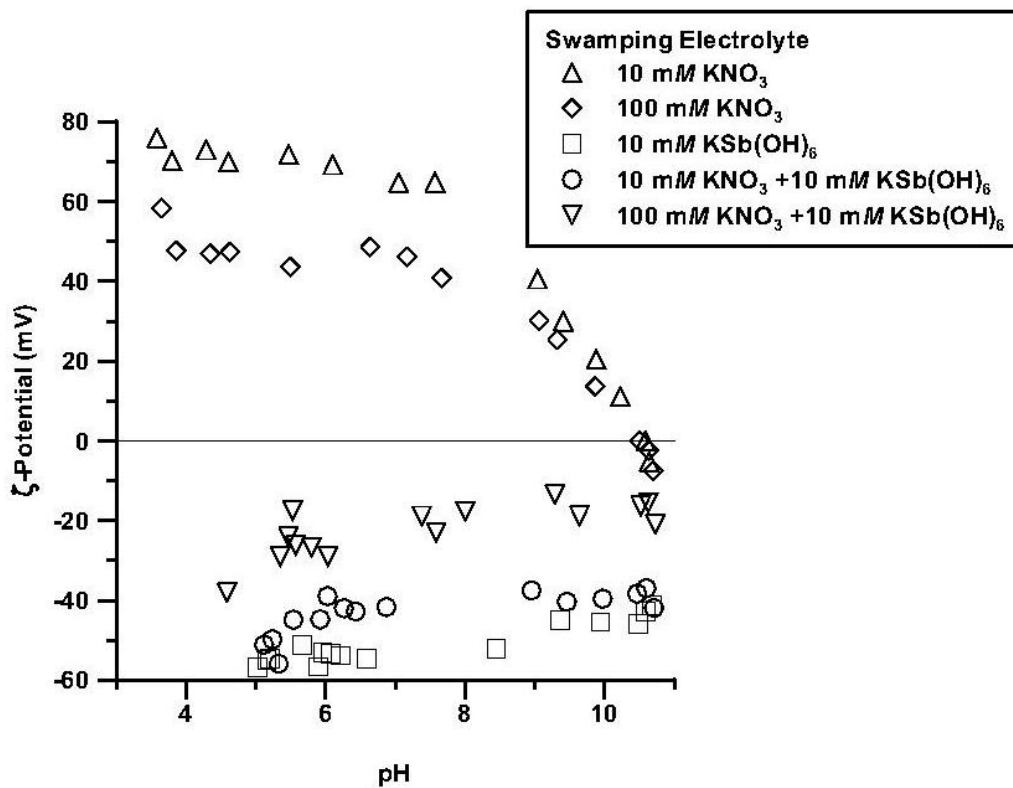


Figure 9. The influence of nitrate (NO_3) and antimonate ($\text{Sb}(\text{OH})_6$) on the ζ -potential (mV) of gibbsite as a function of pH, and counterion type and concentration (ionic strength).

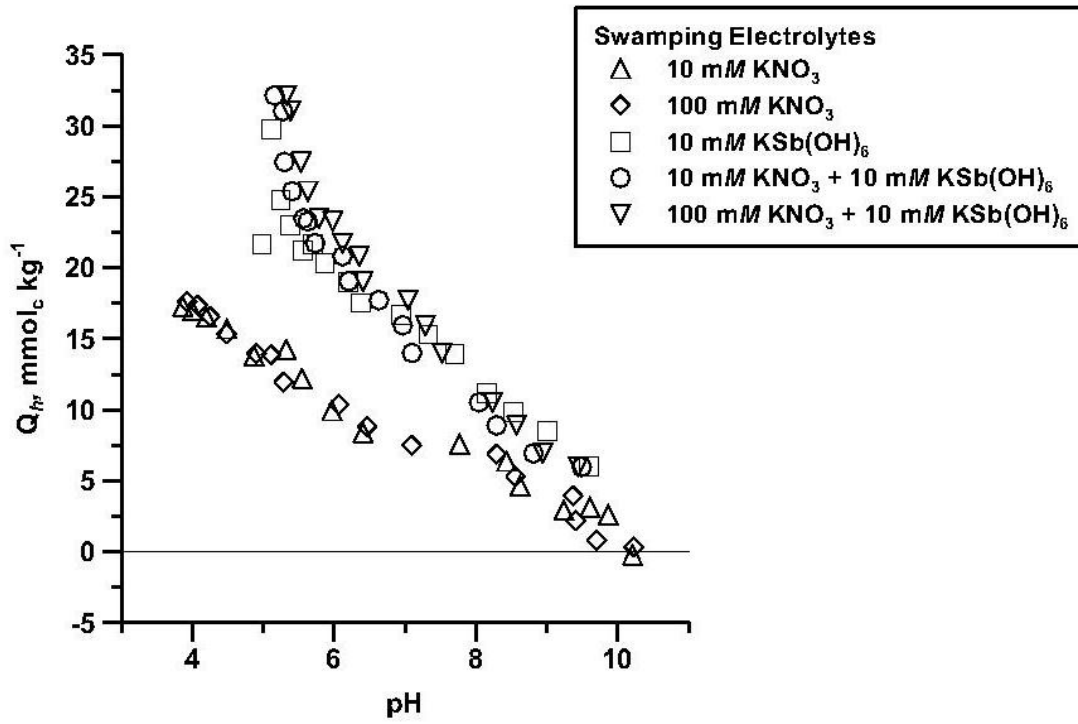


Figure 10. The influence of nitrate (NO₃) and antimonate (Sb(OH)₆) on proton adsorption (Q_h , mmol_c kg⁻¹) by gibbsite as a function of pH, and counterion type and concentration (ionic strength).

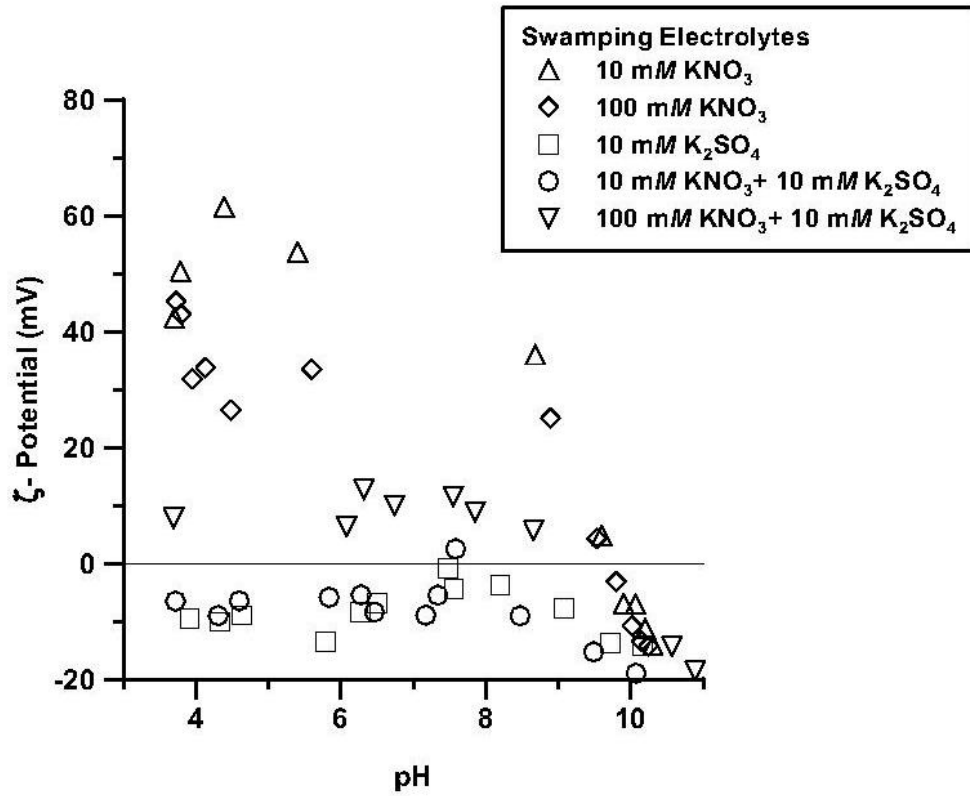


Figure 11. The influence of nitrate (NO_3) and sulfate (SO_4) on the ζ -potential (mV) of goethite as a function of pH, and counterion type and concentration (ionic strength).

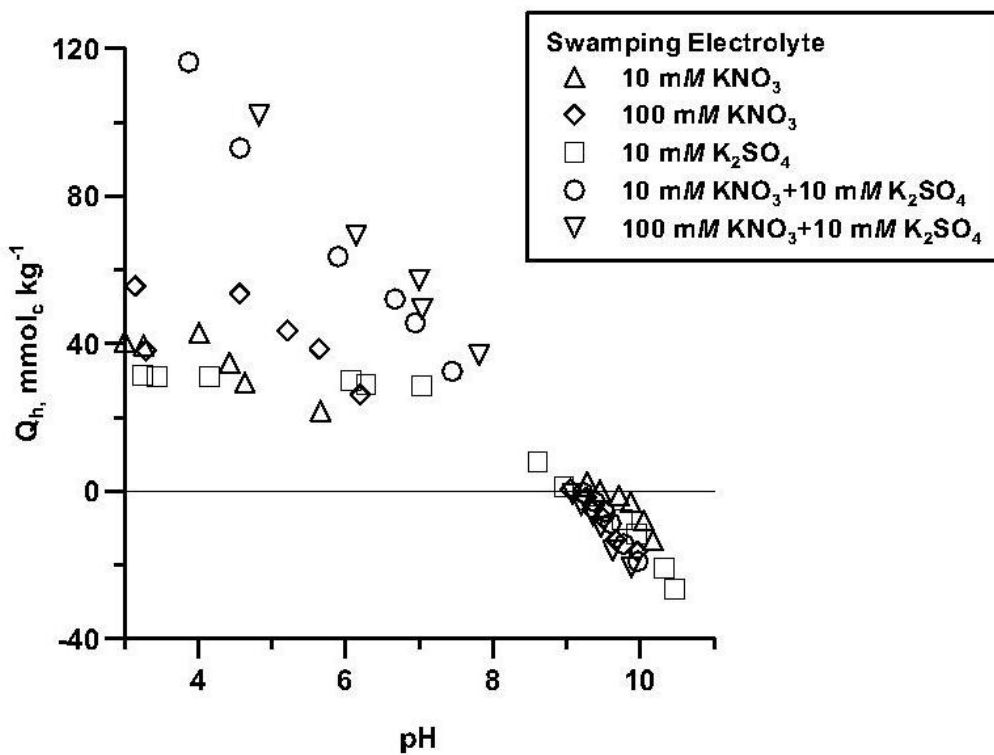


Figure 12. The influence of nitrate (NO₃) and sulfate (SO₄) on proton adsorption (Q_h , mmol_c kg⁻¹) by goethite as a function of pH, and counterion type and concentration (ionic strength).

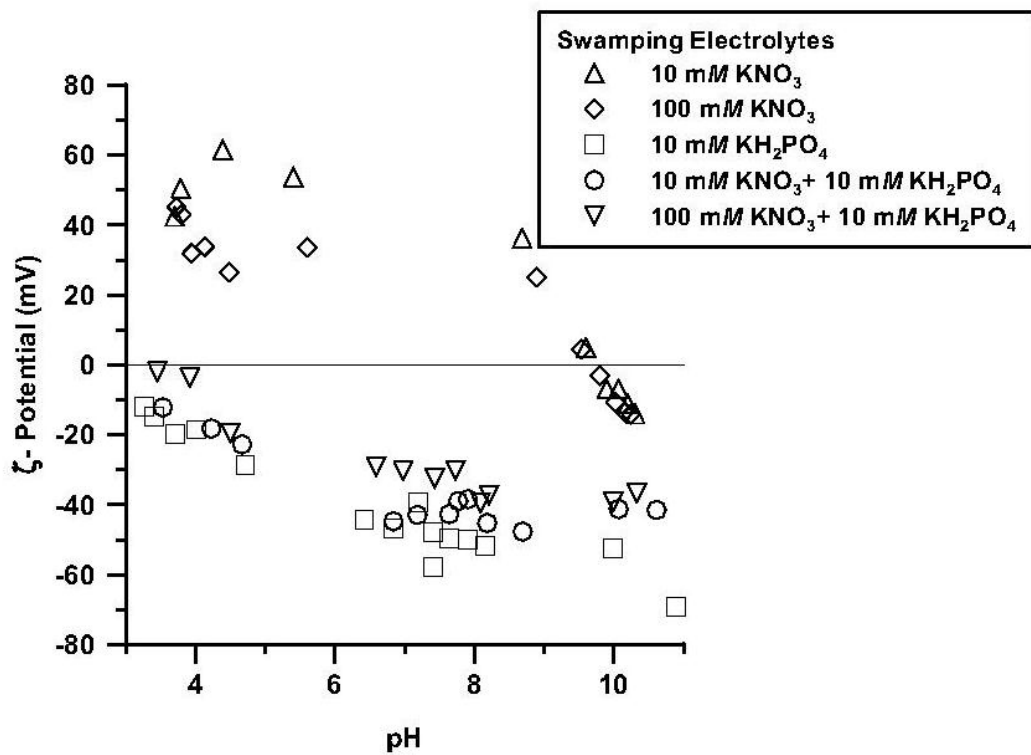


Figure 13. The influence of nitrate (NO₃) and phosphate (PO₄) on the ζ-potential (mV) of goethite as a function of pH, and counterion type and concentration (ionic strength).

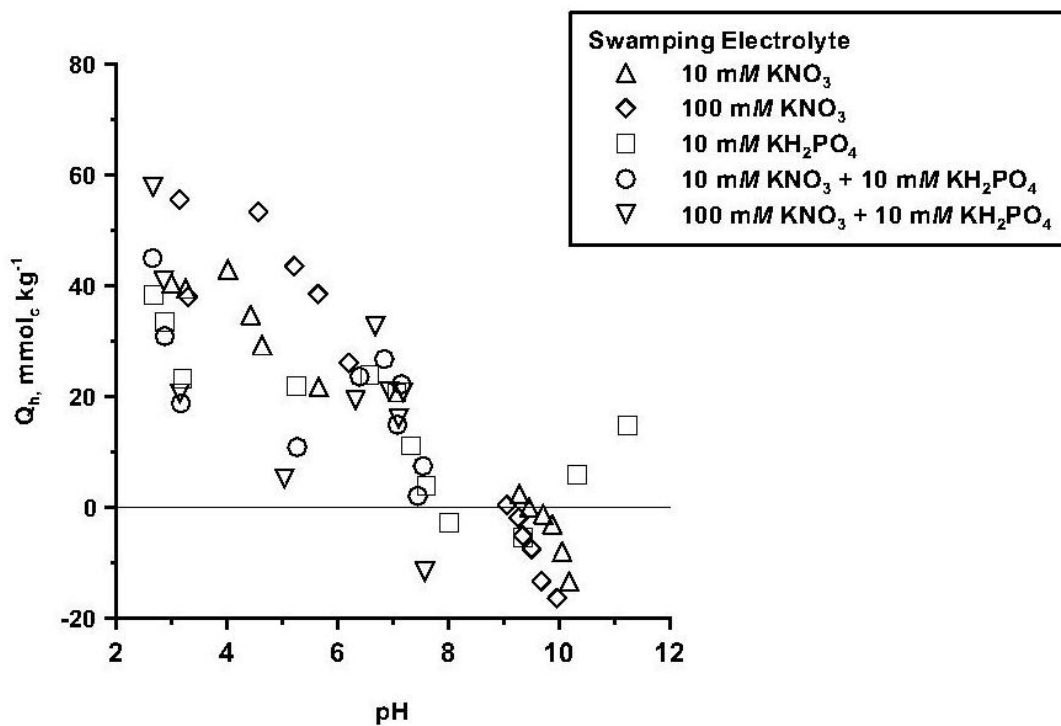


Figure 14. The influence of nitrate (NO₃) and phosphate (PO₄) on proton adsorption (Q_h , mmol_c kg⁻¹) by goethite as a function of pH, and counterion type and concentration (ionic strength).

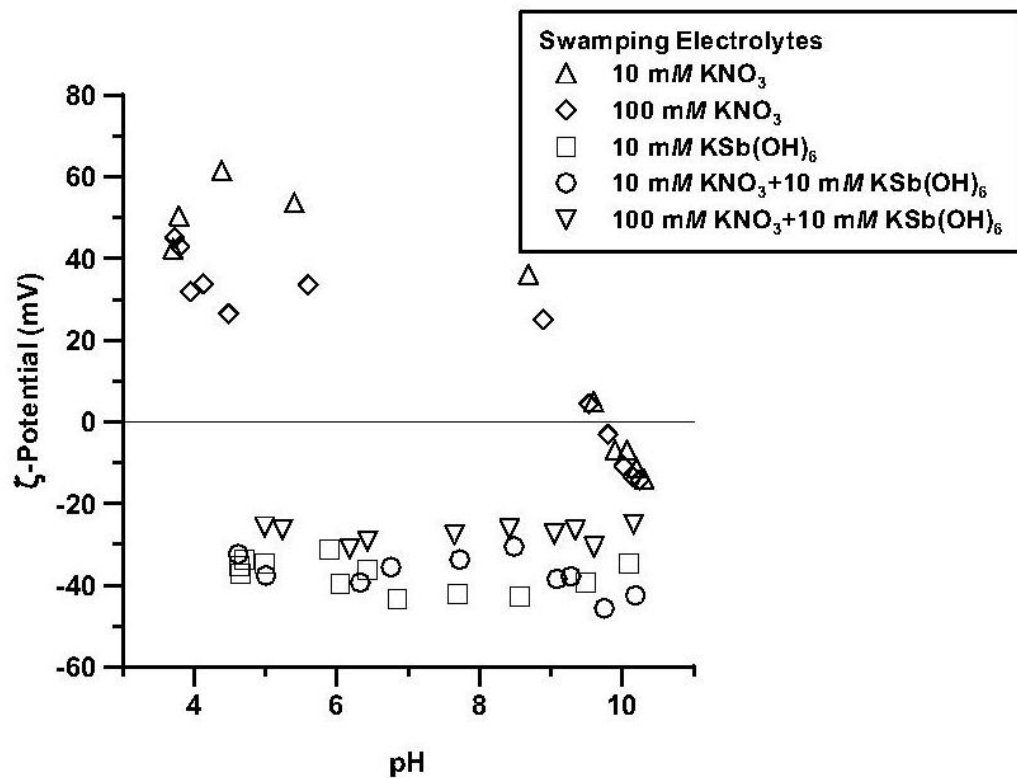


Figure 15. The influence of nitrate (NO₃) and antimonate (Sb(OH)₆) on the ζ-potential (mV) of goethite as a function of pH, and counterion type and concentration (ionic strength).

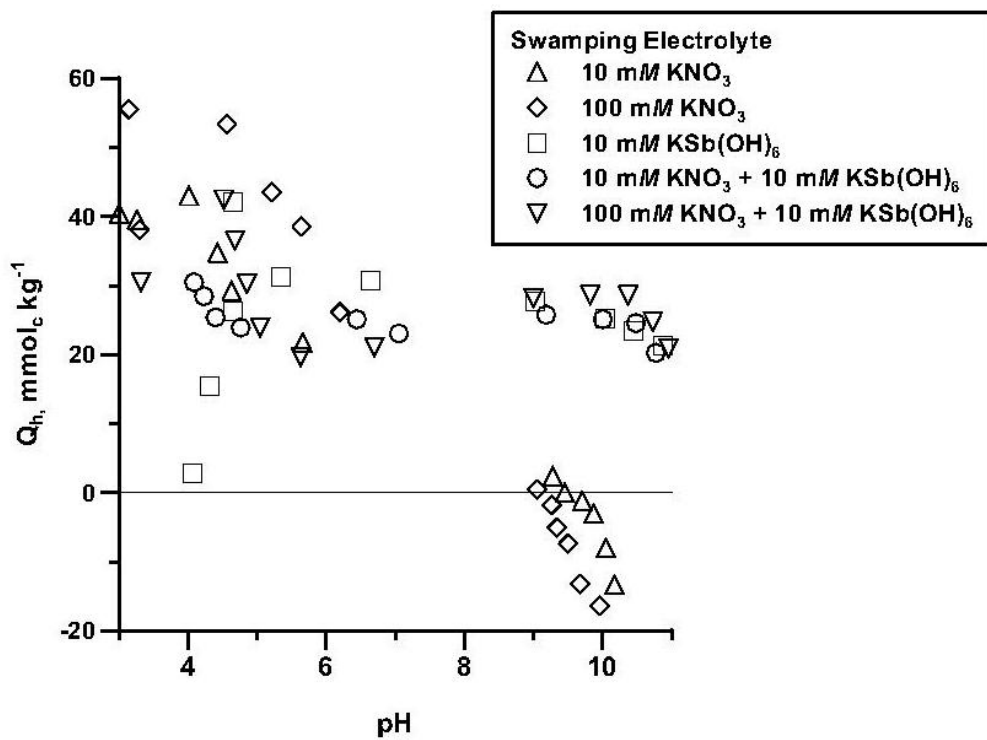


Figure 16. The influence of nitrate (NO₃) and antimonate (Sb(OH)₆) on proton adsorption (Q_h, mmol_c kg⁻¹) by goethite as a function of pH, and counterion type and concentration (ionic strength).

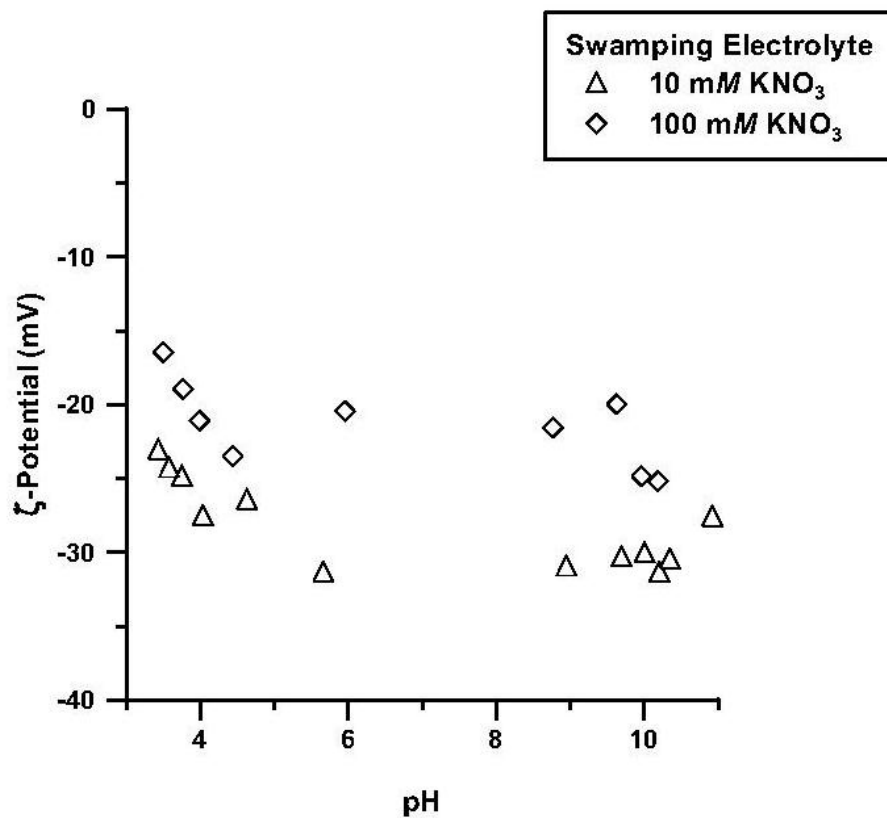


Figure 17. The influence of nitrate (NO_3) on the ζ -potential (mV) of birnessite as a function of pH and counterion concentration (ionic strength).

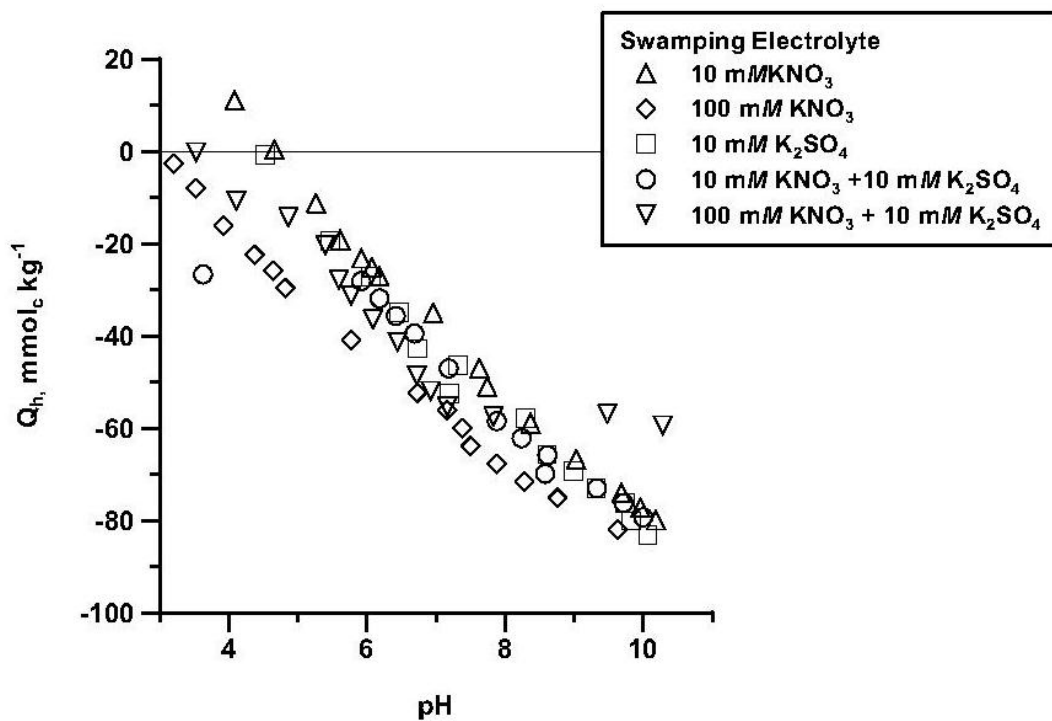


Figure 18. The influence of nitrate (NO_3) and sulfate (SO_4) on proton adsorption (Q_h , $\text{mmol}_c \text{kg}^{-1}$) by birnessite as a function of pH, and counterion type and concentration (ionic strength).

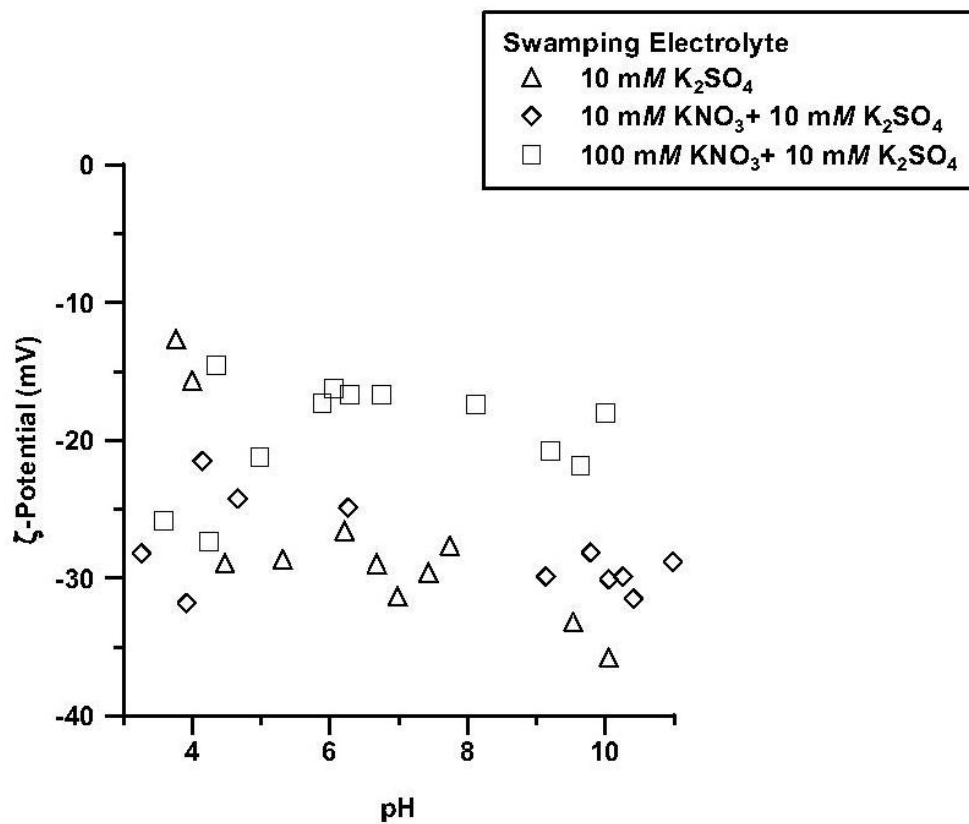


Figure 19. The influence of nitrate (NO₃) and sulfate (SO₄) on the ζ-potential (mV) of birnessite as a function of pH, and counterion type and concentration (ionic strength).

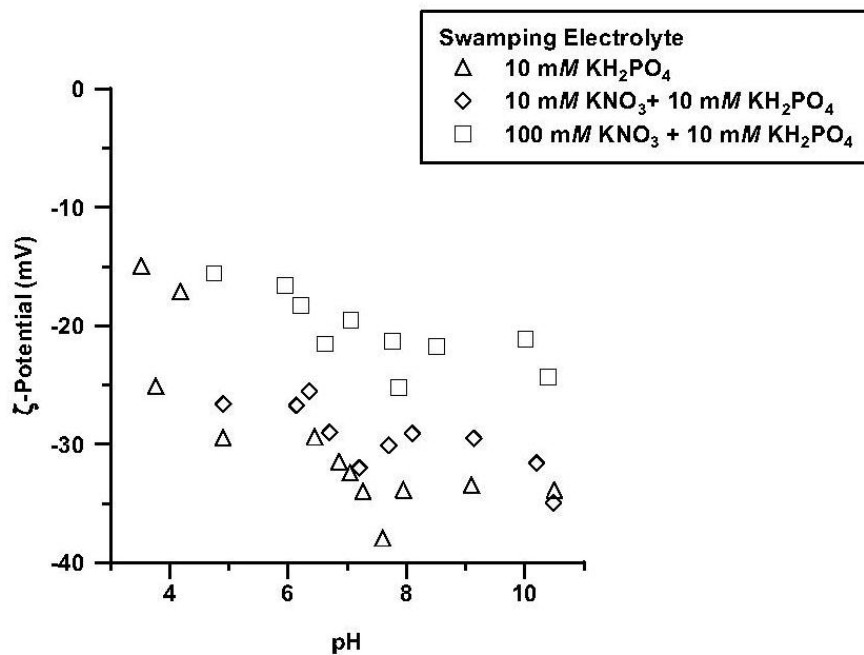


Figure 20. The influence of nitrate (NO_3) and phosphate (PO_4) on the ζ -potential (mV) of birnessite as a function of pH, and counterion type and concentration (ionic strength).

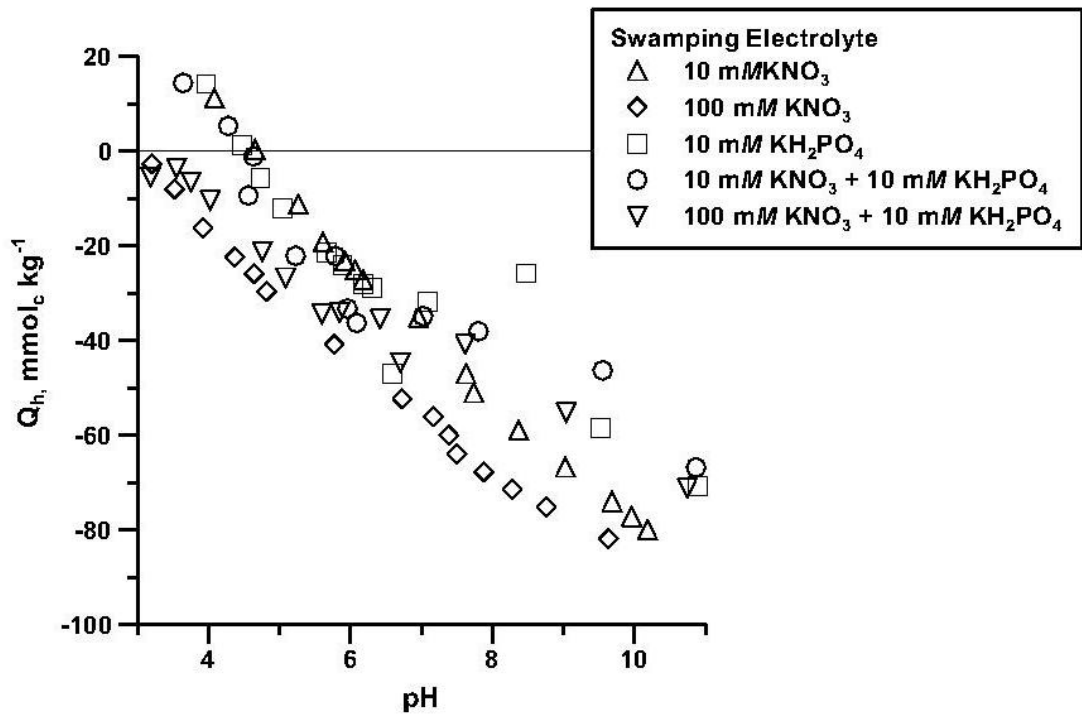


Figure 21. The influence of nitrate (NO₃) and phosphate (PO₄) on proton adsorption (Q_h , mmol_c kg⁻¹) by birnessite as a function of pH, and counterion type and concentration (ionic strength).

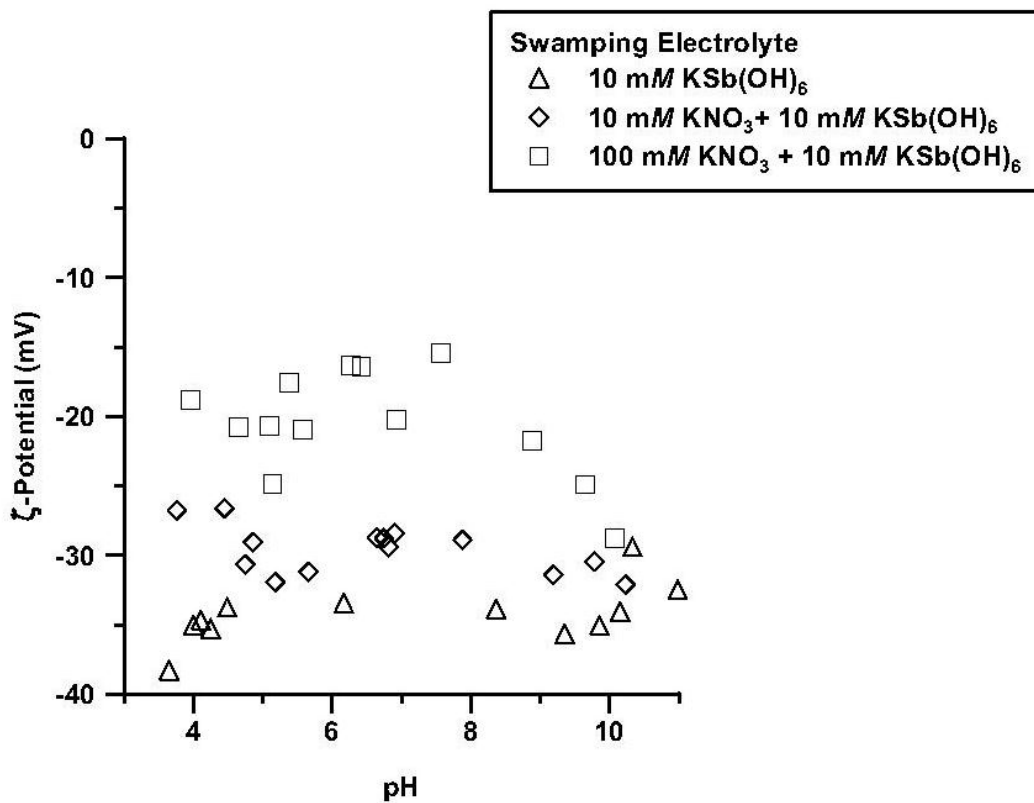


Figure 22. The influence of nitrate (NO_3) and antimonate (Sb(OH)_6) on the ζ -potential (mV) of birnessite as a function of pH, and counterion type and concentration (ionic strength).

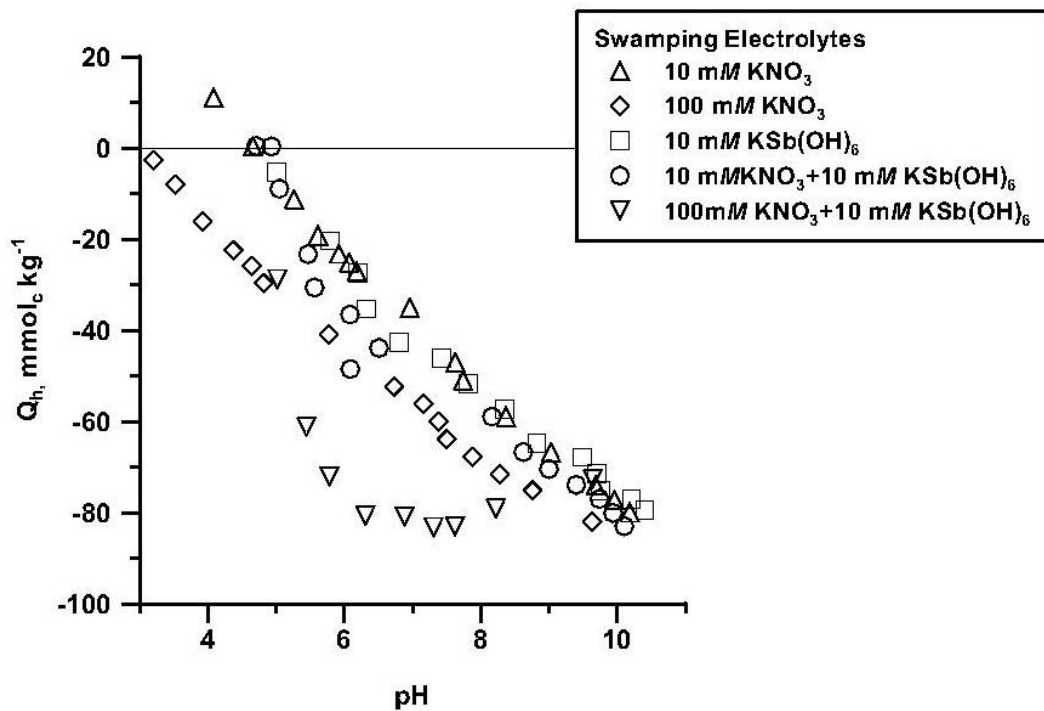


Figure 23. The influence of nitrate (NO₃) and antimonate (Sb(OH)₆) on proton adsorption (Q_h , mmol_c kg⁻¹) by birnessite as a function of pH, and counterion type and concentration (ionic strength).

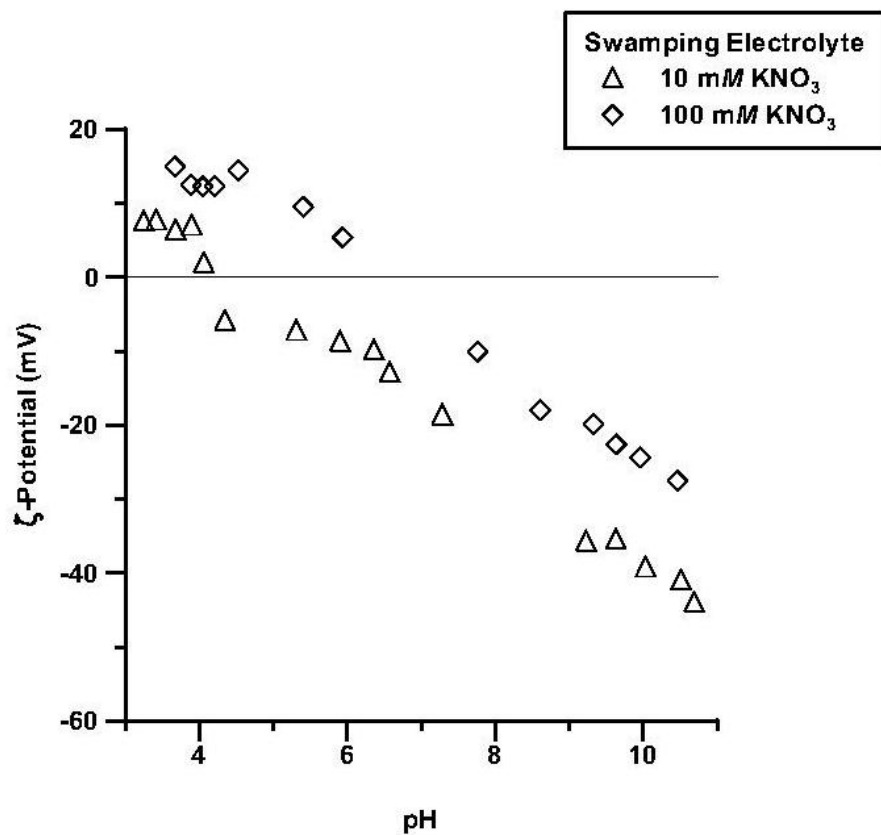


Figure 24. The influence of nitrate (NO₃) on the ζ -potential (mV) of kaolinite as a function of pH, and concentration (ionic strength).

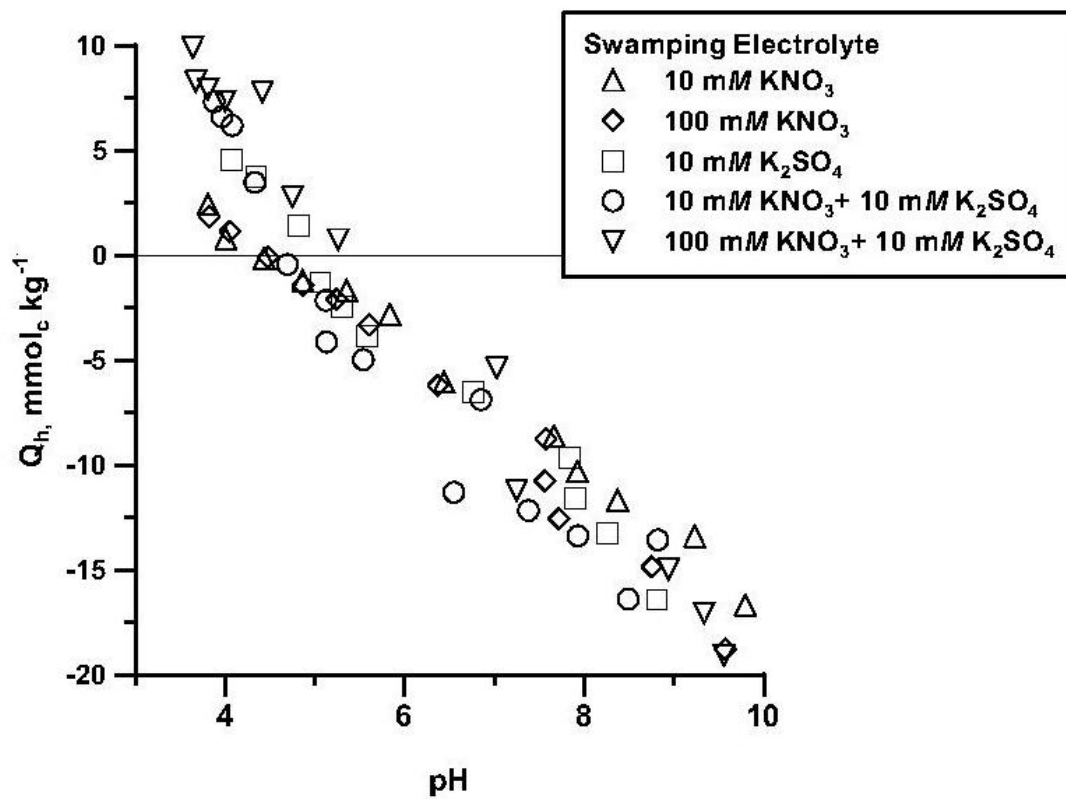


Figure 25. The influence of nitrate (NO₃) and sulfate (SO₄) on proton adsorption (Q_h, mmol_c kg⁻¹) by kaolinite as a function of pH, and counterion type and concentration (ionic strength).

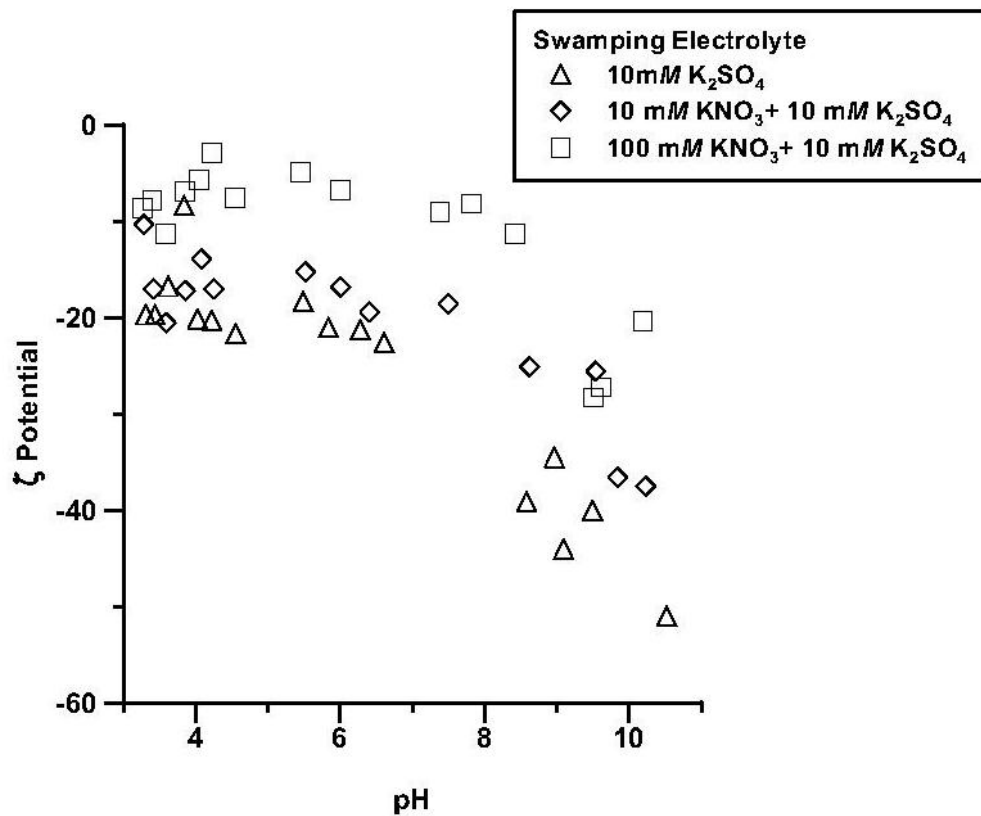


Figure 26. The influence of nitrate (NO_3) and sulfate (SO_4) on the ζ -potential (mV) of kaolinite as a function of pH, and counterion type and concentration (ionic strength).

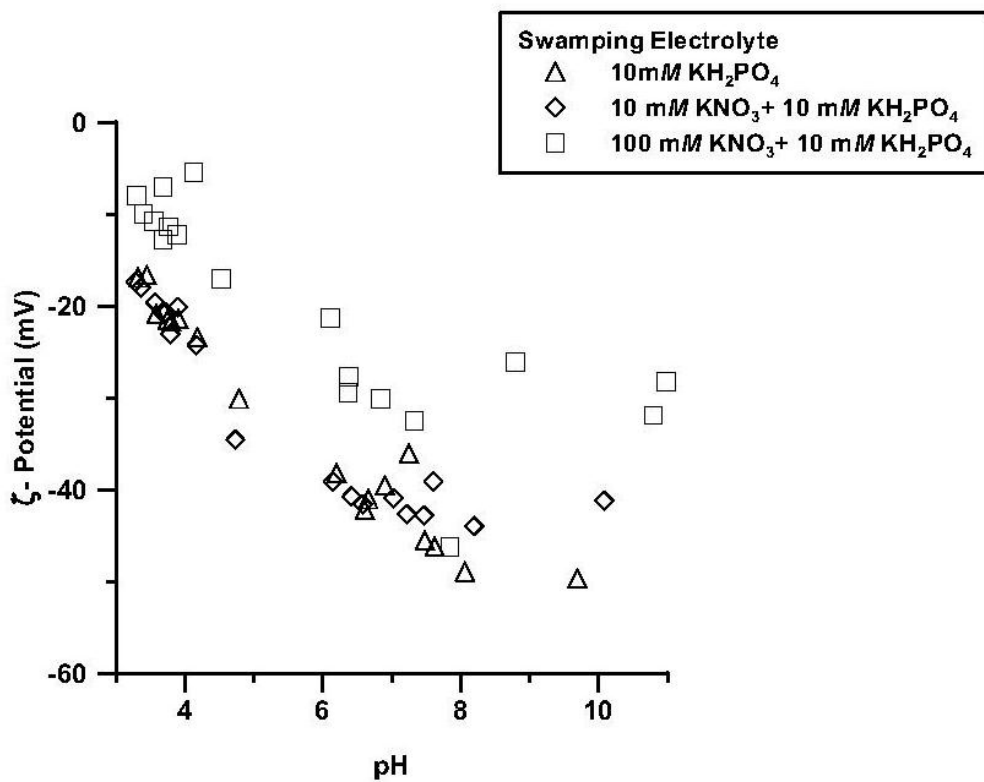


Figure 27. The influence of nitrate (NO₃) and phosphate (PO₄) on the ζ-potential (mV) of kaolinite as a function of pH, and counterion type and concentration (ionic strength).

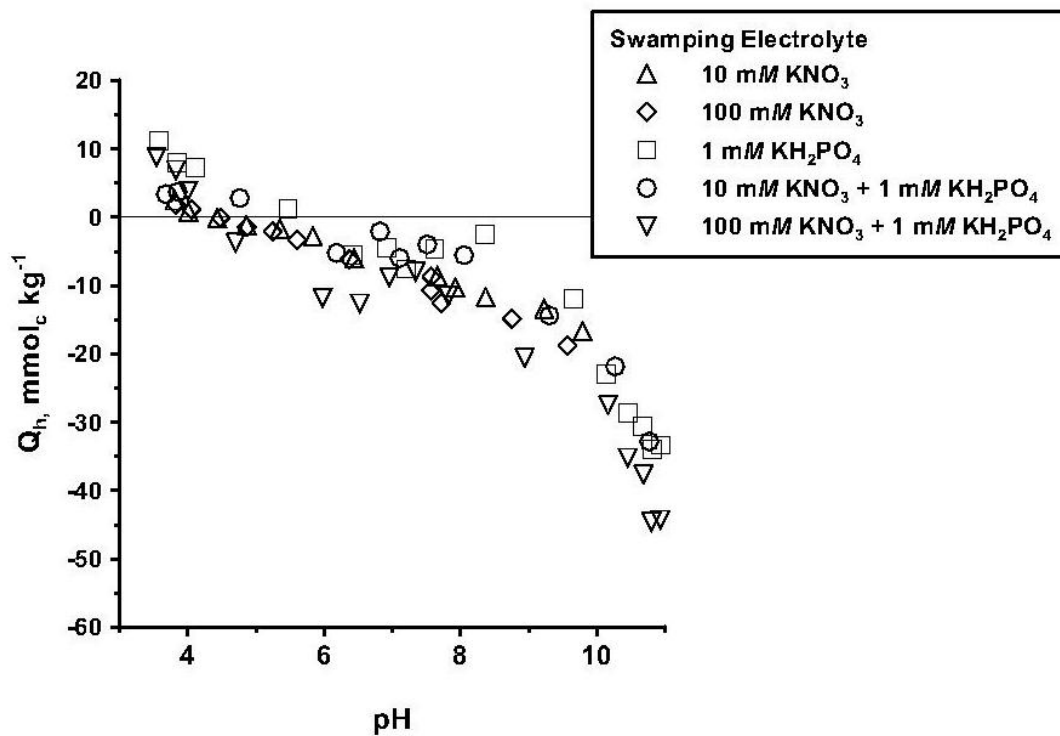


Figure 28. The influence of nitrate (NO₃) and phosphate (PO₄) on proton adsorption (Q_h , mmol_c kg⁻¹) by kaolinite as a function of pH, and counterion type and concentration (ionic strength).

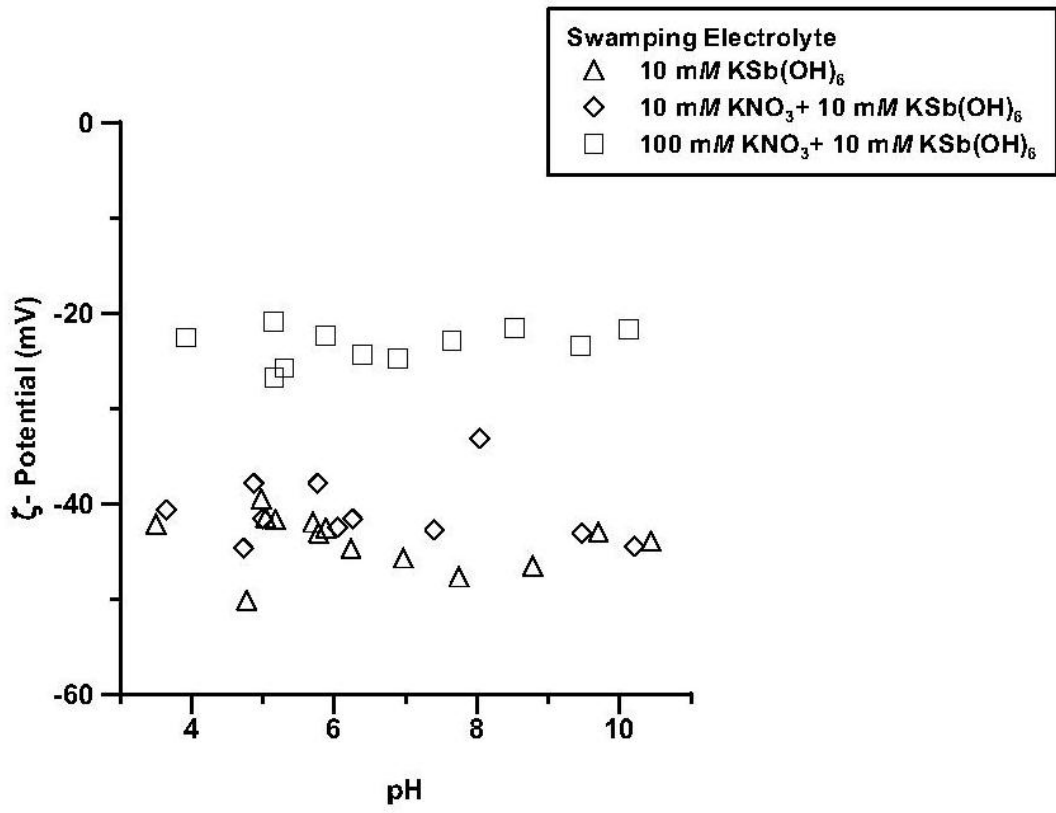


Figure 29. The influence of nitrate (NO_3) and antimonate (Sb(OH)_6) on the ζ -potential (mV) of kaolinite as a function of pH, and counterion type and concentration (ionic strength).

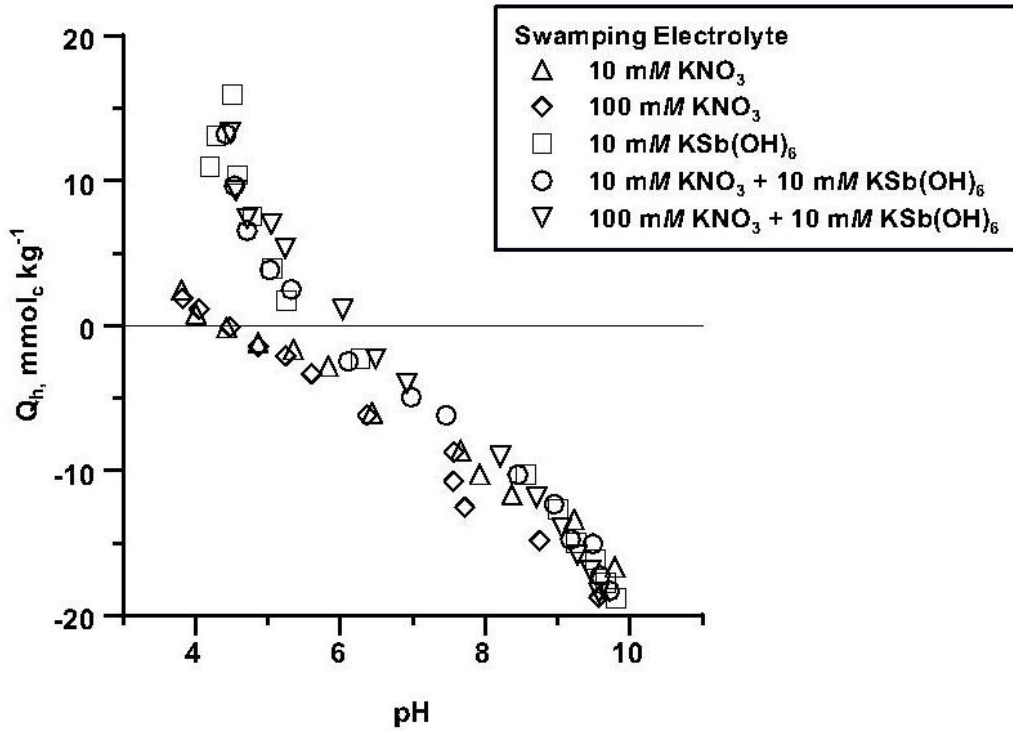


Figure 30. The influence of nitrate (NO₃) and antimonate (Sb(OH)₆) on proton adsorption (Q_h , mmol_c kg⁻¹) by kaolinite as a function of pH, and counterion type and concentration (ionic strength).

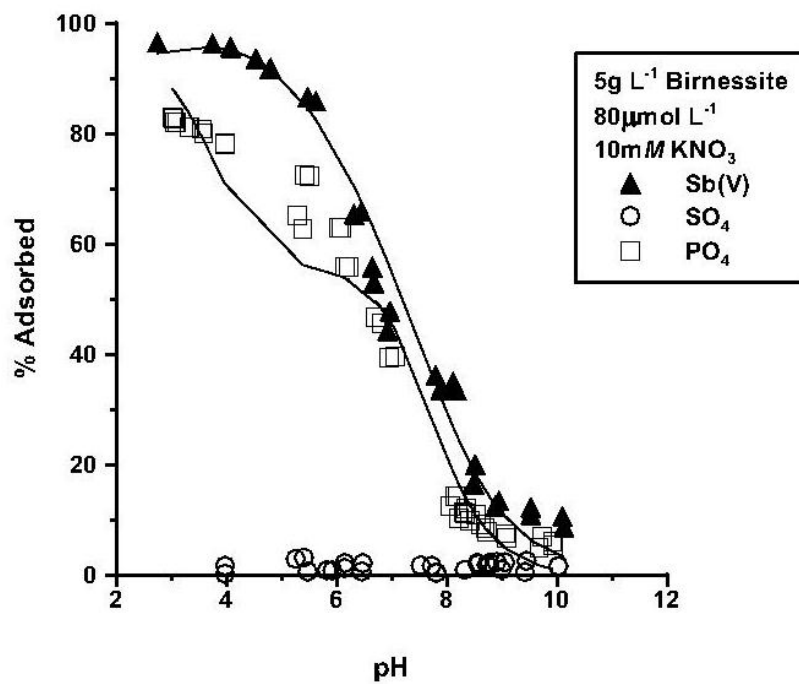


Figure 31. The adsorption of antimonate (Sb(V)), sulfate (SO₄), and phosphate (PO₄) by birnessite in 10 mM KNO₃ as a function of pH. The solid lines represent the diffuse layer model description of the adsorption data.

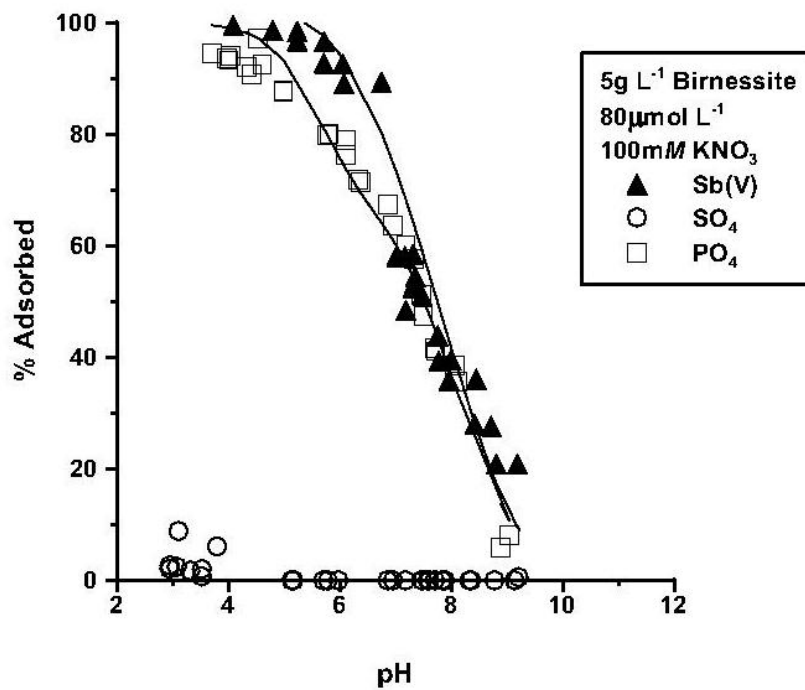


Figure 32. The adsorption of antimonate (Sb(V)), sulfate (SO₄), and phosphate (PO₄) by birnessite in 100 mM KNO₃ as a function of pH. The solid lines represent the diffuse layer model description of the adsorption data.

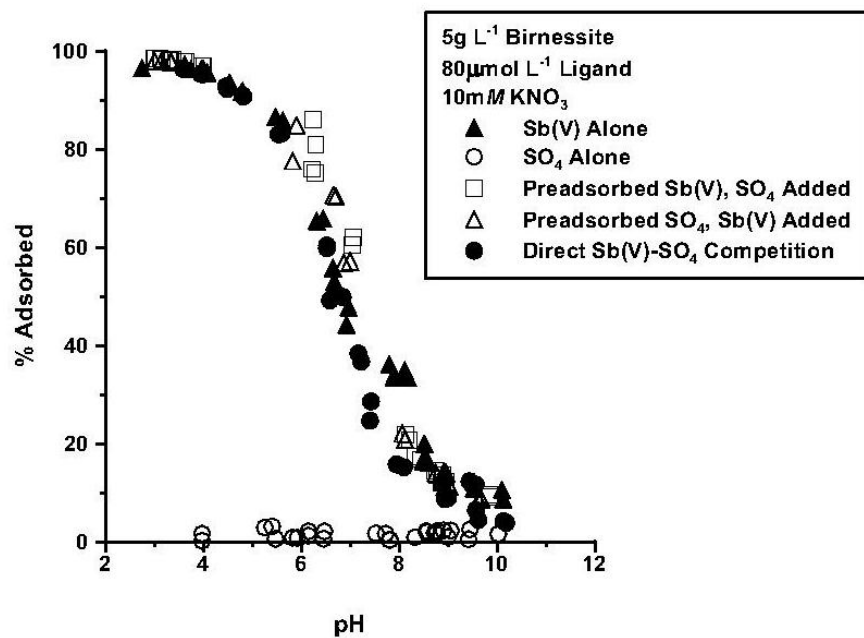


Figure 33. The influence of sulfate (SO₄) on the adsorption of antimonate (Sb(V)) by birnessite in 10 mM KNO₃ as a function of pH and order of ligand addition.

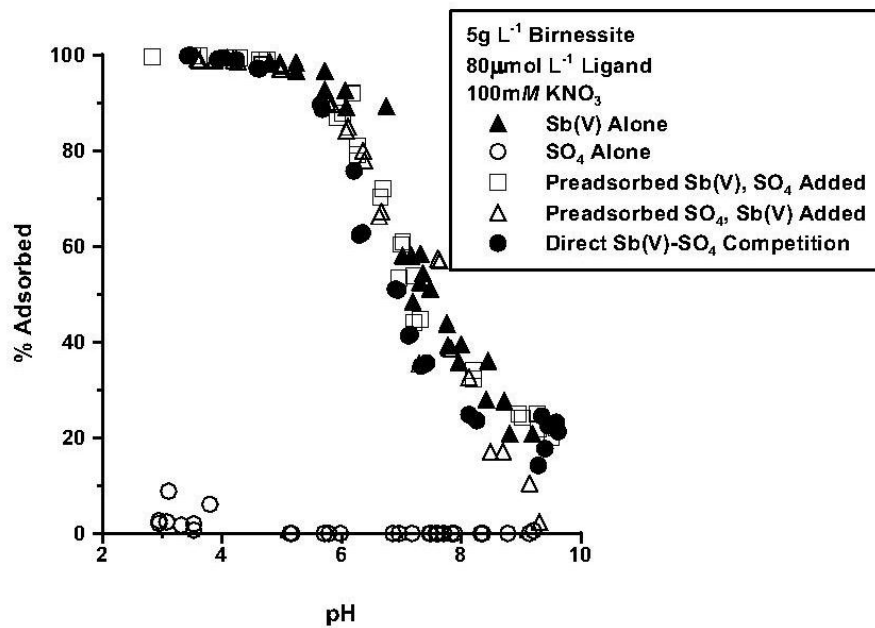


Figure 34. The influence of sulfate (SO₄) on the adsorption of antimonate (Sb(V)) by birnessite in 100 mM KNO₃ as a function of pH and order of ligand addition.

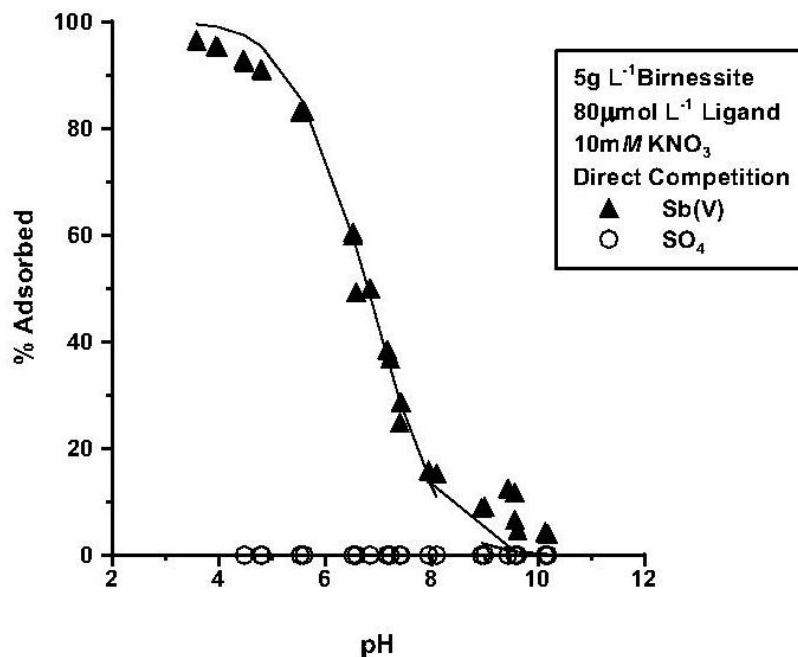


Figure 35. The predicted and experimentally-determined adsorption of antimonate (Sb(V)) and sulfate (SO₄) by birnessite under direct competition in 10 mM KNO₃ as a function of pH. The solid lines represent the diffuse layer model description of the adsorption data.

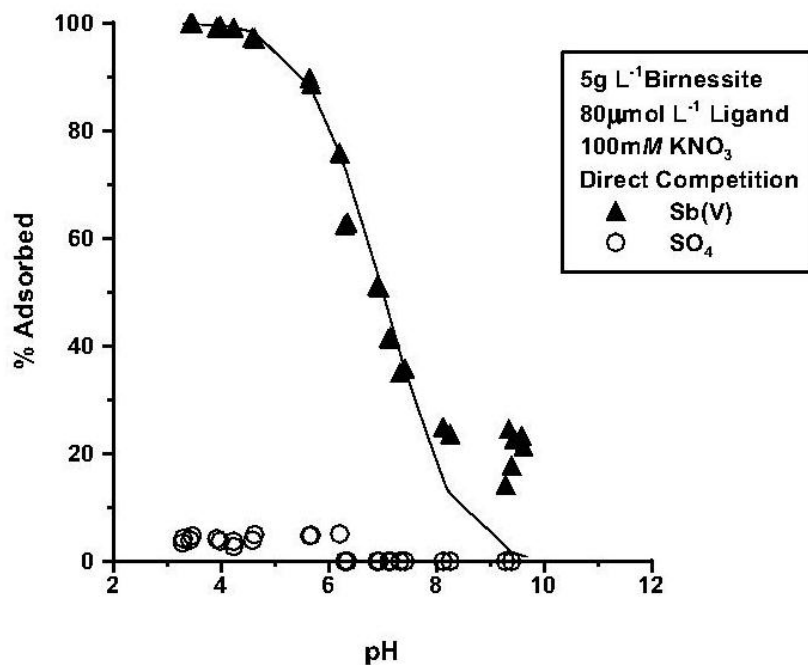


Figure 36. The predicted and experimentally-determined adsorption of antimonate (Sb(V)) and sulfate (SO₄) by birnessite under direct competition in 100 mM KNO₃ as a function of pH. The solid lines represent the diffuse layer model description of the adsorption data.

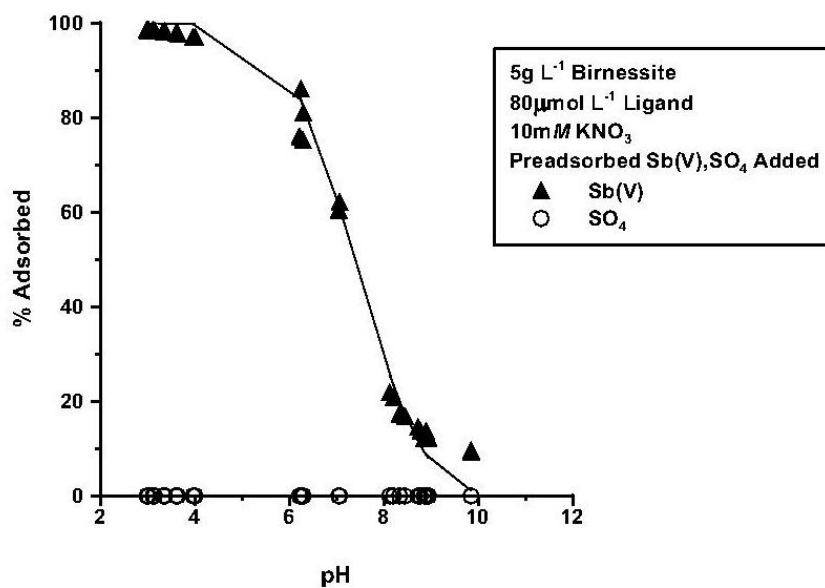


Figure 37. The predicted and experimentally-determined adsorption of antimonate (Sb(V)) and sulfate (SO₄) by birnessite under indirect competition in 10 mM KNO₃ as a function of pH. The solid lines represent the diffuse layer model description of the adsorption data.

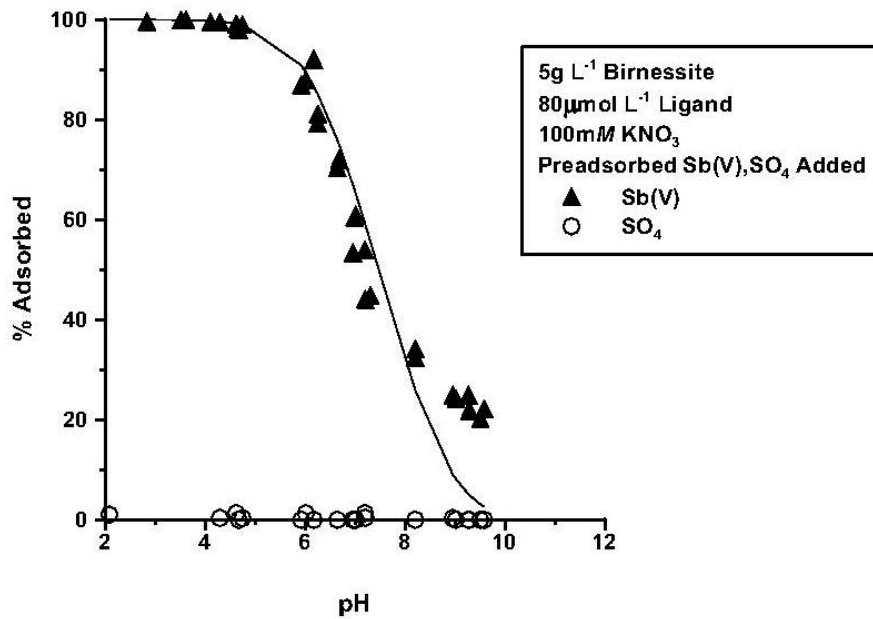


Figure 38. The predicted and experimentally-determined adsorption of antimonate (Sb(V)) and sulfate (SO₄) by birnessite under indirect competition in 100 mM KNO₃ as a function of pH. The solid lines represent the diffuse layer model description of the adsorption data.

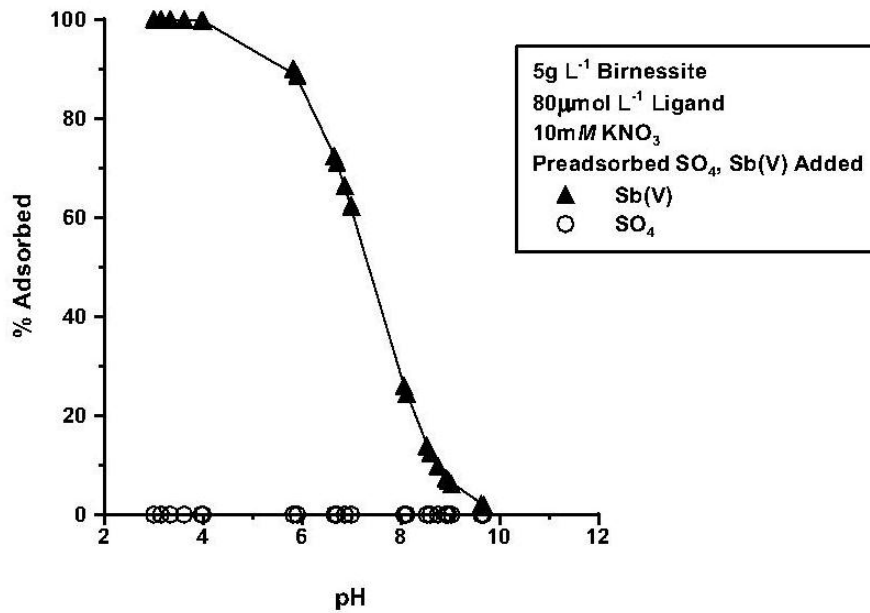


Figure 39. The predicted and experimentally-determined adsorption of antimonate (Sb(V)) and sulfate (SO₄) by birnessite under indirect competition in 10 mM KNO₃ as a function of pH. The solid lines represent the diffuse layer model description of the adsorption data.

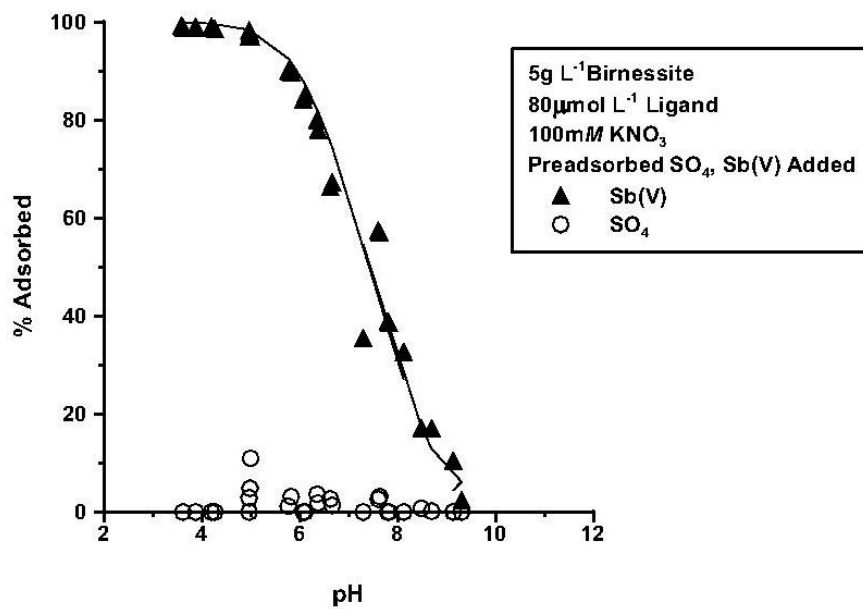


Figure 40. The predicted and experimentally-determined adsorption of antimonate (Sb(V)) and sulfate (SO₄) by birnessite under indirect competition in 100 mM KNO₃ as a function of pH. The solid lines represent the diffuse layer model description of the adsorption data.

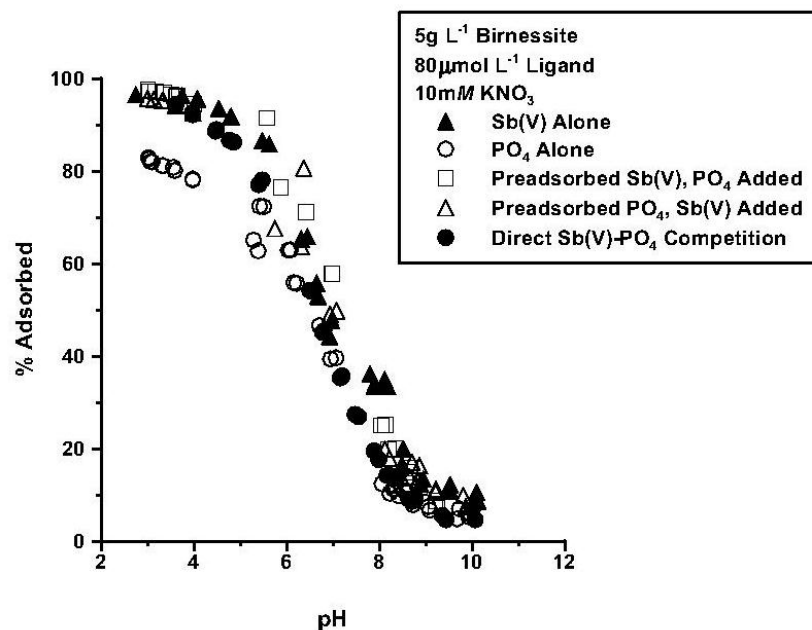


Figure 41. The influence of phosphate (PO₄) on the adsorption of antimonate (Sb(V)) in 10 mM KNO₃ as a function of pH and order of ligand addition.

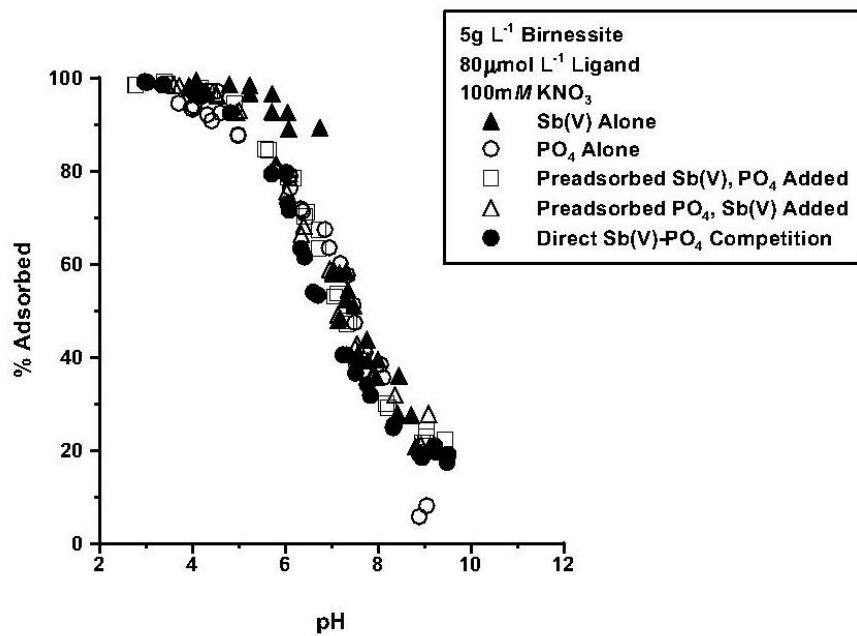


Figure 42. The influence of phosphate (PO₄) on the adsorption of antimonate (Sb(V)) in 100 mM KNO₃ as a function of pH and order of ligand addition.

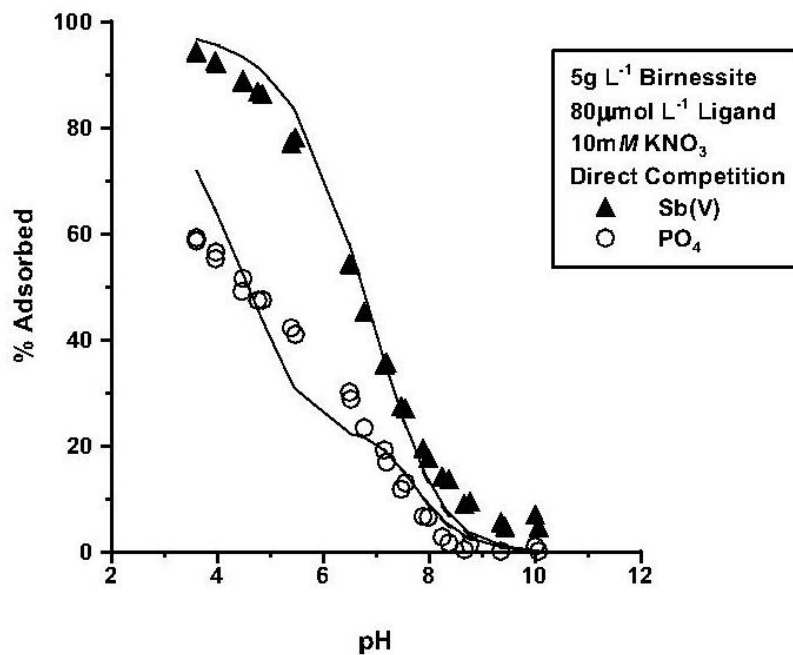


Figure 43. The predicted and experimentally-determined adsorption of antimonate (Sb(V)) and phosphate (PO₄) by birnessite under direct competition in 10 mM KNO₃ as a function of pH. The solid lines represent the diffuse layer model description of the adsorption data.

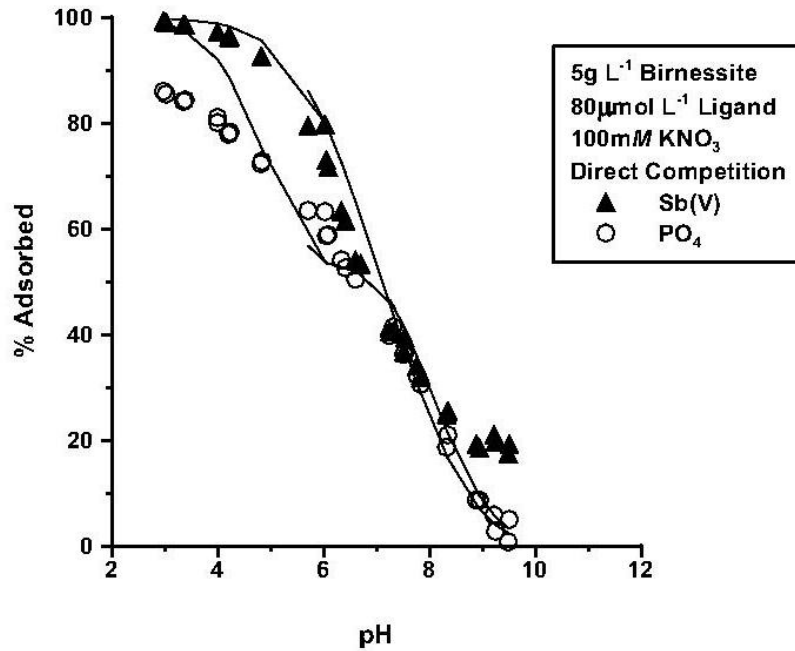


Figure 44. The predicted and experimentally-determined adsorption of antimonate (Sb(V)) and phosphate (PO₄) by birnessite under direct competition in 100 mM KNO₃ as a function of pH. The solid lines represent the diffuse layer model description of the adsorption data.

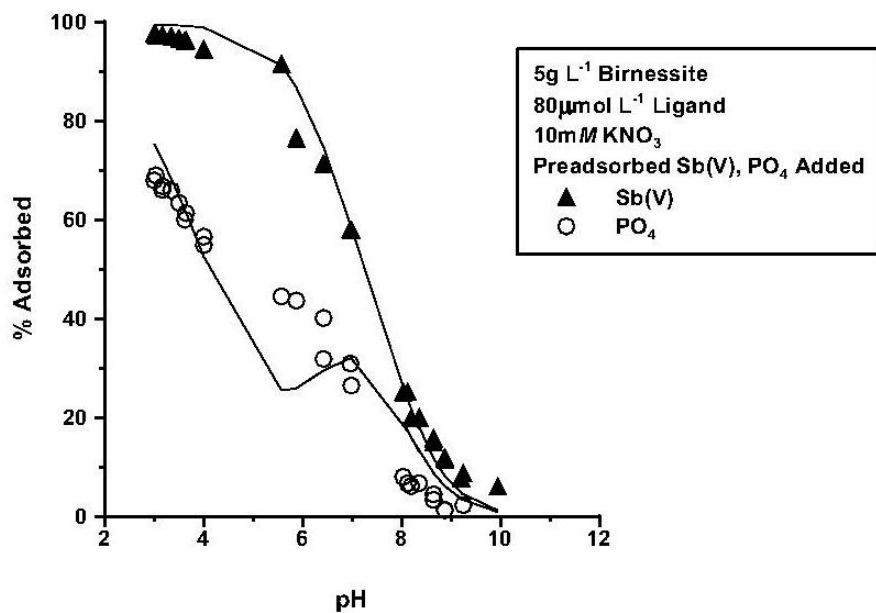


Figure 45. The predicted and experimentally-determined adsorption of antimonate (Sb(V)) and phosphate (PO₄) by birnessite under indirect competition in 10 mM KNO₃ as a function of pH. The solid lines represent the diffuse layer model description of the adsorption data.

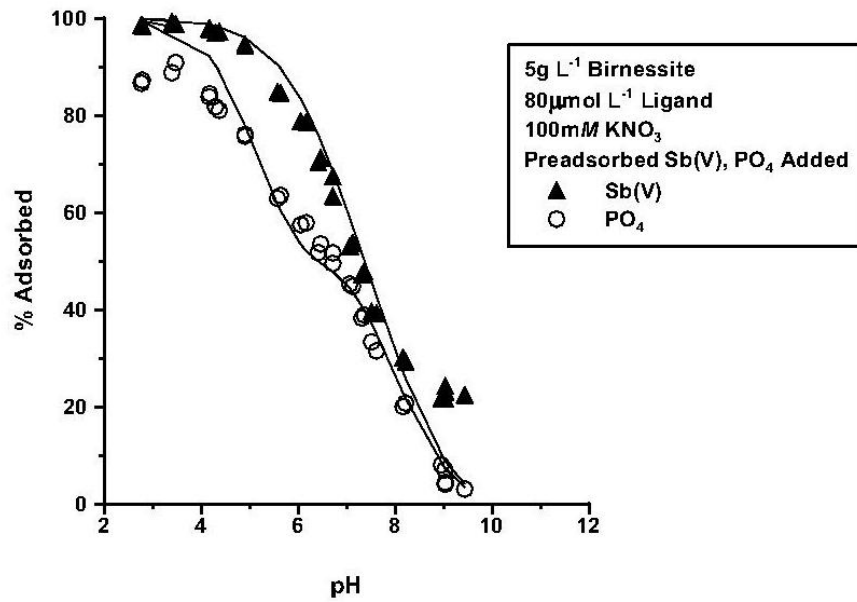


Figure 46. The predicted and experimentally-determined adsorption of antimonate (Sb(V)) and phosphate (PO₄) by birnessite under indirect competition in 100 mM KNO₃ as a function of pH. The solid lines represent the diffuse layer model description of the adsorption data.

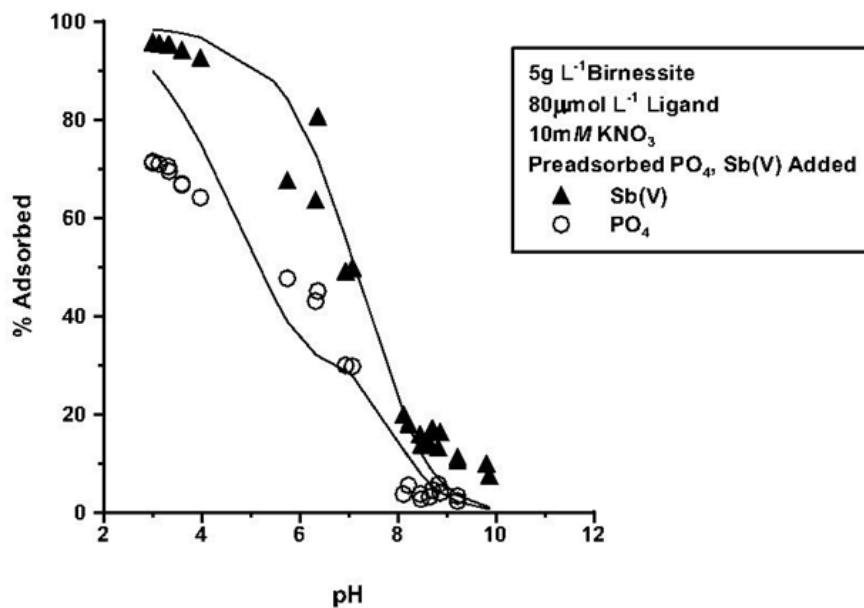


Figure 47. The predicted and experimentally-determined adsorption of antimonate (Sb(V)) and phosphate (PO₄) by birnessite under indirect competition in 10 mM KNO₃ as a function of pH. The solid lines represent the diffuse layer model description of the adsorption data.

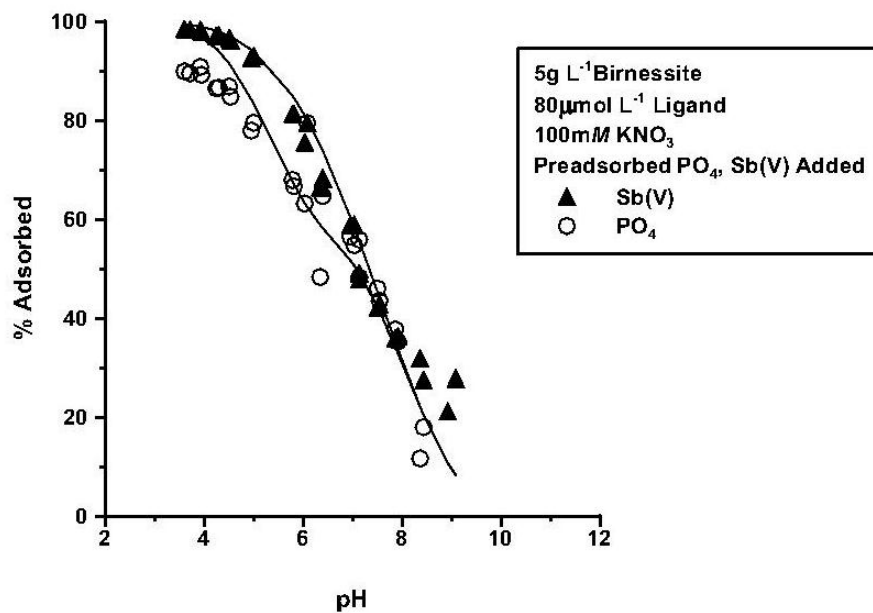


Figure 48. The predicted and experimentally-determined adsorption of antimonate (Sb(V)) and phosphate (PO₄) by birnessite under indirect competition in 100 mM KNO₃ as a function of pH. The solid lines represent the diffuse layer model description of the adsorption data.

REFERENCES

- Accornero, M., L. Marini, and M. Lelli. 2008. The dissociation constants of antimonic acid at 10-40°C. *J. Solution Chem.* 37:785-800.
- Adekola, F., M. Fedoroft, H. Geckeis, T. Kupcik, G. Lefevre, J. Lutzenkircken, M. Plaschke, T. Preocanin, T. Rabung, and D. Schild. 2011. Characterization of acid-base properties of two gibbsite samples in the context of literature results. *J. Colloid and Interface Sci.* 354:306-317.
- Ali, M., and D. Dzombak. 1996. Competitive sorption of simple organic acids and sulfate on goethite. *Environ. Sci. Technol.* 30:1061-1071.
- Ambe, F., S. Ambe, T. Okada, and H. Sekizawa. 1986. In situ Mössbauer studies of metal oxide-aqueous solution interfaces with adsorbed cobalt-57 and antimony-119 ions. 323:403-424. In Davis J.A., and K.F Hayes (ed.), *Geochemical processes at mineral surfaces*, ACS Symposium. ACS, Washington (1986).
- Anderson, R. 2006. Adsorption of 2-ketogluconate by gibbsite, goethite, and kaolinite. M.S. Thesis, The University of Tennessee, Knoxville.
- Antelo, J. M. Avena, S. Fiol, R. Lopez, and F. Arce. 2005 Effects of pH and ionic strength of the adsorption of phosphate and arsenate at the goethite-water interface. *J. Colloid Interface Sci.* 285:476-486.
- Appel, C., L.Q. Ma, R.D. Rhue, and E. Kennelley. 2003. Point of zero charge determination in soils and minerals via traditional methods and detection of electroacoustic mobility. *Geoderma* 113:77-93.

- Arai, Y. and D. L. Sparks. 2001. ATR-FTIR spectroscopic investigation on phosphate adsorption mechanisms at the ferrihydrate-water interface. *J. Colloid Interface Sci.* 241:317-326.
- Aria, Y. 2010. Arsenic and Antimony. p.383-407. *In* P.S. Hooda, (ed.) Trace elements in soils. John Wiley & Sons, West Sussex, UK.
- Avena, M.J., and C.P. de Pauli. 1998. Proton adsorption and electrokinetics of an Argentinean montmorillonite. *J. Colloid Interface Sci.* 202:195-204.
- Balistrieri, L.S., and T.T. Chao. 1990. Adsorption of selenium by amorphous iron oxyhydroxide and manganese dioxide. *Geochim. Cosmochim. Acta* 54:739-751.
- Bencze, C.G. 1994. Antimony. *In* H.G. Seiler et al. (ed.) Handbook on metals in clinical and analytical chemistry. Marcel Dekker, New York.
- Bertsch, P., and J. Seaman. 1999. Characterization of complex mineral assemblages: implications for contaminant transport and environmental remediation. *National Academy of Sciences* 96:3350-3357.
- Bigham, J.M., R.W. Fitzpatrick, and D.G. Schulze. 2002. Iron Oxides. p.324-360. *In* J.B. Dixon et al. (ed.) Soil mineralogy with environmental applications. SSSA, Madison, WI.
- Biver, M. M. Krachler, and W. Shotyk. 2011. The desorption of antimony(V) from sediments, hydrous oxides, and clay minerals by carbonate, phosphate, sulfate, nitrate and chloride. *J. Environ. Qual.* 40: 1143-1152.
- Boily, J. F., J. Lutzenkirch, A. Blames, J. Beattie, and S. Sjöberg. 2001. Modeling proton binding at the goethite-water interface. *Colloids Surf., A.* 179:11-27.

- Celi, L., E. Barberis, and F. A. Marsan. 2000. Sorption of phosphate on goethite at high concentrations. *Soil Sci.* 165:657-664.
- Chassange, C., F. Mietta, and J.C. Winterwerp. 2009. Electrokinetic study of kaolinite suspensions. *J. Colloid Interface Sci.* 336:352-359.
- Council of the European Union, 1998. Council Directive 98/83/EC on the quality of water intended for human consumption. *J. Euro. Communities* 32-54.
- Del Nero, Mirella, C. Galindo, R. Barillon, E. Halter, and B. Made. 2010. Surface reactivity of α -Al₂O₃ and mechanisms of phosphate sorption: in situ ATR-FTIR spectroscopy and zeta potential studies. *J. Colloid Interface Sci.* 342:437-444
- Dixon, J. B., and G.N. White. 2002. Manganese oxides. p.367-386. *In* J.B. Dixon and S.B. Weed (ed.) *Soil mineralogy with environmental applications.* SSSA, Madison, WI.
- Erdemoğlu M., and M. Sarikaya. 2006. Effects of heavy metals and oxalate on the zeta potential of magnetite. *J. Colloid Interface Sci.* 300:794-804.
- Essington, M. E. 2003. *Soil and water chemistry: an integrative approach.* CRC Press, Boca Raton, FL.
- Essington, M. E. 2011. Antimony(V) adsorption by variable-charge minerals. ER-1741. Interim Report v. 1. September, 2011. The University of Tennessee.
- Feng, X. H., L. M. Zhai, W. F. Tan, F. Liu and J. Z. He. 2007. Adsorption and redox reactions of heavy metals on synthesized Mn oxide minerals. *Environ. Pollution* 147:366-373.

- Filella, M., and P.M. May. 2003. Computer simulation of the low-molecular-weight-inorganic species distribution of antimony (III) and antimony (V) in natural waters. *Geochim. Cosmochim. Acta* 67:4013-4031.
- Fillela, M., N. Belzile, and Y.W. Chen. 2002. Antimony in the environment: a review focused on natural waters. I. Occurrence. *Earth- Science Reviews* 57: 125-176.
- Goldberg, S. 1992. Use of surface complexation models in soil chemical systems. p.233-329. *In* D.L. Sparks. *Advances in Agronomy*. Academic Press, Inc. San Diego, CA.
- Goldberg, S. 2010. Competitive adsorption of molybdenum in the presence of phosphorous or sulfur on gibbsite. *Soil Science* 175:105-110.
- Goldberg, S. and G. Sposito. (1984). A chemical model of phosphate adsorption by soils: I. Reference oxide minerals. *Soil Sci.Soc. Am. J.* 48:772-778.
- Goldberg, S., and N.J. Kabengi. 2010. Bromide adsorption by reference minerals and soils. *Vadose Zone J.* 9:780-786.
- Goldberg, S., I. Lebron, J. Seaman, and D. Suarez. 2012. Soil Colloidal Behavior. p.15 1-39. *In* Huang et al. (ed.) *Second Edition, Handbook of soil sciences: properties and processes*, CRC Press, Boca Raton, FL.
- Guo X., Z. Wu, and M. He. 2009. Removal of antimony(V) and antimony(III) from drinking water by coagulation–flocculation–sedimentation (CFS). *Water Res.* 43:4327-4335.
- He, L.M., L.W. Zelany, V.C. Balingar, K.D. Rithey, and D.C. Martens. 1997. Ionic strength effects on sulfate and phosphate adsorption and γ -alumina and kaolinite: triple-layer model. *Soil Sci.Soc. Am. J.* 61:784-793.

- Herbelin, A.L., and J.C. Westwall. 1999. A computer program for determination of chemical equilibrium constants from experimental data. Version 4.0. Report 99-01, Dept. Of Chem., Oregon State University, Corvallis, OR.
- Hug, S.J. 1997. In situ FTIR measurements of sulfate adsorption on hematite in aqueous solutions. *J. Colloid Interface Sci.* 188:415-422.
- Ilgén, A.G., and T.P. Trainor. 2012. Sb(III) and Sb(V) sorption onto Al-rich phases: hydrous Al oxide and the clay minerals kaolinite KGa-1b and oxidized and reduced nontronite NAu-1. *Environ. Sci. Technol.* 46:843-851.
- Jiang, T., G.J. Hirasaki, and C.A. Miller. 2009. Characterization of kaolinite zeta-potential for interpretation of wettability alteration in diluted bitumen emulsion separation. *Energy Fuels* 24:2350-2360.
- Jodin, M.C., F. Gaboriaud, and B. Humbert. 2005. Limitations of potentiometric studies to determine the surface charge of gibbsite $\gamma\text{-Al(OH)}_3$ particles. *J. Colloid Interface Sci.* 287:581-591.
- Johnson C.A.,H. Moench, P. Wersin, P. Kugler, and C. Wenger. 2005. Solubility of antimony and other elements in samples taken from shooting ranges. *J. Environ. Qual.* 34:248–254.
- Juang, R.S., and W.L. Wu. 2002. Adsorption of sulfate and copper (II) on goethite in relation to the change of zeta potentials. *J. Colloid Interface Sci.* 249:22-29.
- Kabata-Pendias A., and H. Pendias. 1984. Trace elements in soils and plants. CRC Press, Boca Raton, FL.

- Kampf, N., A. Scheinost, and D. Schulze. 2012. Oxide minerals in soils. p.22 1-13. *In* Huang et al. (ed.) Second Edition, Handbook of soil sciences: properties and processes, CRC Press, Boca Raton, FL.
- Karamalidis, A.K., and D.A. Dzomback. 2010. Surface complexation modeling. Wiley, Hoboken, NJ.
- Kosmulski, M. 2009. Surface charge and points of zero charge. CRC Press, Boca Raton, FL.
- Kosmulski, M. 2012. IEP as a parameter characterizing the pH-dependent surface charging of materials other than metal oxides. *Adv. Colloid Interfac* 171:77-86.
- Kosmulski, M., and P. Dahlsten. 2006. High ionic strength electrokinetics of clay minerals. *Colloids Surf., A* 291:212-218.
- Leuz, A.K., H. Monch, and A. Johnson. 2006. Sorption of Sb(III) and Sb(V) to goethite: influence on Sb(III) oxidation and mobilization. *Environ. Sci. Technol.* 40:7277–7282.
- Lintschinger, J., B. Michalke, S. Schulte-Hostede, and P. Schramel. 1998. Studies on speciation of antimony in soil contaminated by industrial activity. *Int. J. Environ. Anal. Chem.* 72:11-25.
- Liu, F., A. De Cristofaro, and A. Violante. 2000. Effect of pH, phosphate and oxalate on the adsorption/desorption of arsenate on from goethite. *Soil Sci.* 166:197-208.
- Liu, F., J.Z. He, C. Colombo, and A. Violante. 1999. Competitive adsorption of sulfate and oxalate on goethite in the absence or presence of phosphate. *Soil Sci.* 164:180-189.

- Lutzenkirchen, J. 1997. Ionic strength effects on cation sorption to oxides: macroscopic observations and their significance in microscopic interpretation. *J. Colloid Interface Sci.* 195:149-155.
- Martell, A., R. Smith, and R. Motekaitis. 2004. NIST critically selected stability constants of metal complexes. NIST standard reference database 46, Version 8.0. NIST, Gaithersburg, MD.
- Martinez-Llado, X. J. de Pablo, J. Gimenez, C. Ayora, V. Marti, and M. Rovira. Sorption of antimony (V) onto synthetic goethite in carbonate medium. *Solvent Extr. Ion Exch.* 26:289-300.
- McComb, K. A., D. Craw, and A. J. McQuillan. 2007. ATR-IR spectroscopic study of antimonate adsorption to iron oxide. *Langmuir.* 23:12125-12130.
- McKenzie, R.M. 1971. Synthesis of birnessite, cryptomelane, and some other oxides and hydroxides of manganese. *Mineral. Mag.* 38:493-502.
- McKenzie, R.M. 1983. The adsorption of molybdenum on oxide surfaces. *Aust. J. Soil Res.* 21:505-515.
- McKenzie, R.M. 1989. Manganese oxides and hydroxides. p.439-461. *In* J.B. Dixon and S.B. Weed (ed.) *Minerals in the soil environment*. Second Edition, SSSA Book Series, no. 1, SSSA, Madison, WI.
- Okkenhaug, G., Y.G. Zhu, L. Luo, M. Lei, X. Li, and J. Mulder. 2011. Distribution, speciation and availability of antimony (Sb) in soils and terrestrial plants from an active Sb mining area. *Environ. Pollut.* 159:2427-2434. .

- Peak, D., R.G. Ford, and D.L. Sparks. 1999. An in situ ATR-FTIR investigation of sulfate bonding mechanisms on goethite. *J. Colloid Interface Sci.* 218:289-299.
- Post, J. 1999. Manganese oxide minerals: crystal structures and economic and environmental significance. *Proc. Natl. Acad. Sci.* 96: 3447-3454.
- Rakshit, S., D. Sarkar, P. Punamiya, and R. Datta. 2011. Antimony sorption at gibbsite-water interface. *Chemosphere* 84:480-483.
- Rietra , R.P.J.J., T. Hiemstra, and W.H. van Riemsdijk. 1999. Sulfate adsorption on goethite. *J. Colloid and Interface Sci.* 218:511-521.
- Rosenqvist, J. P. Perrson, and S. Sjoberg. 2002. Protonation and charging of nanosized gibbsite (α -Al(OH)₃) particles in aqueous suspension. *Langmuir* 18:4598-4604.
- Saeki, K., S. Matsumoto, and R. Tatsukawa. 1995. Selenite adsorption by manganese oxides. *Soil Science.* 160:265-272.
- Sahai, N., and D.A. Sverjensky. 1997. Evaluation of internally consistent parameters for the triple-layer model by the systematic evaluation of oxide surface titration data. *Geochim. Cosmochim. Acta* 61:2801-2826.
- Schwertmann, U., and R.M. Cornell. 2000. *Iron oxides in the laboratory.* Wiley-VCH, Germany.
- Shtangeeva, I., R. Bali, and A. Harris. 2011. Bioavailability and toxicity of antimony. *J. Geochem. Explor.* 110: 40-45.
- Shuai, X. and G. Zinati. 2009. Proton charge and adsorption of humic acid and phosphate on goethite. *Soil Sci. Soc. Am. J.* 73:2013-3020.

- Sposito, G. 1981. The operational definition of zero point of charge in soils. *Soil Sci. Soc. Am. J.* 45:292-297.
- Sposito, G. 1989. *The chemistry of soils*. Oxford, New York, NY.
- Sposito, G. 2008. *The chemistry of soils*. Second Edition, Oxford, New York, NY.
- Stumm, W., C. Huang, and S. Jenkins. (1970) Specific chemical interactions affecting the stability of dispersed systems. *Croat. Chem. Acta* 42:223-245.
- Su, C.M. and J.B. Harsh. 1993. The electrophoretic mobility of imogolite and allophane in the presence of inorganic anions and citrate. *Clays Clay Miner.* 41:461-471.
- Tan, W.F., S. Lu, F. Liu, X. Feng, J. He, and L. Koopal. 2008. Determination of the point-of-zero charge of manganese oxides with different methods including an improved salt titration method. *Soil Sci.* 173:277-286.
- Tao, Z., C. Taiwei, L. Weijuan, D. Jinzhou, D. Xiongxin, and G. Yingjie. 2004. Cation adsorption of NpO^{2+} , UO_2^{2+} , Zn^{2+} , Sr^{2+} , Yb^{3+} , and Am^{3+} onto oxides of Al, Si, and Fe from aqueous solution: ionic strength effect. *Colloid Surface A* 242:39-45.
- Tripathy, S.S., S.B. Kanungo, and S.K. Mishra. 2001. The electric double layer at hydrous manganese dioxide/electrolyte interface. *J. Colloid Interface Sci.* 241:112-119.
- Tschan, M., B. Robinson, C.A. Johnson, A. Burgi, and R. Schulin. 2010. Antimony uptake and toxicity in sunflower and maize grown in Sb^{III} and Sb^{V} contaminated soils. *Plant Soil* 344:235-245.

- Tserenpil S., and L. Cong-Qiang. 2011. Study of antimony (III) binding to soil humic acid from an antimony smelting site. *Microchem. J.* 98:15-20.
- United States Environmental Protection Agency (USEPA). 2006. Drinking water standards and health advisories. EPA 822-R-06-013. Washington, DC: Office of Water U.S. Environmental Protection Agency.
- Violante, A., and M. Pigna. 2002. Competitive sorption of arsenate and phosphate on different clay minerals and soils. *Soil Sci. Soc. Am. J.* 66:1788-1796.
- Wang, X.Q, M.C. He, C.Y. Lin, Y.X. Gao, and L. Zheng. Antimony (III) oxidation and antimony (V) adsorption reactions on synthetic manganite. *Chem. Erde-Geochem.* 72:41-47.
- Xi, J., M. He. and C. Lin. 2009. Adsorption of Sb(V) on kaolinite as a function of pH, ionic strength, and humic acid. *Environ. Earth Sci.* 60:715-722.
- Yao, W., and F. Millero. 1996. Adsorption of phosphate on manganese dioxide in seawater. *Environ. Sci. Technol.* 30:536-541.
- Yoon, R.H., T. Salman, and G. Donnay. 1978. Predicting points of zero charge on oxides and hydroxides. *J. Colloid Interface Sci.* 70:482-493.
- Yu, T. R. 1997. *Chemistry of variable charge soils.* Oxford, New York, NY.
- Yukselen-Aksoy, Y., and A. Kaya. 2011. A study of factors affecting on the zeta potential of kaolinite and quartz powder. *Environ Earth Sci* 62:695-705.

Zakaznova-Herzog V.P., and T.M. Seward. 2006. Antimonous acid protonation/deprotonation equilibria in hydrothermal solutions to 300°C. *Geochim. Cosmochim. Acta* 70:2298-2310.

Zhang, G., H. Liu, R. Liu, and J. Qu. 2009. Adsorption behavior and mechanisms of arsenate at Fe-Mn binary oxide/water interface. *J. Hazard. Mater.* 168: 820-825.

Zhang, G.Y., G.M. Brummer, and X. N. Zhang. 1996. Effect of perchlorate, nitrate, chloride, and pH on sulfate adsorption by variable-charge soils. *Geoderma*. 73:217-229.

VITA

Kalyn Alaine Vergeer was born August 1, 1988 to Bob and Janice Vergeer in Innisfail, Alberta, Canada. She moved to Atlanta, Georgia in January of 1999 and subsequently graduated from North Forsyth High School in 2006. Kalyn then moved to Knoxville, TN to attend the University of Tennessee. She graduated in May of 2011 with a Bachelor of Science in Environmental Science. Kalyn then continued her education at the University of Tennessee, receiving her Master of Science in Environmental and Soil Science in May of 2013.